

Investigation of the intrameniscal forces : experiment on porcine knee joints and formulation of mathematical models

Goh, Peck Keng

2007

Goh, P. K. (2007). Investigation of the intrameniscal forces : experiment on porcine knee joints and formulation of mathematical models. Master' s thesis, Nanyang Technological University, Singapore.

<https://hdl.handle.net/10356/21249>

<https://doi.org/10.32657/10356/21249>

NTU

Downloaded on 13 Mar 2024 15:53:54 SGT

0529619

**Investigation of the Intrameniscal Forces:
Experiment on Porcine Knee joints and
Formulation of Mathematical models**

Goh Peck Keng



School of Chemical and Biomedical Engineering

A thesis submitted to the Nanyang Technological University
in fulfilment of the requirement for the degree of
Master of Engineering

2007

ABSTRACT

Mechanisms of the knee joint have always been of interest to orthopaedic surgeons, prosthesis designers and biomechanical engineers. Meniscal injuries are common and the impact of such injuries on the patients is tremendous. Therefore, it is of great interest to investigate the load transmission mechanism in the knee and especially in the menisci.

In this project, the load transfer mechanism was investigated through the direct measurement of the intrameniscal forces of the porcine knee joint using miniature sensors. Such attempts will provide quantitative indications into the load distribution and provide insights into the failure mechanism of the natural knee. In this report, variation of intrameniscal stress with joint angulations, applied torque and time were determined. This approach is unique as there has been no attempt in measurement of the forces inside the meniscus. In addition, mathematical models of the articular cartilage and meniscus are derived to explain the variation of intrameniscal stress with time.

From the investigations done on the intrameniscal force, it was found that measurement of intrameniscal force is possible. In a porcine knee joint, anterior region of the lateral meniscus experienced high stresses during hyperextension. During hyperflexion, posterior regions of both lateral and medial menisci were under high stresses. Anterior region of the lateral meniscus was under highest stresses during external rotation and posterior region of the lateral meniscus was under highest stresses during internal rotation of the knee joint. In general, higher stresses were observed during external rotation as compared to internal rotation of the porcine knee. Highest stresses typically occur in extreme joint positions (hyperextension, hyperflexion, internal rotation and external rotation) and these suggest that extreme positions with high applied torque and a combination of extreme positions on the knee joint should be avoided.

Experimental results for variation of intrameniscal stress with time implied that there was a load transfer from articular cartilage to meniscus with time. This load shift behaviour will protect the articular cartilage if the knee joint is under static loading. This stress versus time behaviour can be explained by a viscoelastic power-law model.

ACKNOWLEDGMENTS

The author would like to express her gratitude towards the following:

1. A/P F.K. Fuss, the supervisor for this project, for his patient guidance;
2. Asst/P A.C. Ritchie, the co-supervisor for this project, for his helpfulness;
3. Dr. Toshimasa Yanai for his willingness to loan his rubber sensor system;
4. Technicians and friends from Biomedical Engineering Research Centre who provide advice and support;
5. Family and partner for their understanding and moral support.

LIST OF FIGURES

Figure 1: The anterior view of the knee joint (from: Tortora, G.J. and Grabowski, S.R., Principles of anatomy and physiology) [41].....	4
Figure 2: The four-bar linkage (from: Fuss, F.K., Anatomy of the cruciate ligaments and their function in extension and flexion of the human knee joint, <i>American Journal of Anatomy</i> .1989 184 (2): 165-176.) [44]	5
Figure 3: The menisci of the right knee (from: Fuss, F.K.: Anatomy, BG2051 (Lecture notes) [54]).....	8
Figure 4: K-scan 4000 from Tekscan (from: http://www.tekscan.com/medical/catalog/4000.html) [85]	17
Figure 5: Differential Variable Reluctance Transducers from Microstrain (from Jones, R.S. <i>et al.</i> , Direct measurement of hoop strains in the intact and torn human medial meniscus, <i>Clinical Biomechanics</i> .1996 11 (5): 295-300) [38]	20
Figure 6: Location of the sensors (from Jones, R.S. <i>et al.</i> , Direct measurement of hoop strains in the intact and torn human medial meniscus, <i>Clinical Biomechanics</i> .1996 11 (5): 295-300) [38].....	21
Figure 7: The positions of the strain gauges (from: Hollis, J.M. <i>et al.</i> , Change in meniscal strain with anterior cruciate ligament injury and after reconstruction, <i>The American Journal of Sports Medicine</i> .2000 28 (5): 700-704.) [87]	22
Figure 8: Schematic of the sensor placed in the meniscomfemoral joint	24
Figure 9: Flexiforce sensor (from:	29
Figure 10: The working mechanism of Inastomer (from: http://www.inaba-rubber.co.jp/en/b_products/inastomer/index.html) [100].....	30
Figure 11: Force sensor resistor's three layer construction (from: http://www.steadlands.com/interlink/interlinkpages/fsr.htm) [104].....	31
Figure 12: Transmissive sensor (from: Krohn, D.A., Fiber optic sensors : Fundamentals and Applications) [107].....	32
Figure 13: Reflective Sensor (from: Krohn, D.A., Fiber optic sensors : Fundamentals and Applications) [107]	33

Figure 14: Microbending (from: Urbanczyk, W., Selected applications of fiber-optic sensors, <i>Proceedings of SPIE - The International Society for Optical Engineering</i> .1999 3820 221-234.)[108]	34
Figure 15: Blazed grating (from: Othonos, A., Fiber Bragg gratings, <i>Review of Scientific Instruments</i> .1997 68 (12): 4309-4341.) [111]	36
Figure 16: Chirped grating with aperiodic pitch (from: Othonos, A., Fiber Bragg gratings, <i>Review of Scientific Instruments</i> .1997 68 (12): 4309-4341.) [111]	36
Figure 17: Locations of sensor within the meniscus	38
Figure 18: The Pressure conductive sensor	39
Figure 19: Data logging set up for Pressure Conductive sensor.....	40
Figure 20: The Goniometer, Torsiometer and the Force sensing resistor sensor system	41
Figure 21: Schematic for sensors systems connection	42
Figure 22: Pressure conductive sensor calibration curve	43
Figure 23: Specimen with the goniometer, force sensing resistor sensor and piezoelectric sensor with indication of the location of torsiometer in rotational experiments.....	45
Figure 24: Insertion of the pressure conductive sensor	46
Figure 25: Structure to constrain the tibia bone (sensor systems not displayed) and extension-flexion movement of the knee specimen.....	46
Figure 26: One cycle in the Extension-Flexion experiment	47
Figure 27: Internal-external rotation of the porcine knee joint specimen (sensor systems not displayed).....	48
Figure 28: One cycle in the Internal-External Rotation experiment.....	49
Figure 29: Removed menisci	50
Figure 30: Intrameniscal stress, applied moment and angle vs. time graphs for extension-flexion experiment	52
Figure 31: Graphs of Intrameniscal Stress and Moment vs. Normalised angle during extension-flexion motion at each position with the moment curve on top of the	

intrameniscal stress curve. Zero normalised angle representing hyperextension.
..... 54

Figure 32: Graph of intrameniscal stress vs. applied moment for extension-flexion
experiment for each location and experiment..... 57

Figure 33: Graph of Intrameniscal stress- Moment ratio at different locations within
the menisci, at extreme knee positions in the extension-flexion experiments..... 58

Figure 34: Intrameniscal stress, applied moment and angle vs. time graphs for
internal-external rotation experiment 61

Figure 35: Graphs of Intrameniscal Stress and Moment vs Normalised angle during
Internal-External rotation motion at mid-flexion at each position with the
moment curve on top of the intrameniscal stress curve. Positive normalised angle
representing internal rotation. 64

Figure 36: Graph of intrameniscal stress vs applied moment for internal-external
rotation experiment for each location and experiment 67

Figure 37: Graph of Intrameniscal stress-Moment ratio at different locations within
the menisci, at extreme knee positions in the internal-external rotation
experiments..... 68

Figure 38: Static Experiment Setup..... 72

Figure 39: Position of pressure conductive sensor between the articular cartilages .. 73

Figure 40: Graphs of Intrameniscal stress vs time at each position 74

Figure 41: Graphs of articular cartilage contact stress vs time..... 76

Figure 42: Material test setup 77

Figure 43: Stress Relaxation Graph for articular cartilage specimen AC1 79

Figure 44: Stress Relaxation Graph for meniscus specimen M11 79

Figure 45: Standard Linear Solid model..... 80

Figure 46: Result of SLS model 85

Figure 47: First Viscoelastic Power model..... 86

Figure 48: Result of the First Viscoelastic Power model 89

Figure 49: Second Viscoelastic Power Model..... 90

Figure 50: Result of Second Viscoelastic Power-law model with $D=0.73$ 93

Figure 51: Result of Second Viscoelastic Power-law model with $D=0.88$ 94

Figure 52: Result of Second Viscoelastic Power-law model with $D=0.58$ 94

Figure 53: Model and schematics of joint interfaces..... 102

LIST OF TABLES

Table 1: Peak stresses at each meniscal location, in each experiment, at internal rotation and external rotation of the knee joint specimens 70

Table 2: Parameters of the articular cartilage power-fit curves for stress relaxation tests 78

Table 3: Parameters of the meniscus power-fit curves for stress relaxation tests 79

LIST OF SYMBOLS

$a, b:$	Geometry parameters for contact area
$E:$	Young Modulus
$F:$	Force
$K:$	Spring stiffness
$R:$	Radius
$W:$	Normal load
$\epsilon:$	Applied Strain
$\dot{\epsilon}:$	Rate of change of strain
$\eta:$	Dashpot viscosity
$\lambda:$	Wavelength
$\sigma:$	Stress
$\dot{\sigma}:$	Rate of change of stress
$\nu:$	Poisson's Ratio
$X:$	Displacement
$\dot{X}:$	Rate of displacement

TABLE OF CONTENTS

Abstract i

Acknowledgments..... ii

List of Figures iii

List of Tables vii

List of Symbols viii

Table of Contents ix

1.0 Introduction..... 1

 1.1 Objective.....3

 1.2 Organization of Report3

2.0 Review of Literature..... 4

 2.1 The Knee Joint.....4

 2.2 Structure of Meniscus7

 2.2.1 Structure.....7

 2.2.2 Constraint and mobility7

 2.3 Functions of Meniscus.....10

 2.4 Meniscal Injuries10

 2.5 Cartilage material model.....12

2.6 Review of related studies.....13

2.6.1 The level of compressive load affects conclusions from statistical analyses to determine whether a lateral meniscal autograft restores tibial contact pressure to normal: A study in human cadaveric knees (Huang, A. *et al.*, 2003) [27]14

2.6.2 Measurement of meniscomfemoral contact pressure after repair of bucket-handle tears with biodegradable implants (Becker, R. *et al.*, 2005) [35]16

2.6.3 A novel method for measuring medial compartment pressures within the knee joint in-vivo (Anderson, I.A. *et al.*, 2003) [36].....18

2.6.4 Selected Knee Osteotomies and Meniscal Replacement: Effects on Dynamic Intra-joint Loading (Andrish, J.T. *et al.*, 2001) [37]19

2.6.5 Direct measurement of hoop strains in the intact and torn human medial meniscus (Jones, R.S. *et al.*, 1996) [38]20

2.6.6 Change in meniscal strain with anterior cruciate ligament injury and after reconstruction (Hollis, J.M. *et al.*, 2000) [4]22

2.6.7 Summary of the six experiments discussed24

2.7 Review of Sensors27

2.7.1 Fuji Film27

2.7.2 Metallic Strain Gauge28

2.7.3 Piezoelectric sensors28

2.7.4 Piezoresistive sensors29

2.7.5 Optic Fibre Sensor31

2.7.5.1 Intensity modulated sensors.....32

2.7.5.2 Phase modulated sensors34

2.7.5.3 Wavelength modulated sensors34

3.0 Material..... 37

3.1 Specimen.....37

3.1.1 Specimen selection37

3.1.2 Specimen Preparation37

3.2 Sensor System.....39

3.2.1 Calibration of Pressure Conductive sensor.....42

4.0 Experiments 44

4.1 Dynamic Experiment- Variation of intrameniscal stress with extension-
flexion angles, internal external rotation angles and torque applied44

4.1.1 Methodology.....44

4.1.2 Results for extension-flexion experiments51

4.1.3 Results for Internal-external rotation experiments60

4.2 Static Experiment -Variation of intrameniscal stress with time72

4.2.1 Methodology.....72

4.2.2 Results.....73

4.3 Material Testing.....77

4.3.1 Methodology.....77

4.3.2 Results.....78

5.0 Material Model 80

5.1 The Standard Linear Solid Model.....80

5.2 First Viscoelastic Power Model.....86

5.3 Second Viscoelastic Power Model90

6.0 Discussion..... 96

7.0 Conclusion and Recommendations 103

8.0 Papers Published/In-Review..... 105

9.0 References..... 106

Appendix A

Appendix B

1.0 INTRODUCTION

The knee joint is the most complex and largest synovial joint in the human body, where stability and mobility have to co-exist. In addition, the knee joint has to be able to withstand high loadings. Loads of more than five times body weight have been calculated to be exerted on the knee joint in normal daily activities [1, 2]. Due to the high load and the demand for precise balance between stability and mobility, the knee joint is prone to acute and chronic injuries. These may arise through degenerative disease, natural degeneration of the body, and external traumas resulting from sports activities.

One of the structures that are frequently injured is the knee menisci. In the past, the common treatment for torn or degenerated meniscus was total or partial meniscectomy. This procedure has been largely superseded and replaced by meniscal repair and meniscal replacement [3] as meniscectomy increases the stress exerted on the articular cartilage [4] and long term studies have provided proof that meniscectomy causes ligament laxity, early degenerative arthritis, and symptomatic knees [5]. Examples of symptoms are pain, locking or buckling of the knee joint.

The main meniscal function is to distribute stress across the knee during weight bearing, provide shock absorption, serve as secondary joint stabilizers, provide lubrication [6] and serve as proprioceptive structure to the knee joint [7]. Investigation on the biomechanics of the meniscus is imperative to the understanding of knee mechanics.

Measurement of the intrameniscal loads is important as the meniscus is frequently injured and it plays multiple important roles in the mechanics of the knee joint. By measuring the intrameniscal forces, the injury mechanism can be understood better and effects can be reduced by clinical modification and intervention. In addition, the information gained from intrameniscal force measurement can serve as a gauge to pinpoint possible injury sites based on injury mechanism and as a guide for restoration of function to injured meniscus through repair or replacement.

Studies made on the knee mechanics have included experimental and theoretical approaches [4, 8-38]. The results from these investigations differ considerably. The noticeable difference in the results from various studies has been highlighted by Komistek *et al.* [39]. The evident difference in contact force measured implies a need for further research.

Experimental methods offer accurate and direct measurement of pressure within the knee provided that experimental conditions *in vitro* replicate *in vivo* conditions. In order to ensure accuracy, the measurement method employed in the experiment must not affect the load transmission mechanism significantly, and the measurement system as a whole must be rigorously calibrated to ensure accuracy. This study therefore concentrates on using an experimental approach, which involves the implantation of sensors in the meniscus to determine the intrameniscal forces. At the present time, direct measurement done on the meniscus includes contact stresses in the meniscomfemoral joint and hoop strain in the meniscus. However, no attempt has been made to measure the intra-meniscal forces.

To measure intrameniscal forces, one of the most important issues is the type of sensor used. Sensors considered include Fuji film, piezoelectric sensors, piezoresistive sensors, strain gauge, and optical sensors. For this project, piezoresistive sensors were used to measure intrameniscal pressure due to its small size, fast response speed and ease of use.

Experiments were conducted to investigate the variation of intrameniscal stresses with change in extension-flexion angle, internal-external rotation angle, applied torque and time. Five dynamic experiments were carried out with pressure conductive sensors to investigate the relationship of the intrameniscal stress to flexion and rotation angles. Another five experiments were conducted to examine the change in intrameniscal stress with time during fixed load and position.

Further investigation of the stress relaxation properties of the meniscus was conducted by testing samples of the material. Mathematical models were developed using the parameters obtained from the material tests to explain the variation of intrameniscal stress with time.

1.1 Objective

The aims of this project are:

1. To measure intrameniscal stresses at varying flexion-extension angle, internal-external rotation angle and applied torque.
2. To examine the variation of intrameniscal pressure with time with constant knee load.
3. To measure the material properties of the meniscus and articular cartilage for development of a viscoelastic model.
4. To use the experimentally obtained results to develop mathematical models to explain the load transfer in the menisci and articular cartilage.

1.2 Organization of Report

The first two chapters serve as an introduction to the investigation, describing the anatomy of the knee with attention on the meniscus, past attempts in the measurement in the knee and different types of sensors available and applicable for such usage.

The third chapter provides the description of the materials used. This is followed by Chapter 4 which gives accounts on the experiment methodology and results.

The derivations of three mathematical models are included in Chapter 5. In Chapter 6, the experimental results, practical applications and the derivation of mathematical model are discussed. The project is concluded in Chapter 7. In Chapter 8, a list of publications for the project is provided.

2.0 REVIEW OF LITERATURE

2.1 The Knee Joint

“Knowledge of the anatomy and biomechanics of the knee is critical for successful rehabilitation following knee injury and/or surgery”(according to McGinty *et al.*) [40]. This is especially important as the knee joint is the largest and the most complex synovial joint in the human body. Also, the joint is located between two of the longest bones of the body, giving rise to huge moment arm and high force and hence is prone to damage and injury. Furthermore, during single-stance in walking for bipedal species, the entire load of a few times body weight must be supported by one knee.

The motion of a knee joint is made up of three articulations, one between the patella and the femur and two between the two femoral condyles and the tibial plateau. The joints are referred to as the patello-femoral joint and the tibiofemoral joint respectively. The knee joint, with the exception of the patella, is shown in Figure 1.

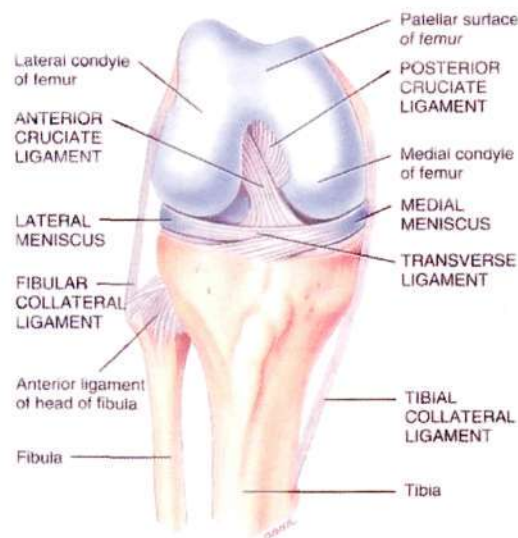


Figure 1: The anterior view of the knee joint (from: Tortora, G.J. and Grabowski, S.R., Principles of anatomy and physiology) [41]

The knee joint is classified as a diarthrodial joint [42]. In a knee joint, the epiphyseal ends of the femur and tibia are separated by a synovial cavity and are contained within a fibroelastic joint capsule. The articulation surfaces of the femur and tibia are covered by hyaline cartilage, which is also known as the articular cartilage. The main function of the articular cartilage is to help to spread the forces over the joint and to provide a low friction and wear-resistant surface for joint movement. Similarly, the

meniscus provides shock absorption and bearing surface. It allows two bones of different shapes to fit more congruently and direct the flow of synovial fluid to the areas of greatest friction.

Even though there is an evident lack of congruency between the articulating surfaces which leads to high flexibility, the knee joint is extremely stable. The reasons for this stability are mainly due to strong ligaments such as the cruciate ligaments. The collateral ligaments contributed to the stability in the knee joint in extension.

The cruciate ligaments (shown in Figure 1) are essential to the kinematics of the knee joint. They consist of guiding bundles which are constantly taut. The polycentric knee is based on the four-bar linkage which is formed by these two guiding bundles. The instantaneous centre of rotation for the joint is at the point where the bundles cross each other. The four-bar linkage is shown in Figure 2. The four-bar linkage of the cruciate ligaments has been assumed for more than 100 years, yet it has not been proved before 1989, independently by O'Connor *et al.* in 1989 [43] and Fuss in 1989 [44].

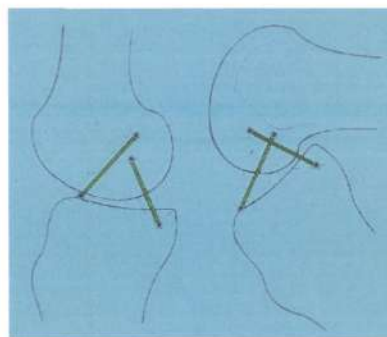


Figure 2: The four-bar linkage (from: Fuss, F.K., Anatomy of the cruciate ligaments and their function in extension and flexion of the human knee joint, *American Journal of Anatomy*.1989 184 (2): 165-176.) [44]

Furthermore, the guiding bundles, also known as isometric bundles, prevent drawer motions (anterior-posterior gliding of the tibia plateau). If cruciate ligament ruptures, instability will be introduced to the knee. Of the two cruciate ligaments, the anterior cruciate ligament (ACL) insufficiency is more harmful than the posterior cruciate ligament (PCL) insufficiency as ACL is stressed twice per stride as compared to the

once per stride of the PCL [45]. Unfortunately, ACL injuries are common and ACL tear frequently leads to meniscal injuries [46]. The ACL can be repaired or replaced with the central third of the patellar ligament, a tendon or an artificial ligament. Notably, the ACL is usually destroyed in human arthritic knee [47]. Therefore, when knee replacement is required in arthritic knee, the function of ACL must be compensated with the structure of the prosthesis.

There are two types of collateral ligaments, namely the medial collateral ligament and the lateral collateral ligament (shown in Figure 1). The medial collateral ligament is also known as the tibial collateral ligament. It extends from the medial epicondyle of the femur to the medial surface of the tibia. The lateral collateral ligament, also known as the fibular collateral ligament, extends from the lateral femoral epicondyle to the head of the fibula. The collateral ligaments restrict the internal and external rotation and prevent abduction and adduction during knee extension [48].

The tibiofemoral joint is described as a ginglymus joint in some literature [49]. However, the axis of rotation changes and both internal and external rotations can be observed in the joint. Also, it can be seen that at different positions of the knee, the magnitude of axial rotation is different. As the joint articulates, limited posterior-anterior and medial-lateral translation can also be observed. Therefore, to classify knee joint as a ginglymus joint is a massive over-simplification of the joint. There have also been reports stating that the knee joint has six degrees of freedom, namely, flexion-extension, internal-external rotation, valgus-varus rotation, anterior-posterior translation, medial-lateral translation and compression-distraction translation [40, 50].

In essence, the tibiofemoral joint is a bicondylar joint. In a constrained bicondylar joint, there are only two degrees of freedom. For an unconstrained bicondylar joint, the joint has four degrees of freedom.

2.2 Structure of Meniscus

2.2.1 Structure

The menisci are a pair of semi-lunar bodies of fibrous cartilage which lie between the femoral condyles and the tibial plateau. Structurally, the menisci reduce in thickness towards the centre of the joint forming a wedge-shaped cross section. The meniscal body consists mainly of water and a dense elaborate type I collagen network [51]. The fibrous structure has a layered appearance, and the articulating surface is made up of fine fibrils arranged in a random mesh-like woven matrix. The deep zone fibres are arranged in a circumferential manner with smaller radial fibres interwoven between the circumferential fibres [52]. Different locations at the meniscus shows variations in tissue configuration and composition, fulfilling different functional demands [51].

Mature cartilage is mostly avascular except the peripheral aspect of the meniscus and therefore, it does not have blood vessels to bring nutrients to and remove waste product from the tissue. It obtains nutrient and removes waste product by either diffusion or mechanical pumping. Therefore, repeated loading and unloading of the joint which provides a pumping action, is essential to the cartilage's well-being. [53]. The avascularity of the cartilage also affects its ability to heal after injury.

2.2.2 Constraint and mobility

Menisci are free on both articular surfaces and are attached at their margins and extremity. There are six meniscal ligaments, holding the menisci in position. The top view of the menisci is shown in Figure 3.

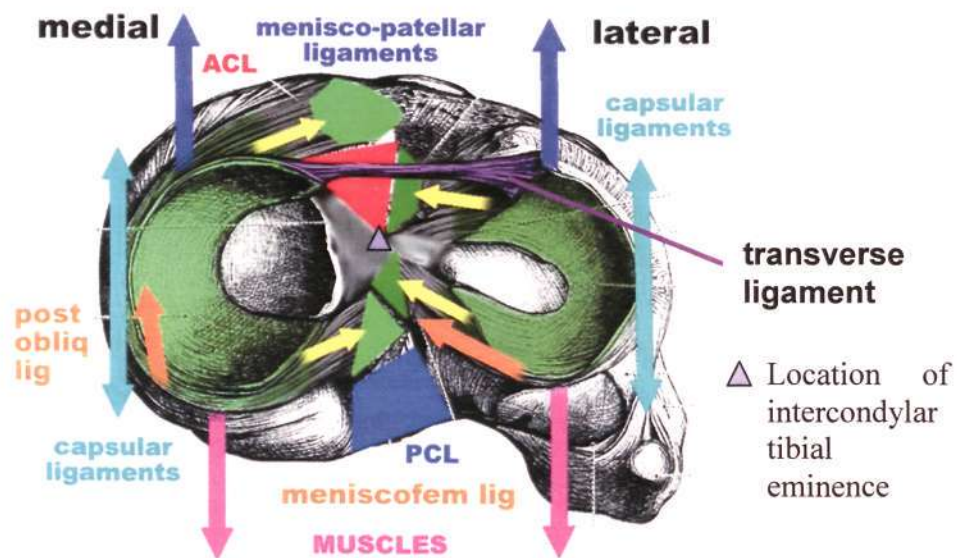


Figure 3: The menisci of the right knee (from: Fuss, F.K.: Anatomy, BG2051 (Lecture notes) [54])

The two menisci are connected at the convex margin by the transverse ligament (in purple in Figure 3). The thickness of the transverse ligament varies and may be totally absent from some subjects [55].

The anterior cruciate ligament (ACL) attachment site at the tibial plateau is shown by the red area and the posterior cruciate ligament (PCL) attachment site is shown by the blue area in Figure 3.

The meniscal attachments to the tibial plateau are shown by the yellow arrows. The meniscal attachment sites are shown by the green areas in Figure 3. The anterior attachment of the medial meniscus to the tibial plateau is in front of the ACL. Its posterior attachment is behind the spine (intercondylar tibial eminence), in between the posterior attachment of the lateral meniscus and the PCL. The anterior attachment of the lateral meniscus to the tibial plateau is in front of the spine, lateral-posterior of the ACL. Its posterior attachment is situated behind the spine and in front of the posterior attachment of the medial meniscus [55].

From the posterior lateral meniscus, the meniscomfemoral ligaments extend to the inside of the medial condyle near the PCL [56]. The meniscomfemoral ligament was once described as the “third cruciate ligament”, however, due to the variability in size and presence of the meniscomfemoral ligament, its exact function is in question [57]. It was found from a review study that out of 1022 cadaveric knees examined, 48.2% have an anterior meniscomfemoral ligament and 70.4% have posterior meniscomfemoral ligament, while 31.8% have both ligaments [58]. The high incidence of meniscomfemoral ligament implies that the meniscomfemoral ligaments have a functional role.

As the femoral condyles compress onto the menisci, the menisci are pushed radially outwards. Radial displacement of the menisci is resisted by the anchorage of the circumferential fibres at the outer edge of the menisci to the intercondylar bone [59]. Thus, the menisci are always kept between the femoral condyles and the tibial plateau.

The menisci have high mobility, with the lateral meniscus having a higher maximum displacement of approximately twice that of the medial meniscus [60]. As the knee extends, the menisci are pushed anteriorly by the femoral condyles and therefore, shifting the contact anteriorly relative to the tibial plateau. Similarly, as the knee flexes, the menisci are pushed posteriorly. The movements of the menisci are also influenced by the ligamentous and muscular attachments. In extensor mechanism, the menisci are moved anteriorly by their connection to the meniscopatellar fibres and the lateral meniscus is moved anteriorly by the meniscomfemoral ligament as the extension constraining fibres of posterior cruciate ligament become taut. In flexor mechanism, the medial meniscus is pulled posteriorly by the semimembranosus expansion. In addition, the medial meniscus anterior horn is moved posteriorly by the attachment to the anterior cruciate ligament. During flexion, the lateral meniscus is drawn posteriorly by the popliteus expansion [61].

2.3 Functions of Meniscus

The primary function of the meniscus is to facilitate the load transmission in the knee joint. It creates a larger surface for load transmission by conforming to the femoral condyles and tibial plateau contributing to a higher degree of congruency between the two mating surfaces. It is estimated that the menisci transmit between 50 to 70 percent of the load across the joint with at least 50 percent load in flexion range of 0 degree to 90 degree [26]. Another suggested function of the menisci is that it provides shock absorption. The viscoelastic menisci have been suggested to function as a damper to the shock spikes generated in the knee joint during activities. Experimental studies have shown that the shock-absorbing capacities of a normal knee are about 20% higher than knees that have undergone meniscectomy [7]. Other proposed functions of the menisci include assisting in the lubrication of the joint and serving as proprioceptive structures to provide feedback mechanism for a sense of joint position [7]. In addition, it serves as a secondary stabilizer when certain primary knee stabilizers are compromised [62].

2.4 Meniscal Injuries

Meniscal injuries can be acute or chronic. The term “chronic” describes conditions of long duration [63]. Chronic injuries occur when there is a long period of repeated exposure to an injurious force which may take place during normal daily activities like work or sports. Acute injuries describes injuries that are severe or of short duration [63]. Often acute injuries occur during sport activities where there is a sudden flexion, extension, rotation or a combined extension or flexion with rotation of the knee joint [64-66].

The medial meniscus is twenty times more susceptible to injuries than the lateral meniscus [67]. This is due to the higher mobility of the lateral meniscus [68]. Meniscal tears can be classified as primary or secondary. A meniscal tear is classified as a primary tear when the damage is direct and as a secondary tear when it is related to damage of the same or other structure. Older patients may not have a specific injury mechanism as their meniscal injuries are often due to degenerative processes [69].

Injuries to the medial meniscus are often associated with rupture of the anterior cruciate ligament. This is due to the increase in magnitude of the internal rotation of the tibia. This excessive twisting action leads to the increase in force exerted by the femoral condyles on the menisci.

In a study by Drosos and Pozo in 2003 [70] on 392 patients, it was found that while traumatic and degenerative tears have similar incidence for patients below 40 years old, degenerative tears become predominant at 76 percent occurrences thereafter. In the same study, it was found that among the patients with meniscal injuries not related to sporting activities, 50 percent sustained their injuries in the action of crouching or getting up from a squatting position. It was also reported by Childress in 1957 [71] that patients who are in occupations that require a squatting position are more likely to sustain injuries in the posterior part of the medial meniscus.

The three basic types of tears are longitudinal, radial and horizontal. Longitudinal or circumferential tear propagates parallel to the outer margin of the meniscus and a displaced longitudinal tear is termed bucket-handle tear. A radial or transverse tear runs in a path perpendicular to the main axis of the meniscus and this compromises the meniscus integrity and reduces the ability of the meniscus to distribute hoop stress. A horizontal tear divides the meniscus into superior and inferior portions. A single tear which occurs in a combination of the longitudinal, radial and horizontal planes is termed a complex tear.

The treatment of the meniscus after injuries is important. Knee evaluation often includes the McMurray's meniscal test and the Apley's tests to check for meniscal injuries. In severe cases, surgical procedures, such as meniscectomy, meniscal repair and meniscal transplantation have to be performed.

When meniscectomy is performed, it was shown that the weight bearing areas of the tibiofemoral joint decreases tremendously. The decrease in contact surface will increase the wear on the articular cartilage, thereby causing early degeneration of the knee. Long-term studies of meniscectomy in children and adolescents have further shown that the procedure causes ligament laxity, early degenerative arthritis, and symptomatic knees with less than half of the 26 children showing good results [5]. It

is of significance to note that even a 25% loss of meniscus can cause a quadrupling of the stress experienced by the articular cartilage [4].

The second surgical treatment method is meniscal repair. This treatment is usually employed when the tear is located in the vascular regions of the meniscus which have the best prognosis for healing.

Meniscal replacement is an option when meniscectomy is unavoidable and there are contraindications for meniscal repair. It was estimated that over 4000 meniscal transplantations have been performed in the United States and this procedure has been gaining popularity in various countries [72]. This operation involves replacing the damaged or missing meniscus with different types of substitutes such as meniscus allograft, autografts, and tissue engineered constructs [73]. It was found that lateral meniscal allograft implanted using bone plugs can significantly improve contact pressure relative to a meniscectomized knee at the time of implantation [27]. Polyvinyl alcohol-hydrogel (PVA-H) artificial meniscus replacement is now under investigation and may be clinically applicable for meniscus injuries [74]. It has been shown that meniscal transplantation is effectively in at least partially fulfilling the functions of a normal meniscus [75]. Understanding of the load transmission in the menisci and examining the meniscus properties will greatly benefit this field of operation by clarifying the requirements for a suitable replacement.

2.5 Cartilage material model

Like most biological materials, the meniscus displays time-dependent creep and stress relaxation. In essence, it is a viscoelastic material, combining the properties of both elastic and viscous substances. As the meniscus experiences load, it deforms and shifts. The deformation depends on the structure properties and the mechanical properties of the meniscus.

2.6 Review of related studies

To gain understanding of the loading mechanism of meniscus in the knee joint, different approaches have been used. The techniques can be categorised into theoretical and experimental approach.

Several studies have utilised theoretical techniques such as finite element analysis [8-24] and mathematical modelling [25] in the investigation of meniscal biomechanics. Finite element analyses have been used to find the magnitude and location of the contact stresses and areas of the menisci [8-13]. Furthermore, the effects of meniscectomy have also been examined using finite element modelling [8, 10]. It was found that removal of menisci markedly increases the primary and coupled laxities of the joint, decreases total contact areas, and increases contact stresses [8]. Interestingly, the study also found that for small to moderate loads, the lateral meniscus resists a larger portion of the axial load than does its medial counterpart. The relative magnitude of the load between uncovered cartilages as compared with meniscus strongly depends on the initial positioning of the joint, femoral constraints, the joint degeneration and loading among other factors. Modelling is versatile and can be used to obtain information that cannot be measured experimentally. It has the disadvantage that modelling requires assumptions with regard to the boundary conditions, contact model and material properties. These assumptions bring about errors and evaluations of the model have to be done using experimental methods.

For the experimental approaches, one angle of approach is the use of an instrumented artificial knee joint in the measurement of both *in vivo* and *in vitro* knee loads [28-31]. However, to measure *in vivo* loads in human knee using an instrumented knee, issues including biocompatibility, power source, weight, sealing of the sensor, signal transmission and fatigue testing have to be addressed. *In vivo* loads have been measured successfully in the human hip joint [76, 77] but the success of the instrumented knee prosthesis in the measurement of *in vivo* loads is limited.

Another method is through investigation of the material properties and structural organisation of the meniscus which will provide the basis for deduction of load transmission through the meniscus. Although determination of the meniscal load

bearing role is not the primary objective of the studies, the extent of this role can be inferred from their results. In most of the studies, samples of the meniscus were extracted to be used in creep tests, indentation tests, tensile tests and compression tests [32-34].

Additionally, measurements of tibiofemoral contact area are also frequently carried out. This can be done by studying the radiographs of knee specimens whose joint spaces were filled with radiopaque fluid and by casting technique using either bone cements or silicone rubber to obtain precise replication of the surfaces [26].

The last and the most direct approach is measurement utilising miniature sensors on the meniscus. This method provides the least disruption to the system and thus will provide more reliable results. However, technical difficulties such as the type of sensors used, the effect of the sensors on the results and shifting of the sensors have to be dealt with. Six of the more important and relevant experiments were chosen and examined in detail in the next section.

2.6.1 The level of compressive load affects conclusions from statistical analyses to determine whether a lateral meniscal autograft restores tibial contact pressure to normal: A study in human cadaveric knees (Huang, A. *et al.*, 2003) [27]

One of the more popular methods of measuring meniscomfemoral contact pressure is through the use of Fuji film. Huang *et al.* aimed to determine the effect of compressive load magnitude on the efficiency of meniscal autograft on restoring tibial contact mechanism. In this investigation, the Fuji film was encapsulated in polyethylene packets to protect it from joint fluid and change in humidity. Nine fresh frozen human cadaver knees were used for the study. The specimens were obtained from five females and five males of age ranges from 34 to 68 years. Knee joints with joint space narrowing, osteophytes, chondrocalcinosis and experience prior knee surgery were excluded. The contact stresses were measured at randomized flexion angles of 0 degree, 15 degrees, 30 degrees and 45 degrees. Loads applied were also chosen randomly at 0.5 times body weight and 1.5 times body weight.

The most important finding from the study was that the effectiveness of autograft in restoring tibial contact pressure to the intact meniscus condition depends on the level of compressive loading. It was found that at 400N axial load, the autograft gave maximum and mean pressures that were comparable to the normal knee with intact meniscus. However, statistical analyses indicated that at 1200N axial load, meniscal implants fixed with bone plugs did not restore the contact pressure to normal but reduction of contact pressure was observed compared to the meniscectomized knee.

The main weakness of the study is the usage of Fuji film. Fuji film was first utilised over 20 years ago and is still being used today for measurement of *in vitro* pressure and areas for both physiological [78, 79] and artificial [80, 81] human joint. It is a useful tool to get a pressure spread between two surfaces. However, there are many limiting factors that have to be taken into consideration when using the pressure sensitive film. Firstly, it works well when both surfaces are kept flat and parallel but does not work well on irregular surfaces; shear forces may be erroneously be recorded at axial loads. This greatly reduces its suitability to measure pressure between the meniscus and femoral condyles as the interfaces are curved and irregular. Secondly, Fuji film can only measure static pressure and only the maximum pressure is recorded. Thirdly, around 50 hours are required for development following stain production. Fourthly, temperature range must be kept within 5-35 Degree Celsius and relative humidity has to be considered. Fifthly, the film cannot be reused and care must be executed during use. Additionally, film thickness may slightly alter the interface congruency and affect the accuracy of the measured contact areas and pressure distributions [82]. In a study on the Fuji film, the usage of ultra-super low grade film (for pressure range from 0.2 to 0.6 MPa) overestimated the contact area while the use of medium grade (for pressure range from 10 to 50 MPa) gave an underestimation [83].

2.6.2 Measurement of meniscomfemoral contact pressure after repair of bucket-handle tears with biodegradable implants (Becker, R. *et al.*, 2005) [35]

Becker *et al.* conducted a study to investigate in the meniscomfemoral contact pressure after repair of bucket handle laceration using different biodegradable implants and suture. The meniscomfemoral contact pressure was measured using a piezo-resistive system from Tekscan (Boston, USA). The sensor used was K-scan, type 4000 which consisted of two pads of size 203mm by 347mm and 0.08mm thick. (Likewise, Thambyah *et al.* did an *in vitro* experiment on cadaveric knees with Tekscan piezoresistive sensor, K-scan to measure contact pressure in the knee [84].) 13 fresh frozen human cadaver knees were used for the study.

The knee was extended from 90 degrees of flexion to 0 degree under a constant load of 350N. The load was applied by adjusting the tensile force of the quadriceps tendon. The tibiofemoral pressure and contact area were recorded at 0 degree, 30 degrees, 60 degrees and 90 degrees of flexion. Results obtained showed that the meniscomfemoral peak pressure at posterior horn was 1.46 ± 1.54 MPa in medial compartment and 1.08 ± 1.17 MPa in the lateral compartment at full extension. The maximum pressure was measured when the knee joint was in mid flexion at 5.5 ± 1.3 MPa for medial compartment and 4.87 ± 1.25 MPa in lateral compartment. The conclusion for the study is that the design of the biodegradable implant has no effect on the meniscomfemoral peak pressure.

For the study, the sensor used is very thin at 0.08mm which is an advantage. The K-scan 4000 is shown in Figure 4. The dimensions given in the journal paper are the overall width and overall length. The dimensions that are of interest are the matrix width and matrix height which are 28mm and 33mm respectively [85]. A sensor of this size would have lain in between both the meniscomfemoral contact surface and the tibiofemoral contact surface. However, no explanation has been offered for the method of differentiating the meniscomfemoral contact pressure from the tibiofemoral contact pressure. Therefore, the peak pressure obtained may not be the meniscomfemoral contact pressure as stated.

In addition, the flaps at the three sides of each sensor pad would obstruct the soft tissues that surround the joint cavity (Figure 4). The third problem is that K-scan

requires a flat surface to give accurate result. Any bending that will result from the contact of two curved surfaces will provide readings which would be mistaken as the contact stresses.

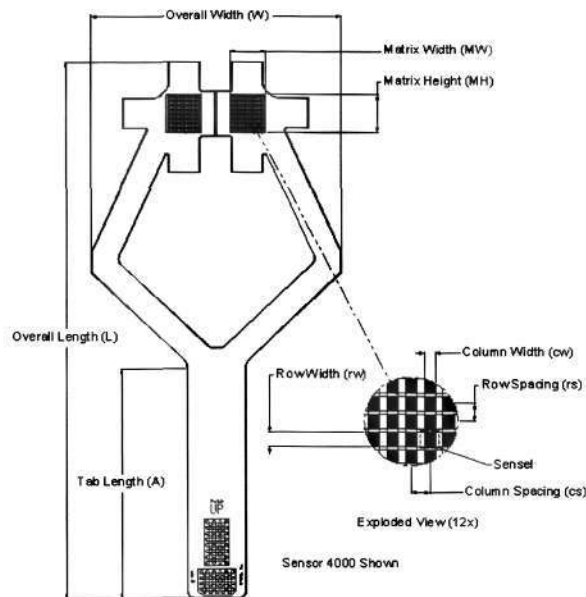


Figure 4: K-scan 4000 from Tekscan (from: <http://www.tekscan.com/medical/catalog/4000.html>) [85]

A wide variation in tibiofemoral contact area and peak pressure values was observed from the result. This may be due to the positioning of the sensor and the bending of the sensor between the curved interfaces. Additionally, similar research using Fuji Film obtained a significant difference in pressure after meniscal repair. The disparity in results implies that the type of sensor used has a major effect on the results obtained even when both type of sensors are flat-sheet type of sensor.

2.6.3 A novel method for measuring medial compartment pressures within the knee joint in-vivo (Anderson, I.A. *et al.*, 2003) [36]

In this study, meniscomfemoral contact pressures were measured *in vivo* by partially covering the loading area with sensor. The aim of the investigation was to assess the effect of valgus knee brace medial compartment force. The meniscomfemoral pressure was measured using a piezoresistive sensor (I-scan 6900 from Tekscan). Cellulose leader tapes were used to hold the sensor between the femoral condyles and the meniscus. The thickness of the sensor with the leader tapes is 0.2mm. Only 11 out of 15 experiments yielded results.

The sensor was inserted through a narrow arthroscopic portal and forceps inserted through a lateral portal were used to pull the sensor into the joint space. Endoscope was used to monitor the positioning process. Sensor system was tested for each patient by exerting varus and valgus thrusts to the leg. Readings from the sensors were also taken for single-leg stance and double-leg stance. Results were based on F_{rel} which is $F_{rel} = F_{brace} / F_{no\ brace}$. F_{brace} and $F_{no\ brace}$ were obtained by summation of the forces from each sensing point and normalised by dividing by force transmitted through the leg during braced and no-braced condition respectively. F_{rel} should vary from zero to one where, zero represents total unloading of the knee and one represents no change in loading. F_{rel} was 0.78 (s.d. 0.29) and 0.70 (s.d. 0.36) for double and single-leg stance respectively. Repeated no-brace measurement on patient 10, 12 and 14 showed variations in the sensor position.

The advantage of such investigation is that *in vivo* measurement can be done with no damage to the knee joint. However, problems such as sensor fixation and determination of sensor position have to be solved. In addition, the investigation lacks systematic protocol as the group of 15 patients in the investigation were separated into three groups with different measurement protocols.

A limitation of the research comes from the sensor used. Although the sensors used have matrix dimensions of 14mm by 14 mm [86] which is smaller in dimension compared to the K-scan, it faces the same problem; I-scan sensor requires a flat surface to give accurate results. The curved meniscomfemoral contact surface would have introduced bending and thereby increased the magnitude of pressure measured.

2.6.4 Selected Knee Osteotomies and Meniscal Replacement: Effects on Dynamic Intra-joint Loading (Andrish, J.T. *et al.*, 2001) [37]

Study by Andrish *et al.* concentrates on the contact stress on the menisci in the menisco-femoral interface and the contact stress on the facets of the patella in the patello-femoral joint during dynamic extension and flexion of the joint. Human cadaveric knee specimens were used in the experiments. Thin-film sensors with thickness of 0.0076mm were used and secured using cyanoacrylate glue. The locations under investigation were the anterior, central and posterior regions of both menisci. Contact stresses were measuring for the joint in flexion angle between 15 degree to 75 degree, with the vastus lateralis, vastus medialis oblique, hamstring muscles under load of 45N tensile load. The result obtained was that the loading on the lateral meniscus was greater than the loading on the medial meniscus.

The sensors used were very thin and this is advantageous as this minimised the effect of foreign entities on the load transmission of the knee joint. Another advantage of the study is the retention of effect of muscles tensions on the joint. However, the method of insertion of the sensors into the joints was not described as the retention of muscles and joint capsule will make precise insertion difficult. The usage of cyanoacrylate glue may also compromise the accuracy of the results. In addition, the contact stress at extreme positions, namely hyperflexion and hyperextension were not measured. It is important to measure the stresses experienced by the joint during the two extreme positions as a large number of meniscal injuries occurs at extreme positions.

2.6.5 Direct measurement of hoop strains in the intact and torn human medial meniscus (Jones, R.S. *et al.*, 1996) [38]

The aim of the study was to investigate in the effect of longitudinal and radial tears on the magnitude of hoop strain on the meniscus. The hoop strain was measured *in vitro* using differential variable reluctance transducer strain gauge from MicroStrain Inc (Vermont, USA). 19 human cadaveric knee joints were tested. Donors with history of knee surgery or pathology were excluded from this study.

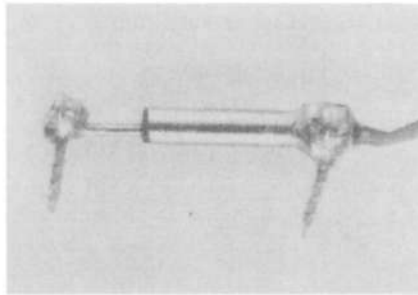


Figure 5: Differential Variable Reluctance Transducers from Microstrain (from Jones, R.S. *et al.*, Direct measurement of hoop strains in the intact and torn human medial meniscus, *Clinical Biomechanics*.1996 11 (5): 295-300) [38]

The DVRT strain sensors were inserted peripherally into the anterior, central and posterior sections of the medial meniscus (Figure 6). The DVRT strain gauge is secured to the meniscus using two barbs and strain is measured through the change in the distance between the two barbs. The load applied on the knee was three body weights at speed of 50mm/min and 500mm/min, during knee flexion angle of 0 degree and 30 degrees. The process was repeated after creation of radial or longitudinal tear in the meniscus.

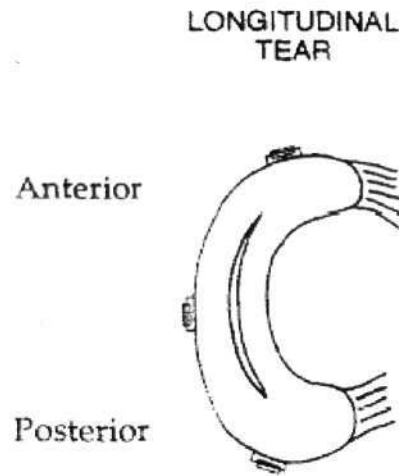


Figure 6: Location of the sensors (from Jones, R.S. *et al.*, Direct measurement of hoop strains in the intact and torn human medial meniscus, *Clinical Biomechanics*.1996 11 (5): 295-300) [38]

Results showed that the posterior section of the intact meniscus was under lower strain as compared to anterior and central sections. However, longitudinal tear in the meniscus caused the strain level to increase in posterior section and decrease in anterior section. 50% radial tear caused the strain in anterior section. Furthermore, the study revealed that the two speed of load application (50mm/min and 500mm/min) showed no difference in strain measurement.

The insertion of sensor into only the medial meniscus may affect the load distribution as difference between the medial and lateral menisci was introduced. More importantly, the sensors in the medial-posterior and medial central position would have intersected with the capsular ligament. The fibres in the capsular ligament extend from the femur to the tibia and would interfere with the extension of the strain gauge. This would result in underestimation of the strain measured. Additionally, medial collateral ligament may interfere with the strain gauge placed at the medial-central position. Lastly, the DVRT provides a linear strain measurement; therefore, the strain readings obtained were only an approximation of the strain in the complex three-dimensional structure of the meniscus.

2.6.6 Change in meniscal strain with anterior cruciate ligament injury and after reconstruction (Hollis, J.M. *et al.*, 2000) [4]

The study by Hollis *et al.* investigated in the change in meniscal strain due to anterior cruciate ligament injury *in vitro*. Hoop strain of the meniscus was measured using differential variable reluctance transducer strain gauge from MicroStrain Inc. (Vermont, USA). Four sensors were utilised, located at posteromedial and anteromedial regions of the medial meniscus and posterolateral and anterolateral regions of the lateral meniscus. A total of nine fresh-frozen cadaveric knees were used in the experiments. All specimens were from cadavers over 60 years of age and did not have significant tibiofemoral or patellofemoral articular cartilage abnormalities and meniscal damage.

The gauges were placed 10mm from the collateral ligament and at the mid line of the meniscus (Figure 7). The measurements were made at full extension, 45 degrees knee flexion and 90 degrees knee flexion. Anterior-posterior force of 0N to 38N was applied to the knee joint while meniscal strain and tibial displacement were recorded at fixed force increments. The knee joint was then loaded at 200N axially along the tibia and the anterior-posterior drawer loading sequence repeated. The entire procedure was repeated after the ACL was sectioned completely. This process was repeated after ACL replacement surgery was conducted for each specimen using patellar tendon graft harvested from the central one-third of the patellar tendon.

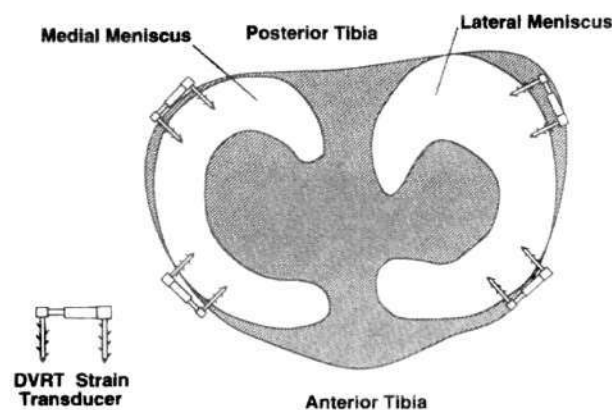


Figure 7: The positions of the strain gauges (from: Hollis, J.M. *et al.*, Change in meniscal strain with anterior cruciate ligament injury and after reconstruction, *The American Journal of Sports Medicine*.2000 28 (5): 700-704.) [87]

The result showed that bisection of the ACL significantly increases the meniscal strain while reconstruction of the ACL returns the meniscal strain to the levels observed in the ACL-intact state. In addition, it was observed that the joint under axial load yielded lower strain readings as compared to the joint which was unloaded. This was due to the stabilising effect of the axial load which resist the anterior-posterior translation resulted from the anterior-posterior loading. The general trend noted was that medial-posterior and lateral-anterior regions tend to be under higher strain. This research supports the hypothesis that the increase in anterior-posterior displacement associated with ACL injury may contribute to the increased in meniscal strain.

The strength of the study is the systematic protocol. The flaws of the study are that the number of the specimens (nine specimens) investigated is small and the limitations posed by the strain gauge. Similar to the study by Jones *et al.*, the capsular ligament interfere with the measurement of the hoop strain using the strain gauges. Furthermore, the DVRT strain gauge measures linear elongation and only provides an approximation of the hoop strain in the menisci. Although load on the meniscus is related to the hoop strain in the meniscus, the relationship is not linear and is yet to be quantified. Therefore, if only hoop strain is measured in an attempt to quantify the meniscus compressive stress, results will be inaccurate.

2.6.7 Summary of the six experiments discussed

From the review of literature, the common limitations in the studies of the stresses and strain of the meniscus lie in the location of measurement and the type of sensor used.

Becker *et al.*, Huang *et al.* and Anderson *et al.* measured the meniscomfemoral contact pressure in their respective investigation. The key disadvantage of measuring the meniscomfemoral contact stresses is the change in the contact surface caused by inserting the sensors in between the two interfaces. It is known that sensor materials covering the full area of contact will influence local contact stresses [88], posing a limitation on the accuracy of the contact stresses measured.

The report from Wu *et al.* [88] showed the effects of inserting a pressensor film into articular joints for the measurement in contact mechanics. Through finite element analysis, it was shown that the usage of Fuji film in measurement of contact stresses will affect the results by 10-26 percent. The percentage error will be affected by loading, geometry of the joint and mechanical properties of cartilage. With consideration of the measurement precision of the Fuji film, joint contact pressures measured in a joint may contain errors as large as 14-28 percent. Figure 8 shows the sensor placed between the femoral condyle and meniscus.

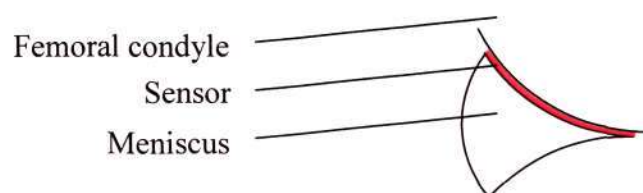


Figure 8: Schematic of the sensor placed in the meniscomfemoral joint

In addition to the finite element analysis by Wu *et al.*, the contact stress can be calculated using the Hertzian theory for arbitrarily curved surfaces. Hertzian equations are shown below.

Hertzian Contact Stresses for arbitrarily curved surfaces [89]:

$$\sigma_z = \frac{1.5W}{\pi ab} \quad (2.6.1)$$

where,

$$a = k_1 \sqrt[3]{\frac{3WR'}{E'}}$$

$$b = k_2 \sqrt[3]{\frac{3WR'}{E'}}$$

$$\frac{1}{E'} = \frac{1}{2} \left[\frac{1 - \nu_A^2}{E_A} + \frac{1 - \nu_B^2}{E_B} \right] \quad (2.6.2)$$

$$\frac{1}{R'} = \frac{1}{R_A} + \frac{1}{R_B}$$

where,

a, b: Geometry parameters for contact area

W: Normal load

R_A: Radius of interface A

R_B: Radius of interface B

R': Reduced radius of curvature

ν_A: Poisson ratio of contacting body A

ν_B: Poisson ratio of contacting body B

E': Reduced Young Modulus

E_A: Young Modulus of contacting body A

E_B: Young modulus of contacting body B

k₁, k₂: Contact coefficients

The contact mechanics is altered with the sensor in between the meniscus and the femoral condyle (Figure 8). The contact pressure can be calculated for sensor and femoral condyle; and for sensor and meniscus from the Hertzian equations shown

above. The contact pressure measured by the sensor cannot be regarded as the contact pressure between the meniscus and the femoral condyle due to the effect of the sensor's material properties. Another factor which will affect the reading is the adhesion between the sensor and the surfaces of femoral condyle and meniscus.

Hoop strain in the meniscus was measured by Jones *et al.* and Hollis *et al.* Due to the different structures in the meniscus; hoop stress represents only part of the load on the meniscus. Although hoop strain is correlated to the compressive load on the meniscus, the correlation factor has not been computed. Therefore, if only hoop strain is measure in an attempt to quantify the meniscus compressive stress, results will be inaccurate. In addition, accuracy of hoop strain measurement is limited by the placement of the strain gauges. Intersection with the capsular ligament will cause the fibres in the capsular ligament to interfere with the extension of the strain gauge. This would result in underestimation of the strain measured.

Fuji film, K-scan and I-scan from Tekscan and DVRT strain gauges were utilized. The limitations of Fuji film are that it works well only on flat and parallel interfaces; can only measure static pressure and only maximum pressure is recorded; requires long development time; is affected by humidity and cannot be reused. The limitation of K-scan and I-scan is that they work well only on flat and parallel interfaces as curved surfaces bend the sensor and create inaccurate readings. DVRT strain gauges measure linear strain; therefore, the strain readings obtained were only an approximation of the strain in the complex 3-dimensional structure of the meniscus. More details on the different sensor system are included in the next sections.

To investigate in the load transfer mechanism of the meniscus, intra-meniscal forces can be measured instead of meniscofemoral contact pressure, meniscotibial contact pressure or hoop strain of the meniscus. This is to avoid errors which are embedded in the contact pressure measurement caused by the insertion of sensor in the meniscofemoral joint or the meniscotibial joint. Effect of the capsular ligament on the measurement of hoop strain using strain gauges can also be avoided when intrameniscal loads are measured using embedded miniature sensors in the meniscus.

2.7 Review of Sensors

Reviews have shown that most sensors used in meniscal biomechanics have been based on metallic strain gauges and semiconductor strain gauges. Since this research relies greatly on choosing an appropriate sensor, it is useful to have a review of the different sensors.

2.7.1 Fuji Film

Although the Fuji Film is very different from the other sensors, it plays an important role in the measurement of contact areas and pressure within a joint. Fuji Prescale pressure sensitive films have been used for pressure sensing in prosthetic knee [80, 81], cadaveric ankle [79] and knee joint [78].

Fuji film is basically divided into five grades: ultra-super-low, super-low, low, medium and high. The first to the fourth grade films measure pressure in the range of 0.2 to 50 MPa and they employ the same composition of two films, A-film and C-films. A layer of colour-forming fluid microcapsules is deposited onto A-film, while C-film is coated with colour-developing chemical. As the two films are placed together and pressure is applied, the microcapsules burst and the colour-forming fluid will be absorbed by C-film and form stains. Due to the different sizes of the microcapsules, the number of microcapsules that will burst differs with the magnitude of pressure applied. High grade film is used for higher pressure ranges from 50-130MPa and it consists of a single sheet on which both colour-forming and colour-developing chemical are deposited.

The magnitude of the pressure applied can be measured by the intensity of the stains formed. Methods of analysis can range from simple usage of densitometer to usage of camera to digitize the film and special software to analyze the resulting image [90].

It is a useful tool to get a pressure spread between two surfaces. However, there are many limiting factors that have to be taken into consideration when using the pressure sensitive film. Firstly, Fuji film can only measure static pressure and only the maximum pressure is recorded. Secondly, it works well when both surfaces are kept flat and parallel but does not work well on irregular surfaces; shear forces may be

erroneously be recorded at axial loads. Thirdly, around 50 hours are required for development following stain production. Fourthly, the relationship between the Fuji film intensity and pressure is nonlinear and varies with temperature and humidity. The temperature range must be kept within 5-35 Degrees Celsius and humidity must be kept stable during the experiment. Due to the difference in environmental conditions, the calibration curves provided by the manufacturer may be invalid [91]. Fifthly, the film cannot be reused and care must be executed during use. Additionally, film thickness may slightly alter the interface congruency and may affect the accuracy of the measured contact areas and pressure distributions [82].

2.7.2 Metallic Strain Gauge

Metallic strain gauges are the most commonly seen sensors due to their robustness and availability in various shape and sizes.

It is connected to a Wheatstone Bridge circuit with full bridge, half bridge or quarter bridge. The bridge in half and quarter circuit is to be completed by precision resistors. The foil-type strain gauge is made up of a grid of wire filaments. When force is applied, the change in dimension of the test piece will be communicated to the filaments. The change in electrical resistance of the foil wire will then unbalance the Wheatstone bridge and produce a signal output. Strain experienced by the foil wire can be found from its relationship to the signal output. The metallic strain gauge depends on dimensional change to produce change in resistance. Metal is sputtered directly on to a flexible backing and are often packaged with Wheatstone bridge, rosette and other patterns.

2.7.3 Piezoelectric sensors

Made up of quartz or ceramic material, piezoelectric sensors are bidirectional transducers that can convert stresses applied into electric potential and vice versa. One of their key characteristics is their wide dynamic range. As the electric signal decays after the application of forces, this may not be a suitable sensor for static loads [92].

2.7.4 Piezoresistive sensors

Piezoresistance is defined by a fractional change in bulk resistivity of the material caused by small mechanical stresses or strain [93]. If the electrical resistance of a material depends upon external strain, the material displays ‘piezoresistivity’ [94]. These sensors were also known as conductor sensors. One of the biomechanical applications of this sensor is in the determination of the foot location on the force plate during gait analysis [95]. This is accomplished by mounting thin sheets of conductor sensor on the force plate.

Piezoresistive Sensors- Flexiforce and K-Scan

Flexiforce (shown in Figure 9) and K-scan sensors are both products of Tekscan and are classified as piezoresistive sensor[96, 97]. K-scan is one of the most frequently utilized sensors in instrumented knee, so it is essential to understand the working principles of the sensor. The Tekscan’s sensors utilize semiconductive ink between the electrical contacts. As force applied increases, the resistance decreases and by measuring the change in current flow, the applied force distribution can be found. The differences between K-scan and flexiforce is that K-scan consists of an arrays of sensing points creating a pressure map while the flexiforce consists of only one sensing point [98].



Figure 9: Flexiforce sensor (from:
<http://www.tekscan.com/flexiforce/flexiforce.htm>)[96]

Piezoresistive sensors- Pressure conductive sensor

The piezoresistive effect can be found in materials which are a composite of elastomer and conductive material. Inastomer (Inaba Rubber Co., Japan) is one example where it consists of insulating rubber material and electro conductive material [99]. The conductive material is carbon and is scattered evenly in the rubber material. When no load is applied, the carbon molecules are not in contact, and therefore, the circuit is open. As load is applied, the conductivity of the material

increases as current conductive pathway is formed by the carbon molecules. As the electrical resistance is dependent on mechanical stress applied, the sensor is classified as piezoresistive sensor [93, 94]. The working principle is illustrated in Figure 10.

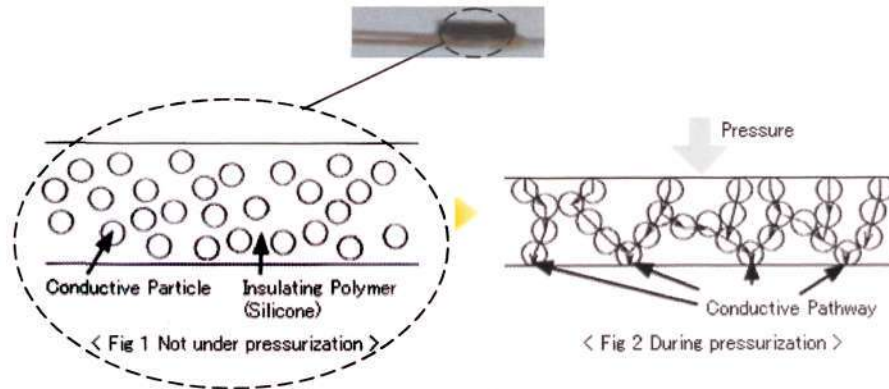


Figure 10: The working mechanism of Inastomer (from: http://www.inaba-rubber.co.jp/en/b_products/inastomer/index.html) [100]

Piezoresistive sensors-Force Sensing Resistor

Force sensing resistor sensors are classified as piezoresistive sensor [101]. It has been used in cases like the measurement of bite force [102] and spinal orthoses [103]. It is a thin polymer device which electrical resistance varies inversely with the magnitude of force applied perpendicularly to the surface of the sensor. The advantage of this sensor is that it can be made into different shapes and sizes to accommodate experimental needs.

Typically, it is made up of three layers of substrate (Figure 11). The first layer is made up of an elastomer printed with semiconductive material. The second layer is a spacer which also acts as an adhesive for the first and third layer. The third layer is made up of a piece of polymer with metallic interdigitating electrodes deposits. When the FSR sensor is loaded, the semiconductive material contacts the electrodes and conductive pathways are formed. As the magnitude of load increases, the resistance of the device decreases. With no load, the force sensing resistor behaves like an open circuit. Force ranges and sensitivities of the sensor can be controlled by the variation of the type of polymer and semiconductive material used.

The working temperature range is -30 to 170 degrees Celsius and it can be used where relative humidity is 100% [90]. In addition, a typical FSR is less than 0.5mm thick and comes in various shapes and sizes. This makes it a suitable candidate in the measurement of joint forces. However, the sensors characteristics that have to be considered in biomechanical usage are its slow rise time and its creep response.

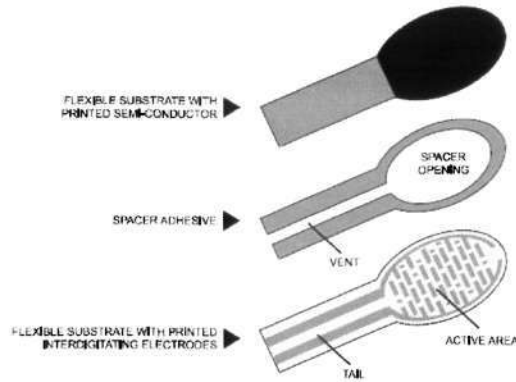


Figure 11: Force sensor resistor's three layer construction (from: <http://www.steadlands.com/interlink/interlinkpages/fsr.htm>)[104]

2.7.5 Optic Fibre Sensor

Almost thirty years have passed since the study of optical fibre sensors began [105]. The advantages of optical fibre sensors over other sensors are that they are immune to electromagnetic interference, are light weight, allow multiplexing, do not require power source and are small in size. Optic fibre sensors are divided into three large groups, namely the intensity modulated, phase modulated and wavelength modulated sensors. Wavelength modulated sensors (chirped FBG sensors) have been reported to be used in the measurement in contact stresses on the tibiofemoral interface in artificial knees during surgery for alignment purposes [106]. No reports have been found on the usage of the intensity modulated and phase modulated sensors in force or pressure measurement in instrumented joints or direct measurement in the mammals' joints.

2.7.5.1 Intensity modulated sensors

The working principal of the intensity modulated sensors is basically to detect the variation of the intensity of light passing through the waveguide. There are three basic mechanisms used in the intensity modulated sensor, which are transmission, reflection and microbending.

For the transmissive sensor, the distance between two probes is measured. This method is normally related to the interruption of a light beam in a switch configuration. As the distance between the two probes increases axially or radially, the intensity of the transmitted spectrum reduces. Figure 12 shows the probes configuration for displacement sensing, whereas in Figure 12a, axial displacement is used and in Figure 12b, radial displacement is used. The response curve of the sensors is shown in Figure 12c, which follows a $1/r^2$ law where r is the distance. This technique can also be used as a force sensor with some modification. To increase the sensitivity of the sensor, the frustrated total internal reflection configuration can be used.

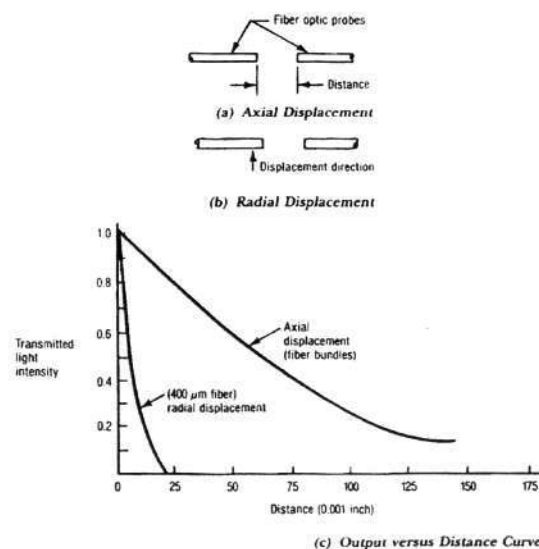


Figure 12: Transmissive sensor (from: Krohn, D.A., Fiber optic sensors : Fundamentals and Applications)[107]

Similarly for reflective sensor, displacement is measured. This sensor comprised of two bundles of fibres or a pair of single fibres. The first bundle of fibre transmits the light to a target and the other bundle traps the reflected light and transmits it to a detector. By observing the intensity of the reflected light, the distance between the

probe and the target can be determined. Figure 13a shows the sensor arrangement of this sensor and the probe configuration is shown in Figure 13b. The response curves for all probe configurations are shown in Figure 13c.

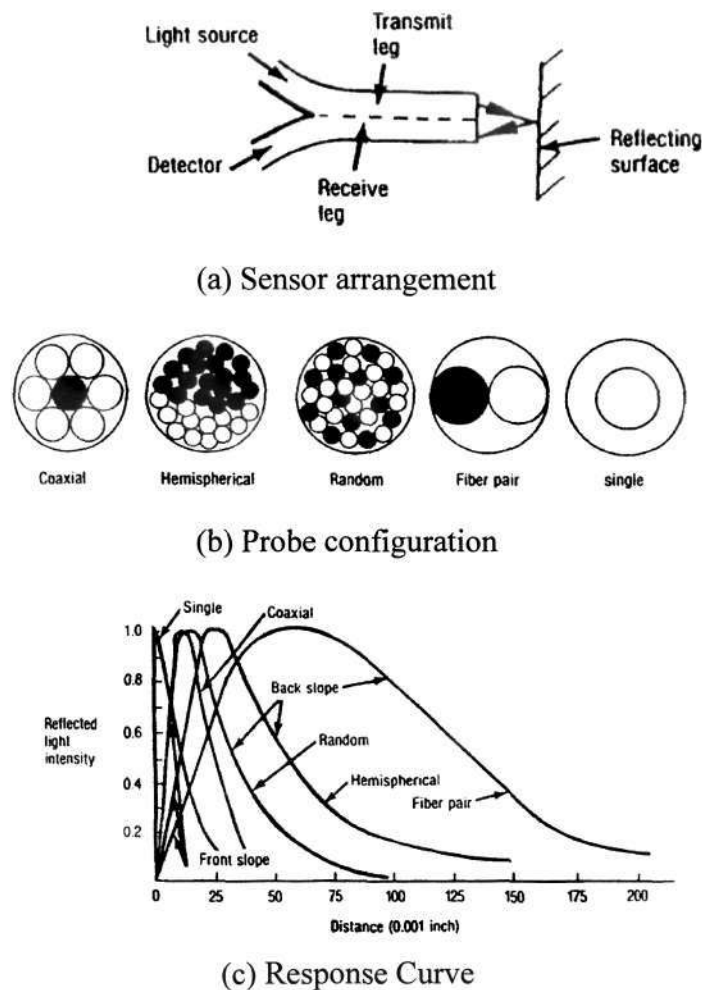


Figure 13: Reflective Sensor (from: Krohn, D.A., Fiber optic sensors : Fundamentals and Applications) [107]

The concept for microbending is simple, making it attractive to users. As a fibre bends, light is lost through the walls of the fibre, decreasing the output intensity. The sensor configuration is shown in Figure 14. Therefore, by monitoring the decrease in transmitted light intensity, the amount of displacement of the top part or the amount of the pressure exerted can be established.

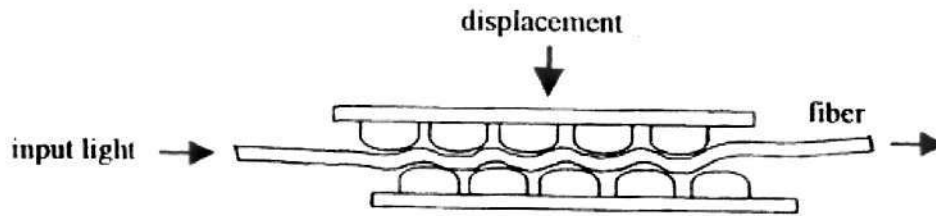


Figure 14: Microbending (from: Urbanczyk, W., Selected applications of fiber-optic sensors, *Proceedings of SPIE - The International Society for Optical Engineering*, 1999 3820 221-234.)[108]

To use transmissive and reflective sensors to measure forces or stresses, some adjustments have to be made. For example, a diaphragm can be used to convert stress or load into displacement which will be measured by the sensors. However, the complexity of the design for the transmissive and reflective sensors may require a larger space and therefore, is not advisable to be used in this application. Also, problems like losses have to be solved.

2.7.5.2 Phase modulated sensors

The working principle of phase modulated sensors involves the use of two single mode optic fibres and one coherent light source. The phase modulated sensor works by splitting the light source into the two fibres. One of the fibres acts as a sensing fibre while the other acts as a reference. As the environment perturbs the sensing fibre, a phase shift occurs relative to the reference fibre. Interferometers that can be used to detect the phase shift are the Mach-Zehnder, the Michelson, the Fabry-Perot and the Sagnac interferometer.

2.7.5.3 Wavelength modulated sensors

In wavelength modulated sensors, the information is encoded in the wavelength. This characteristic brings about the distinct advantage of having marked decrease in dependence of the light source intensity, giving more tolerance to losses due to transmission between connections.

The Fibre Bragg Grating (FBG) is in the family of wavelength-modulated sensors. In addition to the high tolerance to losses, another advantage of the FBG sensor for this

project is its small size. The gauge length of the sensor can be as small as 0.01mm. Force and pressure sensing are achieved through the relationship between strain and wavelength shift.

The basic characteristic of Bragg grating is the periodic modulation of the refractive index in the core of the optic fibre. It serves to filter out the Bragg wavelength which is dependent on the grating pitch and the effective refractive index. Fibre Bragg grating sensors measure the variation of the grating pitch and refractive index caused by environmental perturbations.

In order to fully utilize the concept, several profiles have been generated to obtain different capabilities. There are a few types of structures for Fibre Bragg gratings and the most commonly used profile is the uniform Bragg reflector. The other two profiles are the blazed Bragg grating and the chirped Bragg grating. The blazed Bragg grating has limited suitability for sensing applications; however, it is included for completeness.

The uniform Bragg reflector has the simplest structure, with uniform grating period and change in reflective index. This structure can be used to filter out some wavelength components from a broad band source and to construct a Fabry-Perot cavity. The first configuration is often used for sensing applications. The Fabry-Perot cavity consists of two Bragg reflectors. Basically, the input light will bounce back and forth between the two reflectors and produces a series of output pulses which are progressively smaller in amplitude. The Fabry-Perot cavity acts as a sensor and a tuning element.

The blazed Bragg gratings consist of gratings that are tilted at an angle to the fibre axis. This structure is important for communication purposes where several signals are used at different wavelengths to give a uniform signal-to-noise ratio at the output [109]. Recently, investigation of the usage of blazed grating as macro-bending sensors was also reported [110].

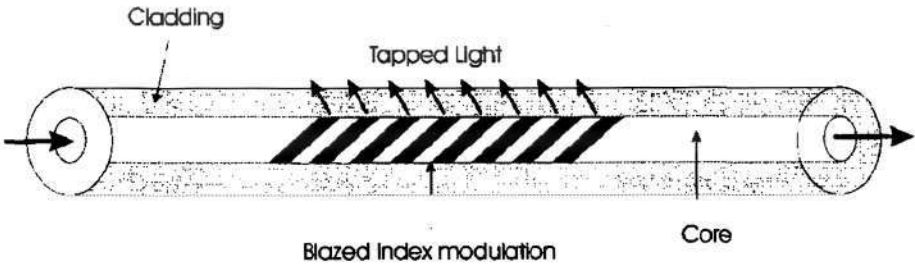


Figure 15: Blazed grating (from: Othonos, A., Fiber Bragg gratings, *Review of Scientific Instruments*.1997 68 (12): 4309-4341.) [111]

Chirped Bragg gratings are created by varying the period as shown in Figure 16. This particular structure has been used in instrumented tibial component in attempt to measure contact stresses for surgical alignment [106]. In this investigation, the chirped gratings act as multiplex of uniform gratings. By observing which of the spectra have shifted and the magnitude of shift, the location of the load and the magnitude of the load can be identified. The sensor is in the form of one whole sheet with arrays of sensing points, behaving somewhat like the Tekscan’s sensor series described in section 2.7.4.

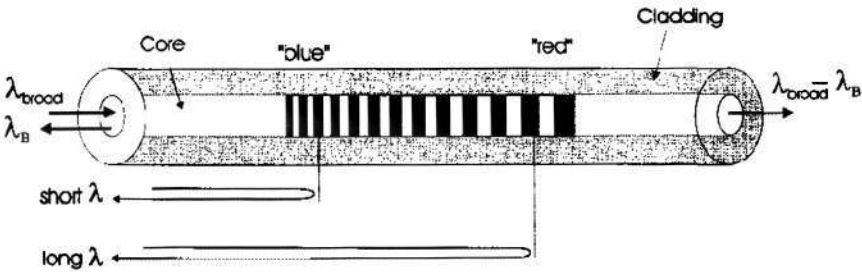


Figure 16: Chirped grating with aperiodic pitch (from: Othonos, A., Fiber Bragg gratings, *Review of Scientific Instruments*.1997 68 (12): 4309-4341.) [111]

3.0 MATERIAL

3.1 Specimen

3.1.1 Specimen selection

A criterion for test specimen is that it must be handled easily, with low possibility of contamination and easy to obtain. As human knee joint is difficult to obtain in Singapore, usage of animal specimens was recommended for the experiment. Apes and bears have knee joints that are very similar to the human knee joints [112]. But these specimens are difficult to obtain.

For the experiments, the knee joint must not be too small, ruling out dog (canine), cat (feline), rabbit (lapine), goat and sheep (ovine) knee joints. As the experiments require manual force application on the joint, big knee joint size is also undesirable. Therefore, ruling out cattle (bovine) and horse (equine) knee joint [112]. Another criterion for the experiment is that the meniscus must be thick and this rules out elephant, hippo and rhino knee joint [113]. Animals with thick meniscus are typically, hoofed and carnivorous animals [113]. Porcine knee joints were selected due to its intermediate size, availability and their thick meniscus.

3.1.2 Specimen Preparation

Porcine knee specimens were obtained from the wet market a few days before the experiments. The specimens were cleaned up and dissected, leaving the mechanically essential structures, which includes the femur, tibia, collateral ligaments, cruciate ligaments, transverse ligament, meniscomfemoral ligaments and the meniscotibial ligaments. The joint capsule was removed to prevent interference with the insertion of the sensor. As the joint capsule is at close proximity to the ligaments, especially the medial collateral ligament, the extraction of the capsule was undertaken with care. The specimens were then deep frozen for the experiments.

Before the experiment, the specimen was thawed and perforations were made on the femur and tibia bones for attachment and fixation purposes. At the start of the experiment, the cuts were made in the six key locations of the meniscus, namely the medial-anterior (MA), medial-central (MC), medial-posterior (MP), lateral-anterior (LA), lateral-central (LC) and lateral-posterior (LP). The cuts of 5mm wide by 6-7mm

deep were made precisely using scalpel to accommodate the sensor. The locations of the cut are shown in Figure 17.

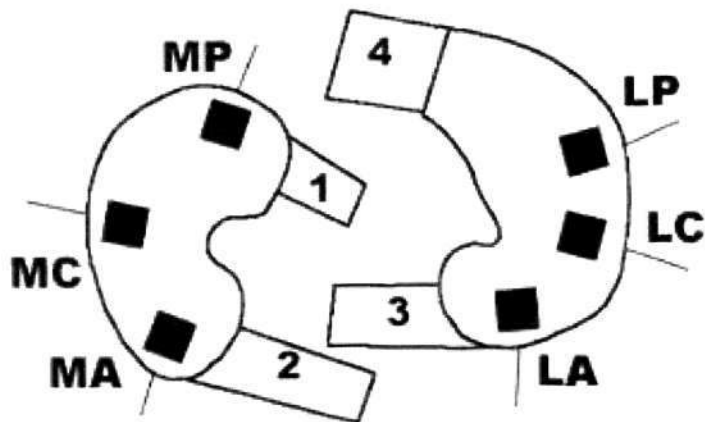


Figure 17: Locations of sensor within the meniscus

3.2 Sensor System

The sensor chosen to measure intrameniscal forces is the pressure conductive sensor (Inastomer sensor from Inaba Rubber Co, Japan) (Figure 18). The reason for the choice over the other sensors is their small size, sensitivity in force measurement and low temperature sensitivity. The disadvantage of the sensor is that it can be damaged by the wet environment within the meniscus. Therefore, a plastic jacket was used to protect the sensor. The overall dimensions of the pressure conductive sensor with the plastic jacket are 5mm by 5mm, with 1mm thickness.

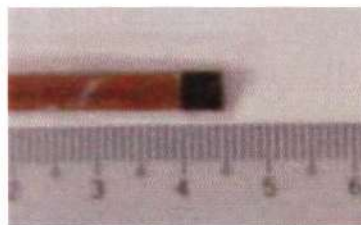


Figure 18: The Pressure conductive sensor

The sensor consists of a composite material where the conductive particles are embedded into rubber material. As pressure is applied on the composite, the conductive particles begin to form conductive pathways, thus causing a reduction in electrical resistance of the material. The specifications sheet of the pressure conductive sensor is included in Appendix A. As the specification sheet is written in Japanese, a short English description is also included.

For the dynamic measurement of variation of intrameniscal force with respect to the change in extension-flexion and internal-external rotation, the applied moment on the joint and the angles of the joint needed to be determined. The sensor systems chosen were the pressure conductive sensor system, piezoelectric sensor system (Three components Force link, Kistler 9317, Switzerland), goniometer and torsiometer system (Biometrics, United Kingdom). Pressure conductive sensors were used to obtain the intrameniscal forces; the piezoelectric sensor was used to determine the applied moment; goniometer and torsiometer were used to measure the joint angle.

The pressure conductive sensor was interfaced with its custom datalogger for data acquisition. However, to synchronize the data between the sensor systems, a new method of data acquisition needed to be found. In order to use the same data acquisition system for the piezoelectric sensor, a signal conditioning board (SCB) (Dewetron, Austria) was selected. As there was no existing SCB which matched the specifications required for the pressure conductive sensor, the SCB had to be custom made. Measuring range of the SCB is from 100 Ω to 1M Ω with operation temperature range from -5°C to 60°C. The accuracy of the SCB is $\pm 0.1\%$. The pressure conductive sensor was connected to the SCB through 9-pin SUB-D connector. One SCB can only be used with one sensor at a time; therefore, the experiments were conducted by measuring one sensing location at one time. The datalogging setup for the pressure conductive sensor is shown in Figure 19. The program used for both the pressure conductive sensor and the piezoelectric sensor was the DasyLab program (Dewetron, Austria).

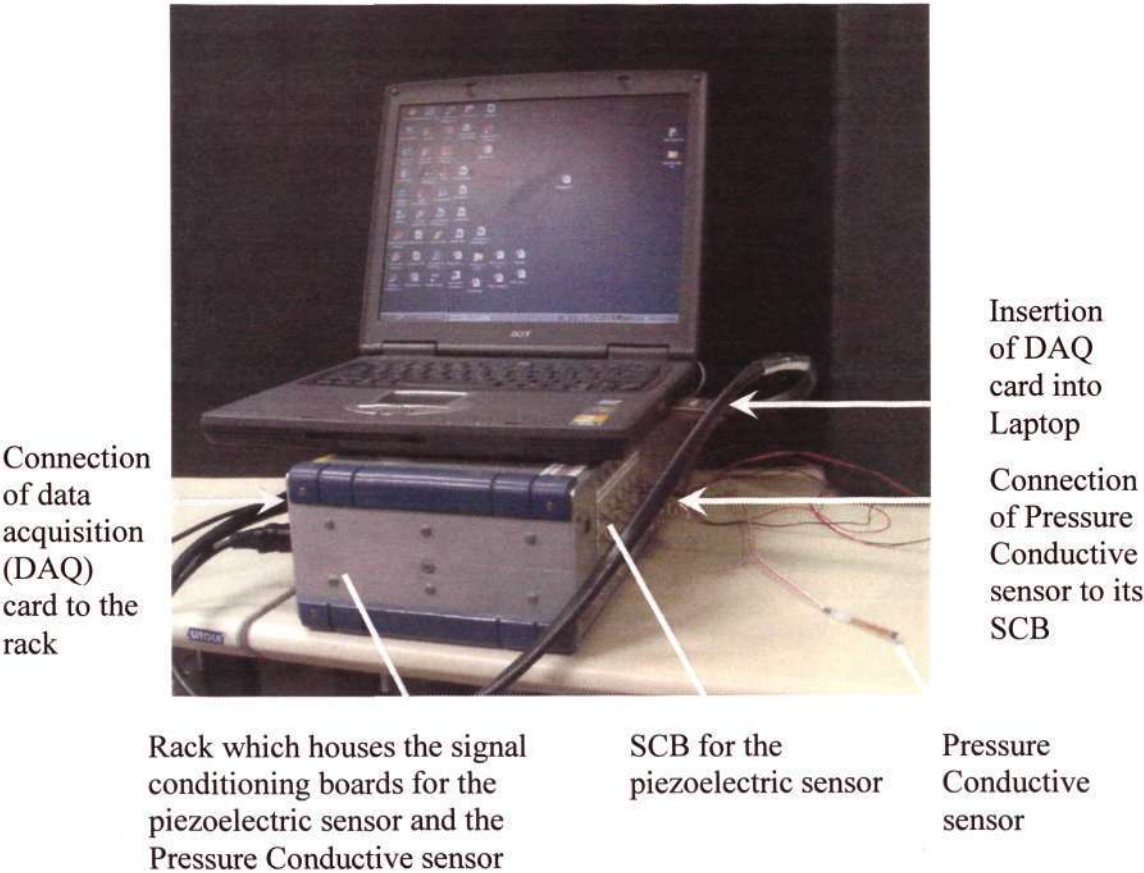


Figure 19: Data logging set up for Pressure Conductive sensor

The goniometer and torsiometer formed another sensor system as they were connected using the same datalogger. To synchronise the goniometer and torsiometer sensor system (sensor system 1) and the piezoelectric sensor and pressure conductive sensor system (sensor system 2), a force sensing resistor sensor was included. The force sensing resistor sensor was connected to the datalogger for the goniometer and torsiometer (Figure 20) and the sensing end was attached to the piezoelectric sensor. By tapping on the piezoelectric sensor before each experiment, both the force sensing resistor sensor and the piezoelectric sensor provided force spike signals. These signals were used to synchronise the test data (intrameniscal force, applied force, angle) after the experiments.

The program used for the goniometer, torsiometer and force sensing resistor sensor system was the DataLog Analysis Software program.



Figure 20: The Goniometer, Torsiometer and the Force sensing resistor sensor system

The connection for the sensor systems is shown in Figure 21.

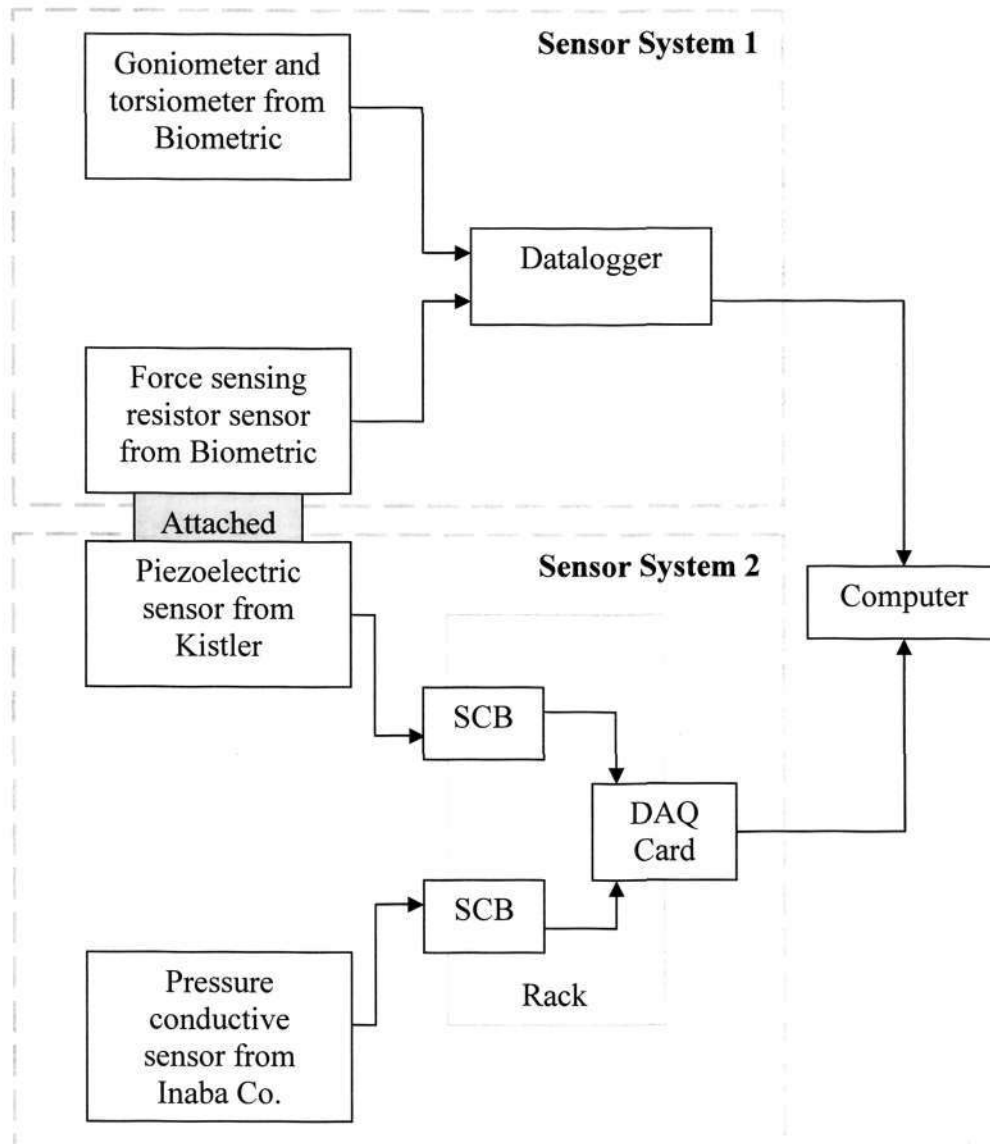


Figure 21: Schematic for sensors systems connection

3.2.1 Calibration of Pressure Conductive sensor

Calibrations were conducted on the sensor in the protective jacket, on an Instron machine (model 3366 in Biomedical Engineering Research Centre, Nanyang Technological University).

The load applied on the sensor by the Instron machine and the resistance of the pressure conductive sensor was recorded. The Instron machine force plate was tapped at the end of each calibration, to provide a spike in the load and resistance data for synchronisation. Ten calibrations were conducted before each experiment. The force vs. resistance calibration graph is shown in Figure 22. Data of ten calibrations were

plotted and the best fit was found. The green curve is the hyperbolic fit, the red curve is the power fit and the blue curve is the combined hyperbolic and power fit. Blue curve is the best fit and the equation was keyed into the DasyLab program for the pressure conductive sensor to obtain the force readings during the experiment.

The equation for the blue curve is:

$$F=0.7\left(\frac{2213.166277}{(R+28.24740814)}+2.163173172\right)+0.3\left(112.7355487R^{-0.4415743657}\right)$$

where,

F: force

R: Resistance

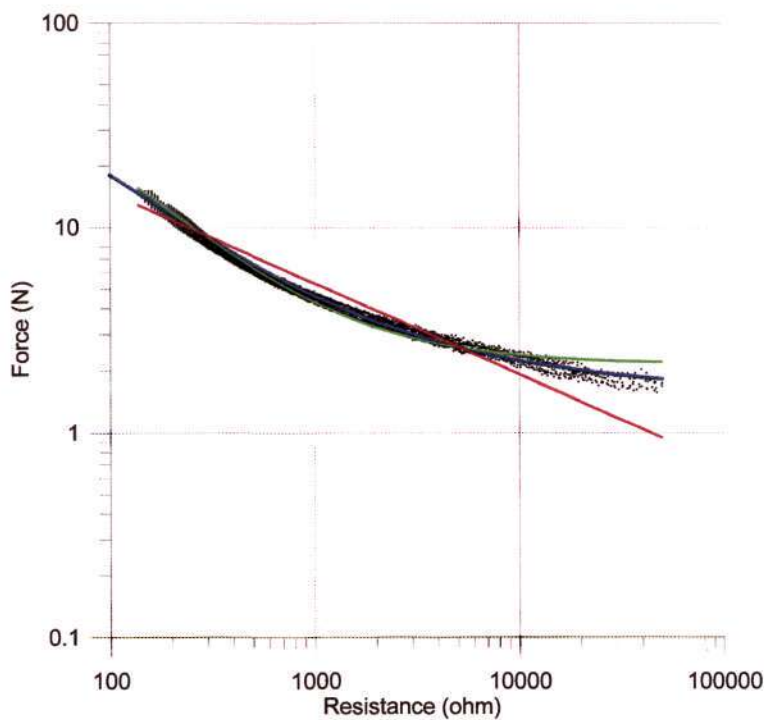


Figure 22: Pressure conductive sensor calibration curve

After each experiment, the sensor was calibrated again to ensure that the calibration curve remained unchanged.

4.0 EXPERIMENTS

4.1 Dynamic Experiment- Variation of intrameniscal stress with extension-flexion angles, internal external rotation angles and torque applied

4.1.1 Methodology

Two right and three left porcine knee specimens were utilised for the dynamic experiments.

For each experiment, the material preparation was followed by the fixation of the goniometer. The datalogger of the goniometer was first connected to the computer to make simple adjustments per channel for gain, power supply, sampling frequency and datum settings. The twin axis goniometer was connected across the joint at the side and the interconnect lead was used to attached the sensor to the input socket of the datalogger. The single axis torsionmeter was connected anteriorly across the joint during the second part of the experiment for the measurement of the internal-external rotation angle.

Next, the thin and robust force sensing resistor sensor was attached to the top of the piezoelectric sensor to provide force spike signal for synchronisation. The force sensing resistor sensor was connected to the same datalogger for the goniometer and torsionmeter (Figure 20).

Subsequently, piezoelectric sensor was fastened to the femur bone. It was taped to the anterior side of the femur with the z-direction of the sensor perpendicular to the femur for the extension-flexion experiment. The alignment was done using the tibia protrusion and it was made sure that there was no sliding movement between the sensor and the bone. The moment arm was set to be 0.125m and positive force was set to be bearing down on the femur, causing flexion motion. For the internal-external rotational experiment, the piezoelectric sensor was fastened at the lateral side of the femur. Similarly, positive force was set to be perpendicular and towards the femur.

Therefore, positive application of force on the femur caused the tibia to rotate internally.

Specimen with the goniometer, force sensing resistor sensor and piezoelectric sensor is shown in Figure 23. Location of the torsionmeter is also indicated in Figure 23. The connections of sensor systems are shown in Figure 21.

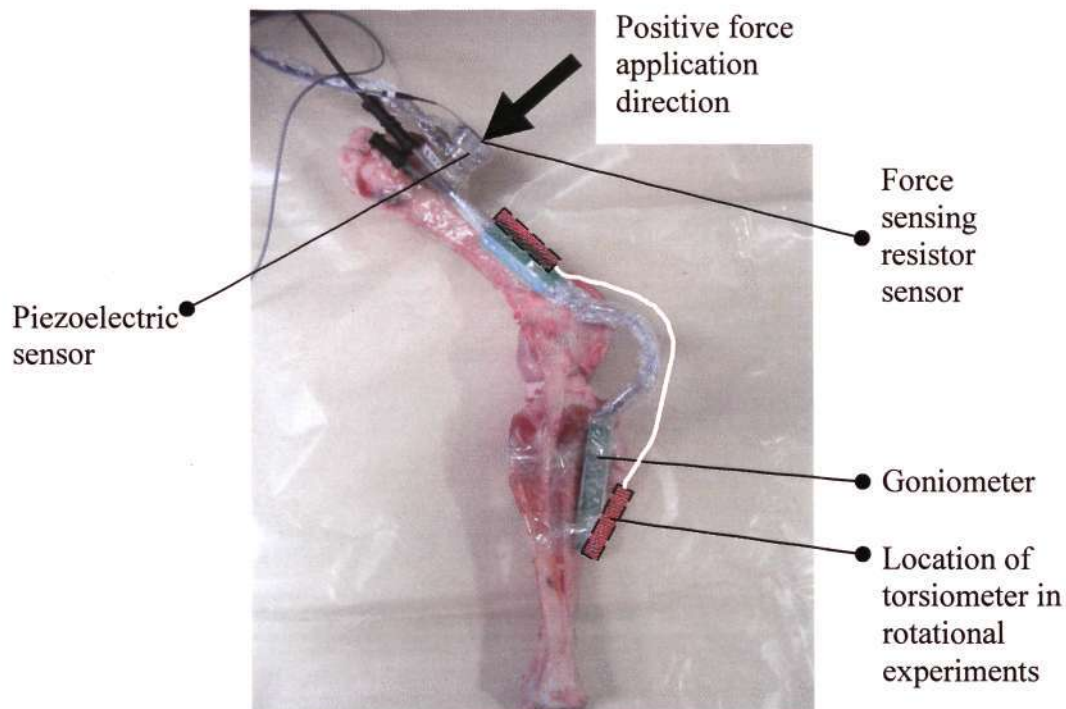


Figure 23: Specimen with the goniometer, force sensing resistor sensor and piezoelectric sensor with indication of the location of torsionmeter in rotational experiments

At each time, only one meniscal location was investigated with one pressure conductive sensor. The pressure conductive sensor was inserted into one of the locations of interest, where cuts were previously made (Figure 17). The insertion of the sensor is shown in Figure 24.



Figure 24: Insertion of the pressure conductive sensor

For the experiment, the specimen was mounted on a custom-made structure where the tibia was fixed and made immobile. The structure is shown in Figure 25.

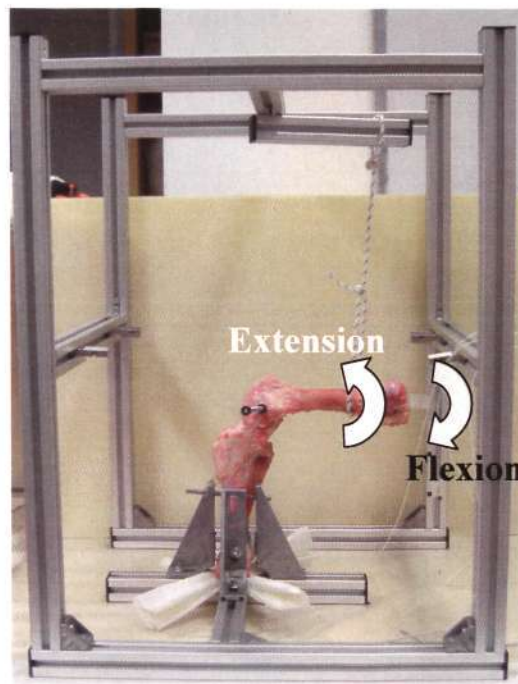


Figure 25: Structure to constrain the tibia bone (sensor systems not displayed) and extension-flexion movement of the knee specimen

The goniometer was zeroed at maximum extension of the joint. By tapping on the force sensing resistor sensor attached on the piezoelectric sensor, shock spike signal will be produced by both sensors, marking the start of the experiment. Force was exerted through the piezoelectric sensor to reproduce extension-flexion movement of the knee. Extension-flexion movement of specimen is shown in Figure 25.

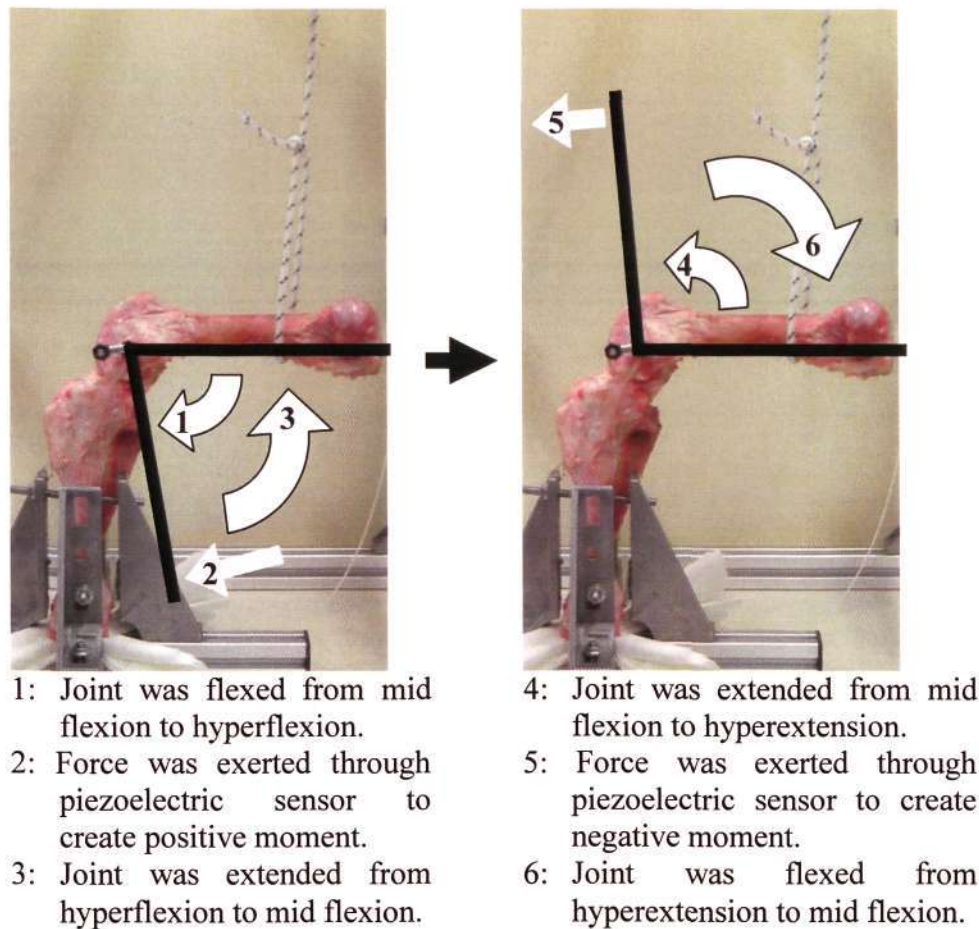


Figure 26: One cycle in the Extension-Flexion experiment

One cycle in the extension-flexion experiment is shown in Figure 26. The cycle started with the porcine knee specimen in mid flexion position. The specimen was then made to flex until hyperflexion was achieved, where force was applied through the piezoelectric sensor. During hyperflexion, positive moment was exerted on the joint as the piezoelectric sensor was attached at the anterior side of the femur, such that positive force was towards the bone (Figure 23). The specimen was subsequently extended until hyperextension was achieved, where negative moment will be applied to the joint. The cycle ended when the specimen was returned to mid flexion position. Special note was taken at hyperextension and hyperflexion.

Five cycles were carried out for each meniscal location and the process was repeated for all six locations in the menisci of each specimen.

The experiment was repeated for internal-external rotation at mid-flexion. The torsionmeter was zeroed at the free hanging angle of the porcine knee specimen at mid flexion. The free hanging angle was obtained by positioning the femur bone so that its long axis was horizontal, with no constraint placed on the tibia bone. The torsionmeter was set to zero at this position. Internal-external rotation of the porcine knee joint specimen is shown in Figure 27.

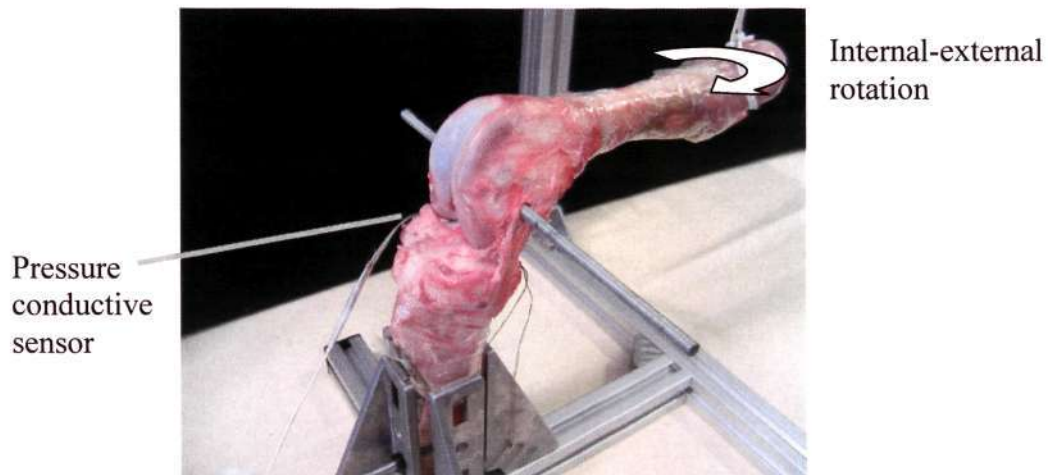
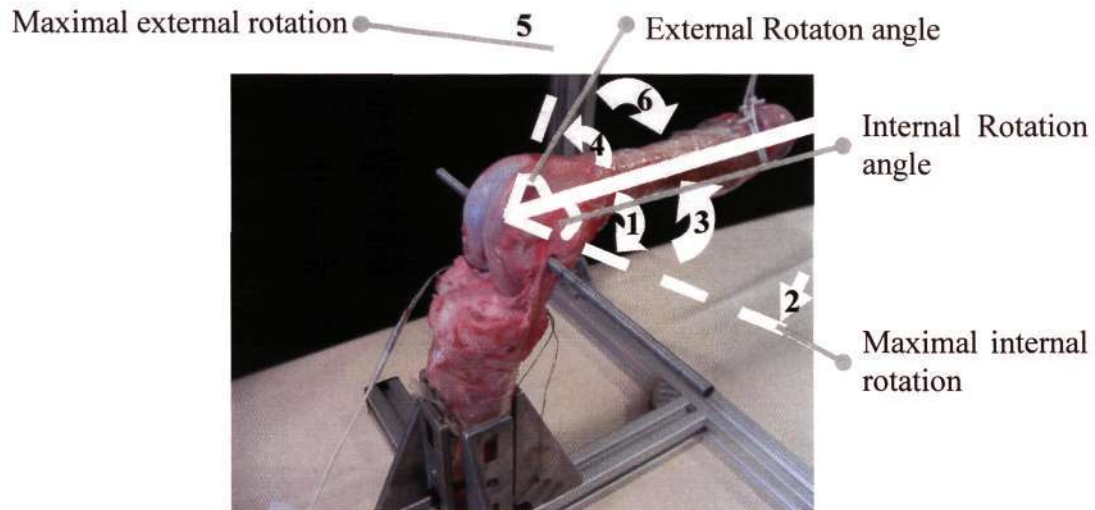


Figure 27: Internal-external rotation of the porcine knee joint specimen (sensor systems not displayed)

Similarly, the shock spike signals were created at the start of the experiment. One cycle in the extension-flexion experiment is shown in Figure 28.



- 1: Joint was internally rotated to maximal rotation.
- 2: Positive moment was applied through the piezoelectric sensor.
- 3: Joint was returned to free hanging angle at mid flexion.
- 4: Joint was externally rotated to maximal rotation.
- 5: negative moment was applied through the piezoelectric sensor.
- 6: Joint was returned to free hanging angle at mid flexion.

Figure 28: One cycle in the Internal-External Rotation experiment

The cycle started with the specimen in mid flexion, free hanging angle. The specimen was then slowly internally rotated, till maximal rotation. Maximal rotations are indicated in Figure 28 by the dotted lines. Positive moment was applied through the piezoelectric sensor. Next, the specimen was externally rotated and negative moment was applied at maximal angle. Five cycles were carried out for each location and the process was repeated for all six locations of the meniscus.

It must be noted that phosphate buffer solution (Sigma, St. Louis, Missouri) was dripped onto the joint at regular intervals to maintain the water content.

After all measurements were taken, the collateral ligaments, cruciate ligaments, all the meniscomfemoral and meniscotibial attachments were bisected. The sensor insertion locations in the menisci were checked to ensure that the pressure conductive sensor was well embedded inside the menisci during experiment.

Figure 29 shows the menisci after the bisection of all the ligaments, meniscomfemoral attachments and meniscotibial attachments. The meniscomfemoral interface is shown in Figure 29a and the meniscotibial interface is shown in Figure 29b. From Figure 29, it can be seen that the sensors were well embedded within the menisci.

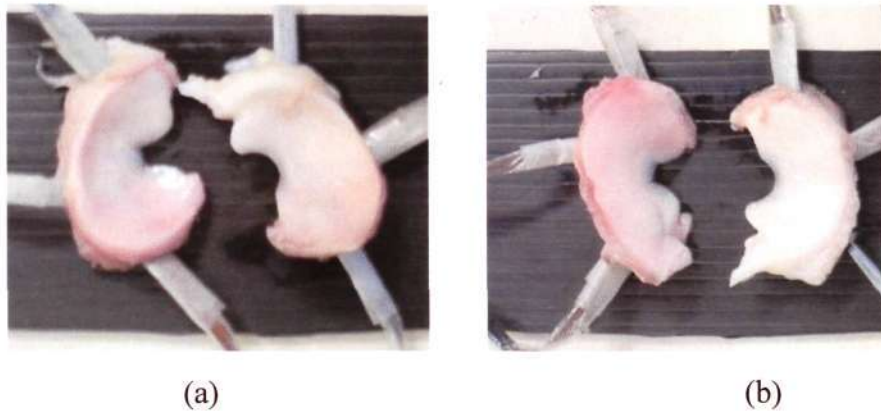


Figure 29: Removed menisci
(a) Meniscomfemoral interface
(b) Meniscotibial interface

4.1.2 Results for extension-flexion experiments

From the calibration graph, intrameniscal forces of the porcine knee joint during extension-flexion of the joint were obtained. The intrameniscal forces were then divided by the constant sensing area of the pressure conductive sensor to acquire the intrameniscal stresses. The results are shown in Figure 30, Figure 31, Figure 32 and Figure 33.

A typical cycle for each location in the menisci is presented in Figure 30 to represent the variation of intrameniscal stress, applied moment and extension-flexion angle with time. The intrameniscal stress is represented by the red curve, the applied moment is represented by the black curve and the joint angle is represented by the green curve. The angle axis is not shown, the intrameniscal stress axis is on the left and the moment axis is on the right.

Each graph represents one location in the menisci, which is stated in the graph title. The locations are shown in Figure 17. Maximum flexion represents the knee position where the biggest angle is shown on the goniometer. Hyperflexion is the state of the knee joint where the moment started to increase. Maximum extension represents the knee position where the smallest angle is shown on the goniometer. Hyperextension is the state of the knee joint where the absolute moment started to increase. Hyperflexion and hyperextension sections are indicated in graph for lateral-anterior region in Figure 30.

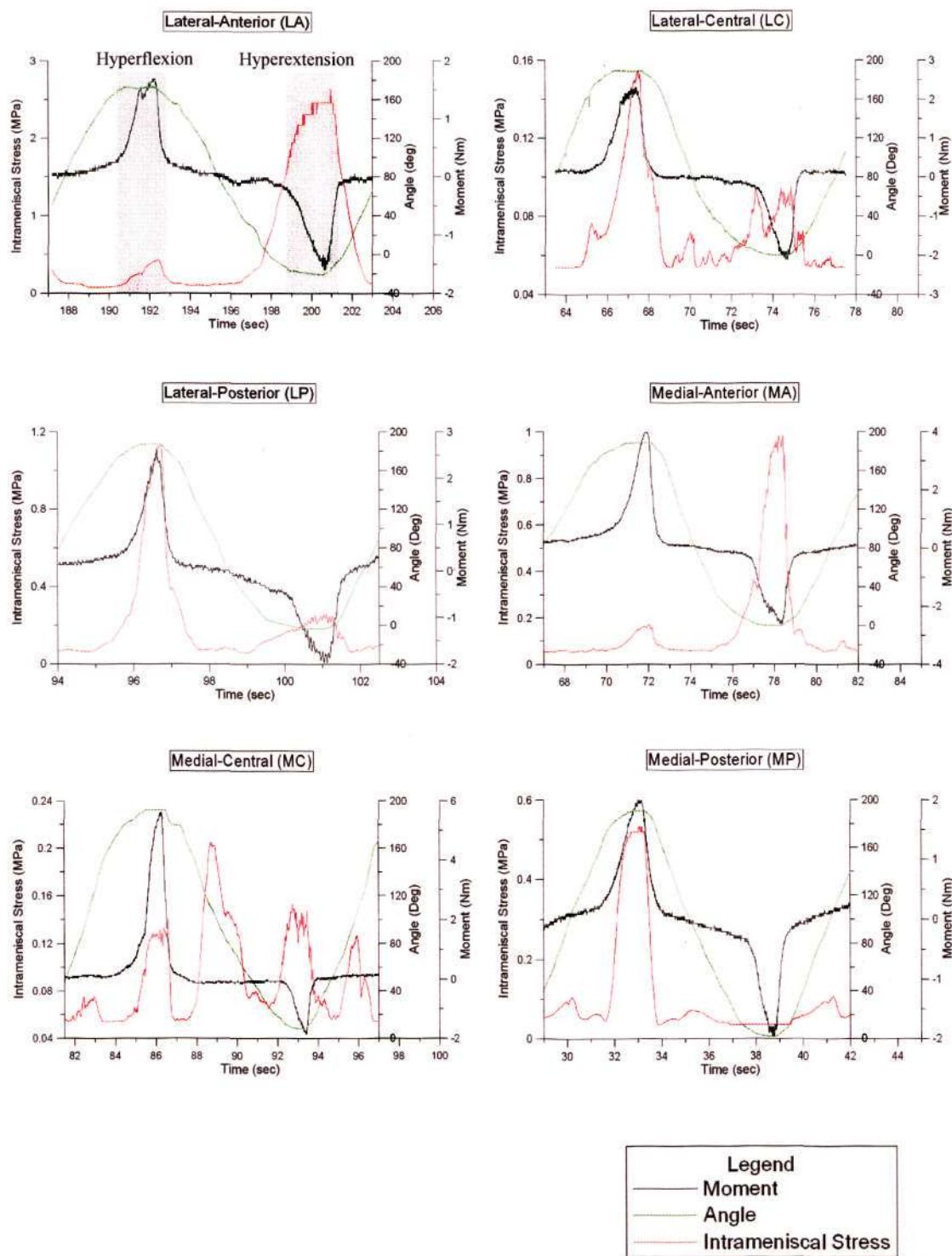


Figure 30: Intrameniscal stress, applied moment and angle vs. time graphs for extension-flexion experiment

From Figure 30, the shift of knee position from mid flexion to hyperflexion to mid flexion to hyperextension back to mid flexion can be traced. The positive applied moment was applied at hyperflexion and negative applied moment at hyperextension.

From Figure 30, the variation of intrameniscal stress with time can be observed. The intrameniscal stress behaviour in lateral-central, medial-central and medial-posterior regions are of interest. It can be seen that there are some stress peaks between terminal positions. The highest peak stress for the medial central location (shown in Figure 30), occurred when the knee specimen was being extended from a flexed knee position.

Five experiments were conducted, one for each specimen. To compare the results for each specimen, intrameniscal stress and moment vs. normalised angle graphs for all the experiments are shown in Figure 31. Each graph represents one location in the menisci, which is stated in the graph title. The locations are shown in Figure 17. In each graph, only one typical cycle is presented for each experiment for neatness. The resultant graphs are colour-coded with black curves representing the first experiment and red curves representing the second experiment as shown in the legend. The upper curves represent the moment vs. normalised angle graphs while the lower curves represent the intrameniscal stress vs. the normalised angle graphs.

Full range extension-flexion angle = measured maximum flexion angle – measured maximum extension angle.

The normalised angle was obtained using:

$$\text{Normalised angle} = \frac{\text{Measured angle} - \text{measured maximum extension angle}}{\text{Full range extension-flexion angle}}$$

The full range extension-flexion angle ranges from 188 degrees to 208 degrees for the 5 specimens. Average of the full range extension-flexion angle is 194 degrees.

Hyperextension ranged from normalised angle of 0 to 0.05 while hyper-flexion ranged from normalised angle of 0.95 to 1. Applied moment for hyperextension is negative while the applied moment for hyperflexion is positive due to the direction of force application.

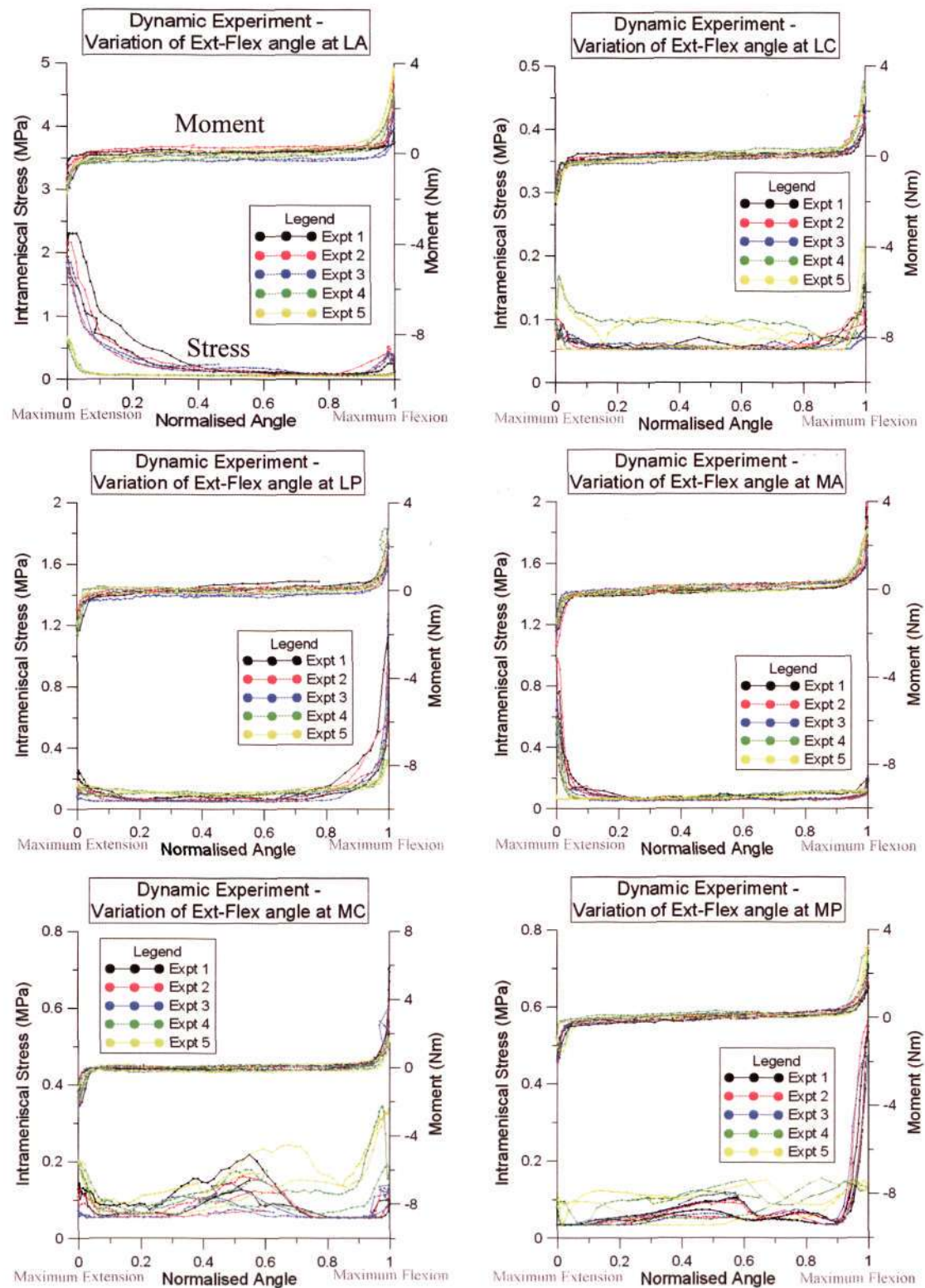
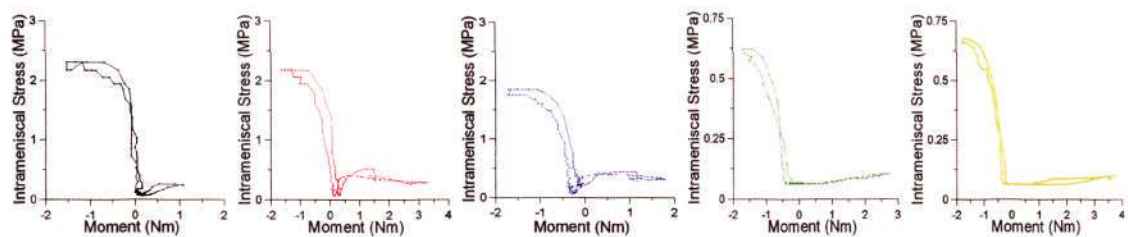


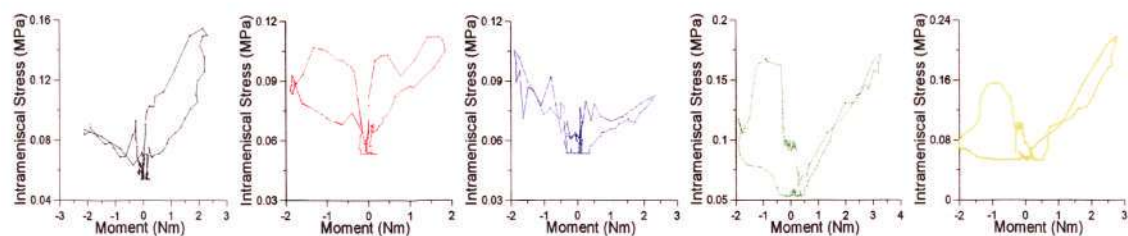
Figure 31: Graphs of Intrameniscal Stress and Moment vs. Normalised angle during extension-flexion motion at each position with the moment curve on top of the intrameniscal stress curve. Zero normalised angle representing hyperextension.

From the graphs, the intrameniscal stress in the lateral-anterior region is higher in hyperextension than in hyperflexion. Experiments 4 and 5 yielded lower intrameniscal stress as compared with the rest of the results at the two extreme positions. At the lateral-central region, the difference in intrameniscal stress experienced during hyperextension and hyperflexion is small. Lateral-posterior region experienced higher intrameniscal stress at hyperflexion as compared to hyperextension. The trend is reversed for the medial-anterior region. The variation of intrameniscal stress of medial-anterior region is similar to that of the lateral-anterior region. The results for lateral-central, medial-central and medial-posterior regions are unique due to the increase in the intrameniscal stress at the middle of an extension-flexion cycle. This behaviour is obvious at the medial-central region, where there is a peak in intrameniscal stress at mid-flexion. At the medial-posterior region, higher intrameniscal stress was experienced during hyperflexion as compared to hyperextension of the knee joint.

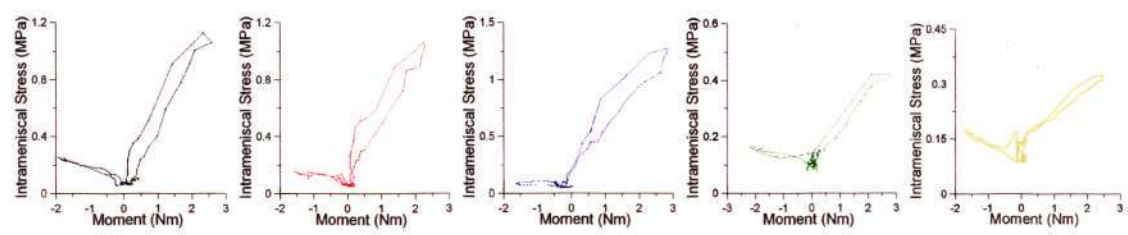
The graphs of intrameniscal stress vs. moment are presented in Figure 32 for all locations and experiments conducted. Likewise, only one typical cycle was chosen to represent each experiment. The graphs are similarly colour-coded, where black represents the first experiment, red representing the second experiment, blue representing the third experiment, green representing the fourth experiment and yellow representing the fifth experiment.



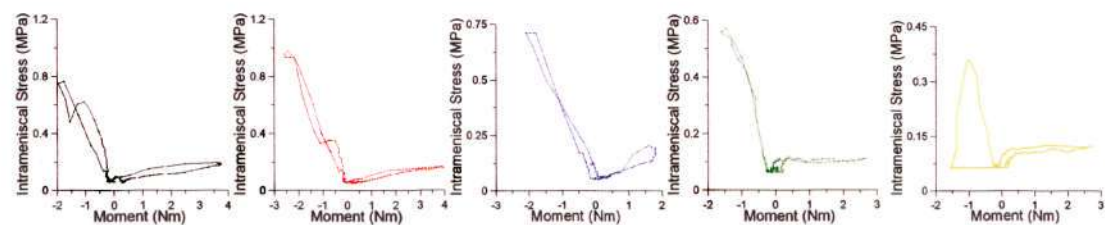
Intrameniscal stress vs. Moment during extension-flexion at LA- experiment 1 to 5



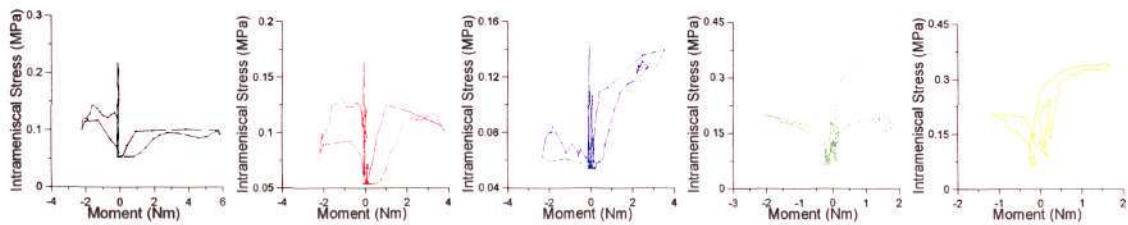
Intrameniscal stress vs. Moment during extension-flexion at LC- experiment 1 to 5



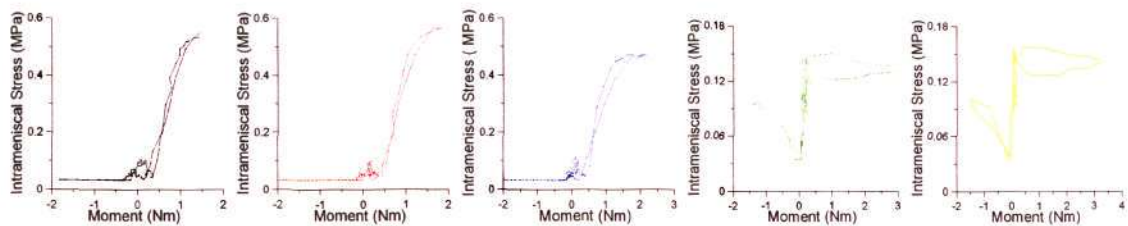
Intrameniscal stress vs. Moment during extension-flexion at LP- experiment 1 to 5



Intrameniscal stress vs. Moment during extension-flexion at MA- experiment 1 to 5



Intrameniscal stress vs. Moment during extension-flexion at MC- experiment 1 to 5



Intrameniscal stress vs. Moment during extension-flexion at MP- experiment 1 to 5

Figure 32: Graph of intrameniscal stress vs. applied moment for extension-flexion experiment for each location and experiment.

From the results, it can be seen that there are loops in the intrameniscal stress vs. moment curve. The curves are similar for all the five experiments at lateral-anterior, lateral-posterior and medial-anterior regions.

There are some variations in the trend of the curves for the lateral-central, medial-central and medial-posterior regions. From Figure 32, it can be observed that for the lateral-central, medial-central and medial-posterior regions, there are increases in intrameniscal stresses when the applied moment is near zero. This means that there is an increase in intrameniscal stresses when little or no moment has been applied to the knee joint. Note that hyperflexion and hyperextension starts when there is moment applied to the knee joint. This indicates that intrameniscal stresses can increase when the joint is not in hyperflexion or hyperextension. This behaviour is also reflected in Figure 30 and Figure 31 where the graphs show an increase in intrameniscal stress when the joint extension-flexion motion was at mid-cycle and the joint was not at any terminal positions.

As the intrameniscal stress is dependent on the corresponding applied moment on the specimen, the ratio of the maximum intrameniscal stress and the corresponding applied moment is required for comparison between meniscal locations at different knee positions.

There are two terminal knee positions (hyperextension and hyperflexion) for each meniscal location. At each of these points, the stress-moment ratio was calculated. The equation used is:

Ratio=
$$\frac{\text{Maximum intrameniscal stress at terminal knee position at each meniscal location}}{\text{Corresponding Applied moment}}$$

The mean ratio at each of these points was then obtained by averaging the corresponding stress-moment ratios of the five specimens. The standard deviation of the ratios of the five specimens was then calculated.

The chart representing the mean and standard deviation of intrameniscal stress-moment ratio at each meniscal location, at hyperextension and hyperflexion is shown in Figure 33.

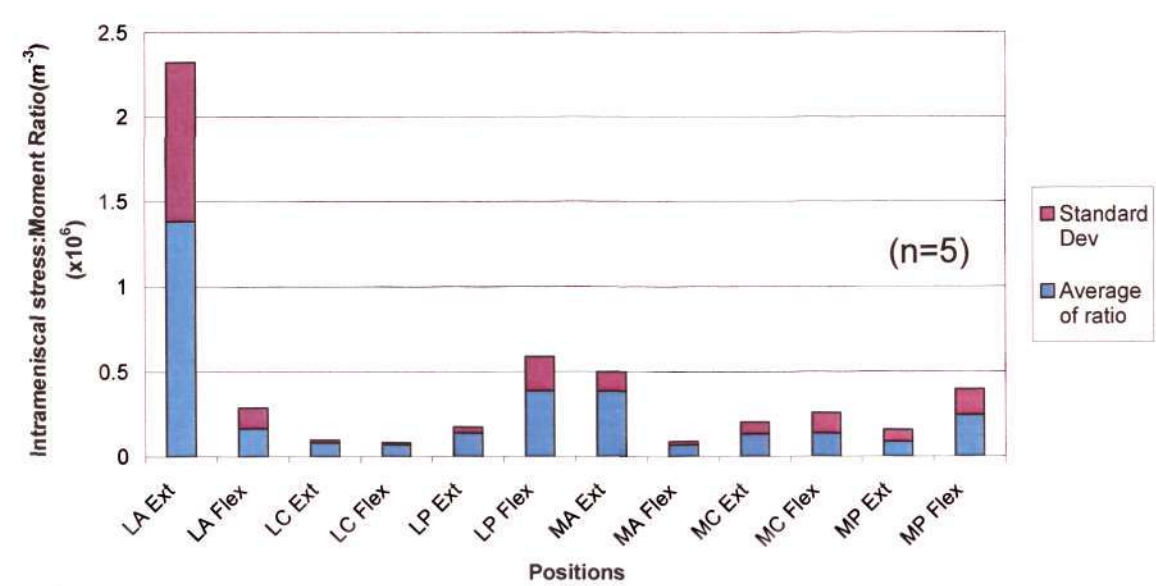


Figure 33: Graph of Intrameniscal stress- Moment ratio at different locations within the menisci, at extreme knee positions in the extension-flexion experiments

From Figure 33, intrameniscal stress-moment ratio at lateral-anterior region during hyperextension of the knee joint is much higher than the stress-moment ratio experienced in the rest of the locations at their terminal joint positions. The mean value of intrameniscal stress-moment ratio at lateral-anterior region at hyperextension is $1.4 \times 10^6 \text{m}^{-3}$. During hyperflexion, the region in the porcine knee menisci that withstood the highest stress-moment ratio is lateral-posterior, follow by the medial-posterior region.

From the results, it can be concluded that highest intrameniscal stress occurs at hyperextension and hyperflexion of the joint, with highest stress at lateral-anterior region during hyperextension and at lateral-posterior and medial-posterior regions during hyperflexion.

4.1.3 Results for Internal-external rotation experiments

The results for the dynamic experiment studying the variation of intrameniscal stress during internal-external rotation of the porcine knee joint at mid-flexion are shown in Figure 34, Figure 35, Figure 36 and Figure 37. The intrameniscal stresses were obtained by dividing the intrameniscal forces by the sensing area.

A typical cycle for each location in the menisci is presented in Figure 34 to represent the variation of intrameniscal stress, applied moment and internal-external rotation angle with time. The intrameniscal stress is represented by the red curve, the applied moment is represented by the black curve and the joint angle is represented by the green curve. Each graph represents one location in the menisci, which is stated in the graph title. The locations are shown in Figure 17.

Internal rotation and external rotation sections are indicated in the graph for lateral-anterior region in Figure 34.

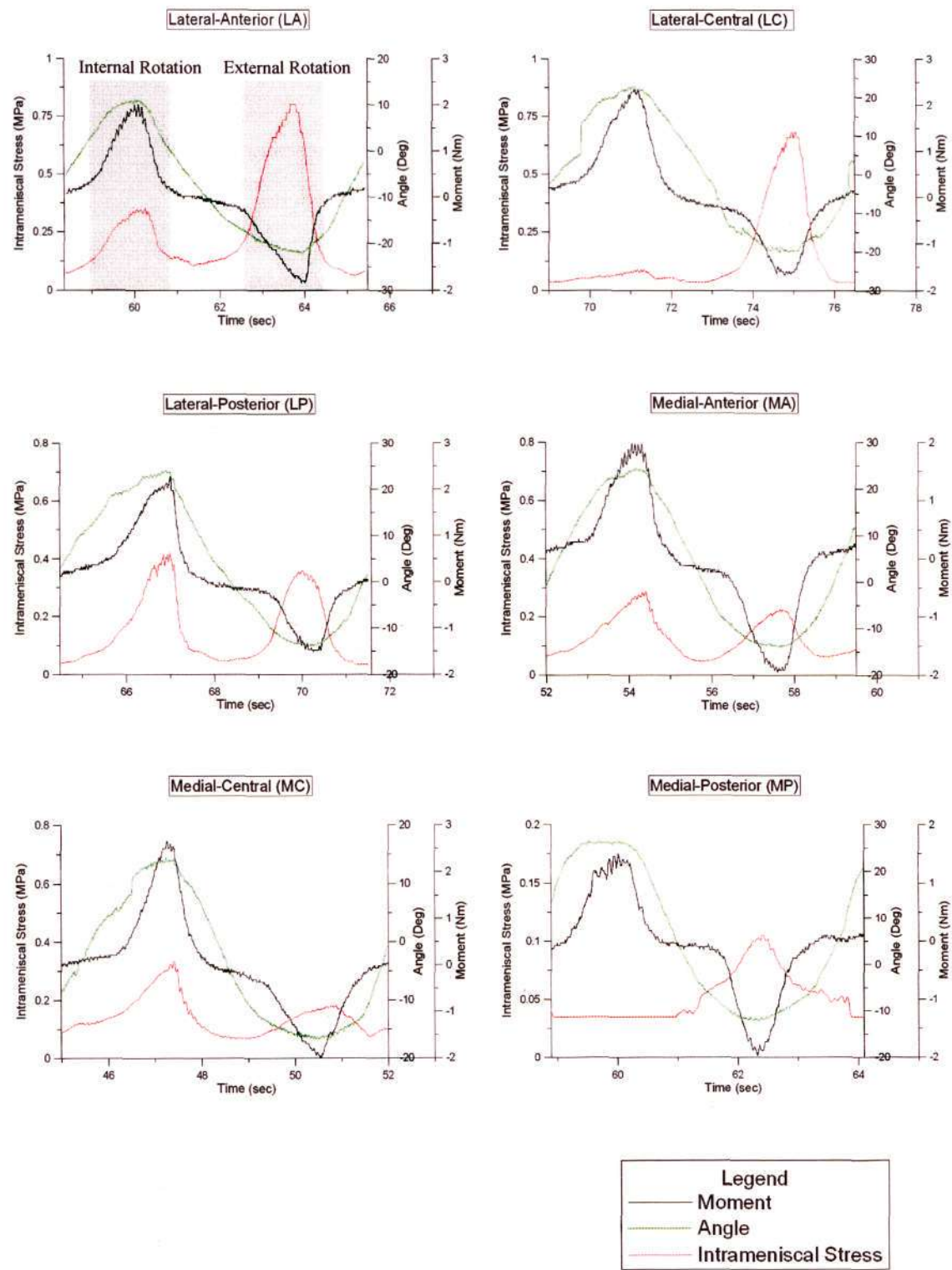


Figure 34: Intrameniscal stress, applied moment and angle vs. time graphs for internal-external rotation experiment

From Figure 34, the shift of knee position from free hanging to internal rotation to free hanging to external rotation back to free hanging position can be traced. The positive applied moment was applied at maximum internal rotation and negative applied moment at maximum external rotation.

Meniscal injuries often occur at internally/externally rotated knee joint. The peaking of stress at maximum moment is what was anticipated since maximum moment implied that maximum force was applied to the joint. However, from the graphs, it can be observed that the intrameniscal stress peak occurs slightly before the peak of applied moment at lateral-anterior and lateral-posterior regions during external rotation of the knee joint. Peak stress occurs slightly after the peak moment at lateral-central and medial-central regions during external rotation of the knee joint.

Five experiments were conducted, one for each of the five specimens. To compare the results for each specimen, intrameniscal stress and moment vs. normalised angle graphs for all the experiments are shown in Figure 35.

In each graph (representing one meniscal location), five curves are shown for the five experiments. The locations are shown in Figure 17. In each graph, only one typical cycle is presented for each experiment for neatness. The results are colour coordinated with black curves representing one typical cycle from the first experiment and red curves representing one cycle from second experiment as shown in the legend. The curves on top represent the applied moment vs. normalised angle graphs while the curves below represent the intrameniscal stress vs. the normalised angle graphs.

Maximum internal rotation angle is represented by +1 while maximum external rotation angle is represented by -1. Normalised angle is zero at the free hanging angle of the knee specimen at mid-flexion as described in section 4.1.1.

Normalised angles were obtained by:

$$\text{External rotation normalised angle} = \frac{\text{External rotation angle}}{\text{Maximum external rotation angle}}$$

$$\text{Internal rotation normalised angle} = \frac{\text{Internal rotation angle}}{\text{Maximum internal rotation angle}}$$

Applied moment for internal rotation is positive while the applied moment for external rotation is negative due to the direction of force application.

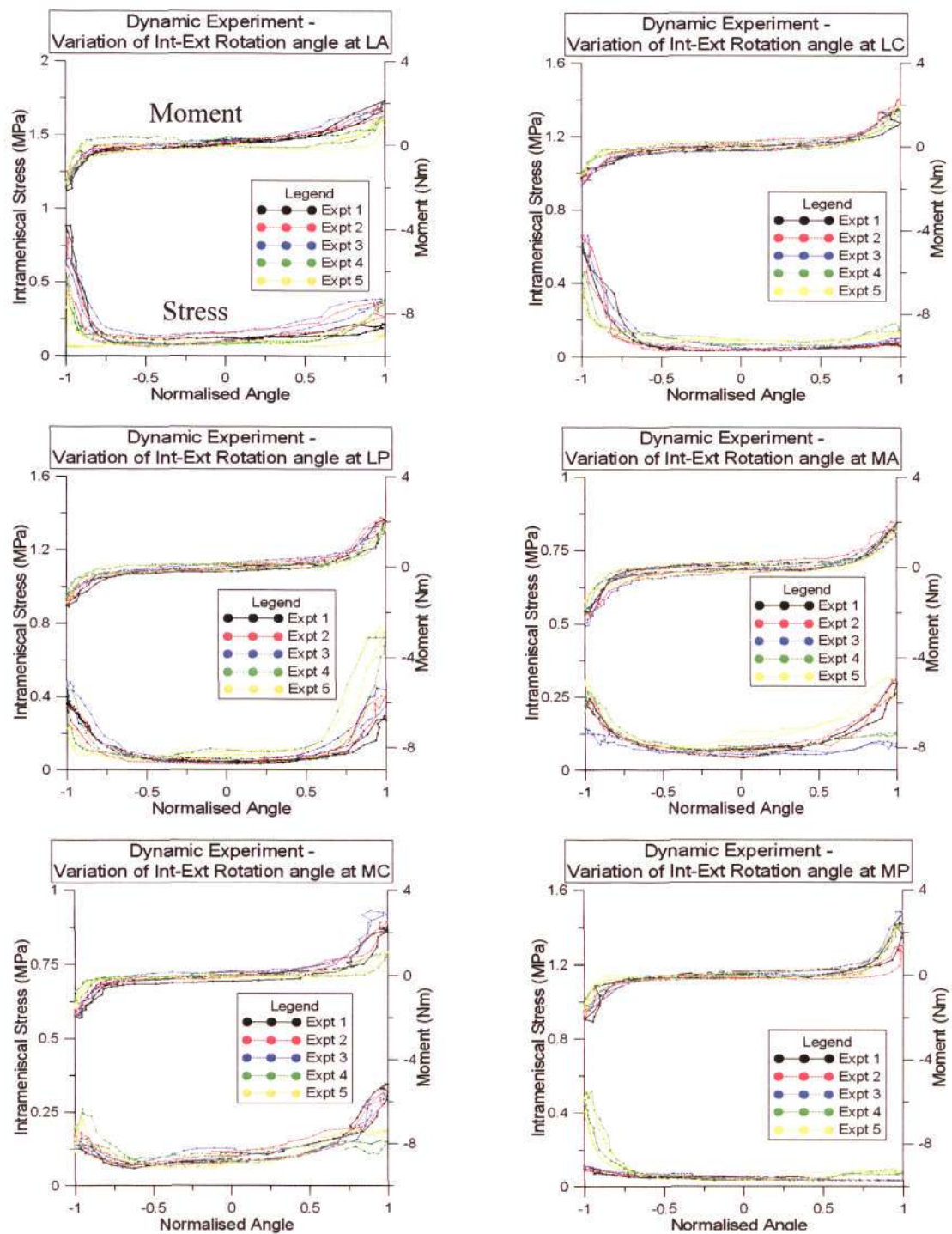
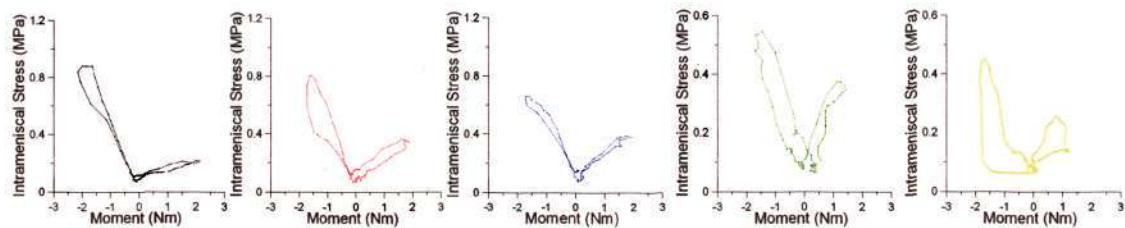


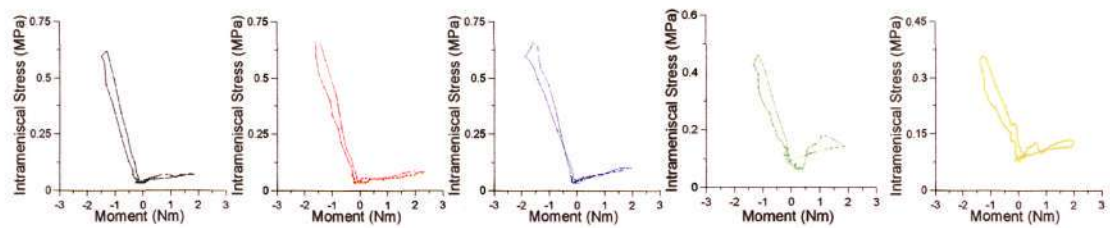
Figure 35: Graphs of Intrameniscal Stress and Moment vs Normalised angle during Internal-External rotation motion at mid-flexion at each position with the moment curve on top of the intrameniscal stress curve. Positive normalised angle representing internal rotation.

Intrameniscal stress is higher at lateral-anterior region during external rotation as compared to internal rotation. Same trend is observed for lateral-central region. The differences in intrameniscal stress experienced during external and internal rotation are small, with slightly higher values during internal rotation, at lateral-posterior, medial-anterior and medial-central regions. Some low value intrameniscal stress is experienced in the medial-central region during mid cycle, away from terminal joint position. Medial-posterior region experienced higher stress during external rotation. However, there is variation in terms of magnitude of differences in intrameniscal stress between experiments. Experiments 4 and 5 gave a much bigger differences in intrameniscal stress measured between internal and external rotation compared to the rest of the experiments. This may be due to the differences in the range of motion between the porcine knee specimens. For experiment 4 and 5, the location of maximum intrameniscal stress may have shifted back and medially, creating higher intrameniscal stresses at medial-posterior region at external rotation of the joint.

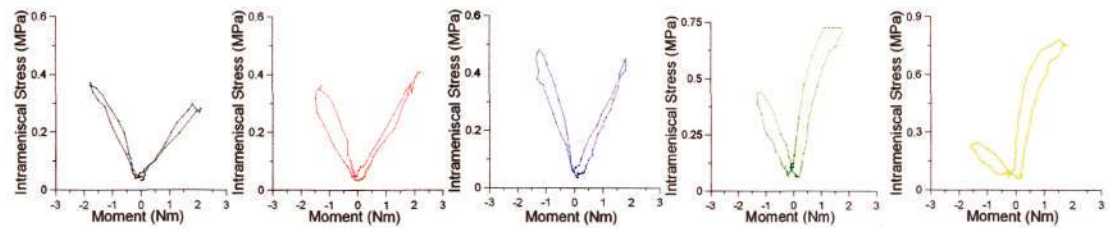
The graphs of intrameniscal stress vs. moment for internal-external rotation are presented next for all locations and experiments conducted.



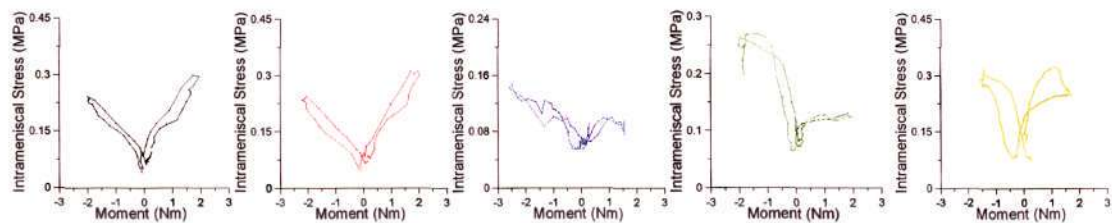
Intrameniscal stress vs Moment during internal-external rotation at LA- experiment 1 to 5



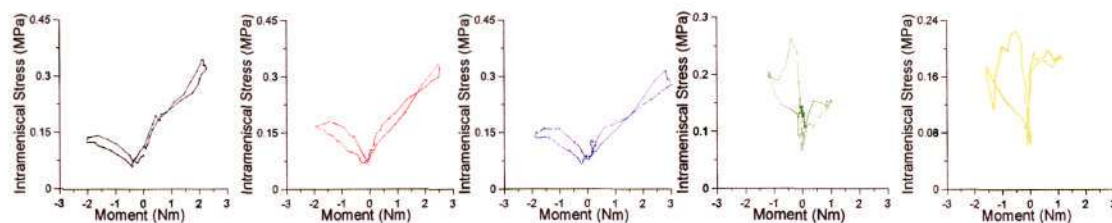
Intrameniscal stress vs Moment during internal-external rotation at LC- experiment 1 to 5



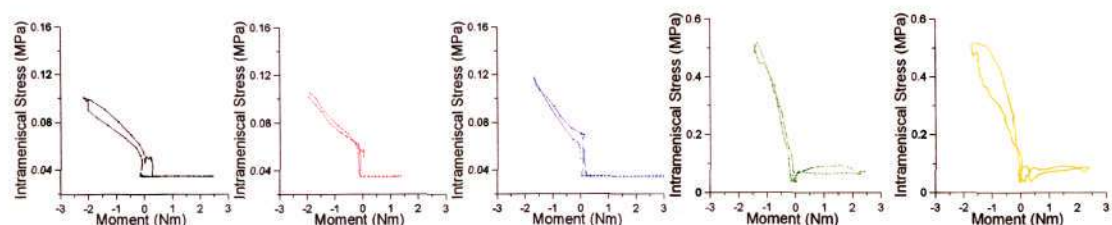
Intrameniscal stress vs Moment during internal-external rotation at LP- experiment 1 to 5



Intrameniscal stress vs. Moment during internal-external rotation at MA- experiment 1 to 5



Intrameniscal stress vs. Moment during internal-external rotation at MC- experiment 1 to 5



Intrameniscal stress vs. Moment during internal-external rotation at MP- experiment 1 to 5

Figure 36: Graph of intrameniscal stress vs applied moment for internal-external rotation experiment for each location and experiment

Similarly, loops can be observed for all graphs. The curves are similar for all the five experiments at lateral-anterior, lateral-central and medial-posterior regions. There is some variation in the trend of the curves for the lateral-posterior, medial-anterior and medial-central regions.

The ratio of intrameniscal stress against applied moment is required for comparison between meniscal locations at different knee positions. The chart representing the mean and standard deviation of intrameniscal stress-moment ratios at each location, at maximal internal and external rotation is shown in Figure 37.

One data point represents one meniscal location at each of the two terminal knee positions (maximum internal rotation and maximum external rotation).

At each of these points, the stress-moment ratio was calculated by:

Ratio=

$$\frac{\text{Maximum intrameniscal stress at terminal knee position at each meniscal location}}{\text{Corresponding Applied moment}}$$

The mean ratio at each of these points was then obtained by averaging the corresponding stress-moment ratios of the five specimens. The standard deviation was calculated from the ratios of the five specimens.

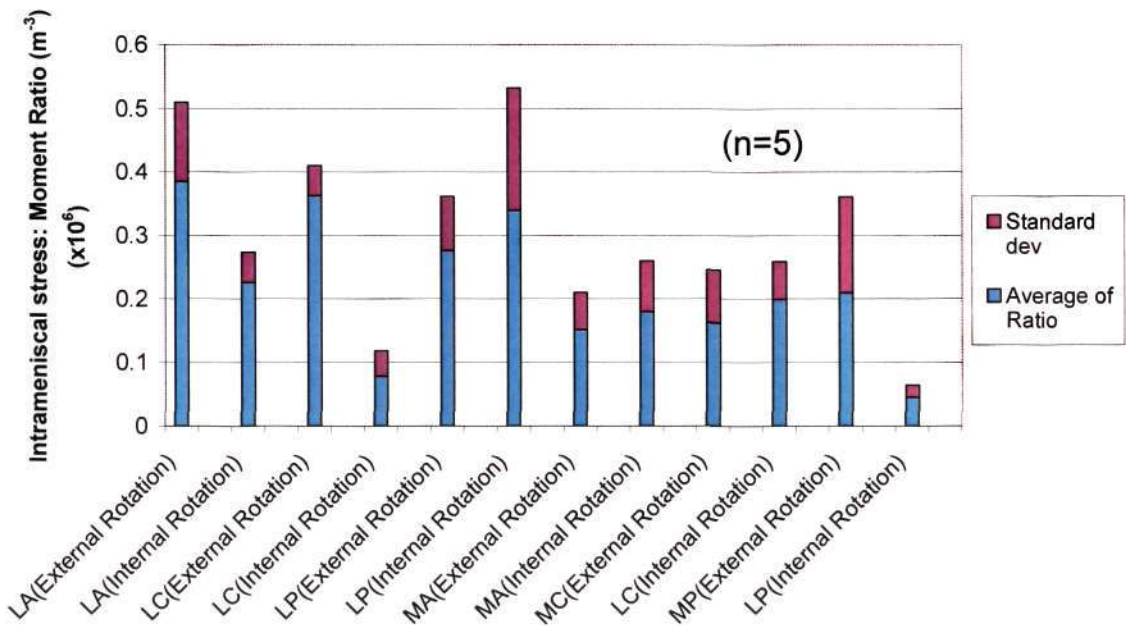


Figure 37: Graph of Intrameniscal stress-Moment ratio at different locations within the menisci, at extreme knee positions in the internal-external rotation experiments

The difference in intrameniscal stress-moment ratio between meniscal locations is not as distinct compared to the result from the extension-flexion experiment (Figure 33). Intrameniscal stress-moment ratio of mean values higher than $0.3 \times 10^6 \text{ m}^{-3}$ occurs at lateral-anterior region during external rotation, lateral-central region during external rotation and lateral-posterior region during internal rotation.

By summation of the stress-moment ratio at each terminal joint position, it was seen that the menisci were overall under higher pressure during external rotation of the joint as compared to internal rotation at the same applied moment. It can also be observed that lateral meniscus have higher stress-moment ratio than in the medial meniscus in external-internal rotation of the porcine knee joints in mid-flexion.

From the result, it can be concluded that highest intrameniscal stress occurs at maximum external and internal rotation. The result implies that overall higher stresses occur at external rotation.

A simple statistical analysis is added to support the conclusion that internal or external rotation of the knee joint specimen is a factor in determining the intrameniscal stresses and that higher stresses occur at external rotation

Table 1: Peak stresses at each meniscal location, in each experiment, at internal rotation and external rotation of the knee joint specimens

Meniscal Locations	Expt no.	Peak Intrameniscal stresses	
		External Rotation	Internal Rotation
Lateral-Anterior (LA)	Expt 1	0.8805	0.2124
	Expt 2	0.8018	0.3606
	Expt 3	0.6593	0.3858
	Expt 4	0.5463	0.3749
	Expt 5	0.4476	0.2576
Lateral-Central (LC)	Expt 1	0.6168	0.07103
	Expt 2	0.6593	0.07787
	Expt 3	0.6593	0.1004
	Expt 4	0.4636	0.1798
	Expt 5	0.3613	0.1356
Lateral-Posterior (LP)	Expt 1	0.3727	0.296
	Expt 2	0.3606	0.4075
	Expt 3	0.4823	0.4508
	Expt 4	0.4401	0.7272
	Expt 5	0.2468	0.7834
Medial-Posterior (MA)	Expt 1	0.2436	0.2997
	Expt 2	0.246	0.3116
	Expt 3	0.1474	0.09986
	Expt 4	0.27	0.1315
	Expt 5	0.3241	0.3241
Medial-Central (MC)	Expt 1	0.1426	0.3441
	Expt 2	0.1812	0.334
	Expt 3	0.1618	0.3158
	Expt 4	0.2627	0.1557
	Expt 5	0.2255	0.1988
Medial-Posterior (MP)	Expt 1	0.1011	0.03499
	Expt 2	0.1052	0.03503
	Expt 3	0.1177	0.03502
	Expt 4	0.5213	0.07405
	Expt 5	0.5211	0.08893

In this statistical analysis, the factor under investigation is the internal rotation and external rotation of the knee joint specimen. The aim of the analysis is to determine the significance of the factor on the intrameniscal stresses measured.

Result:

The data forms a normal probability plot and so an analysis of variance test (ANOVA) is done in EXCEL. Summary of results is shown below.

Sum of intrameniscal stresses at external rotation: 11.5696

Sum of intrameniscal stresses at internal rotation: 7.6041

Average of intrameniscal stresses at external rotation: 0.3857

Average of intrameniscal stresses at internal rotation: 0.2535

Variance for external rotation: 0.04615

Variance for internal rotation: 0.03464

At 95% confidence, the F value is 16.7225 and the F critical value is 5.3541. Since F value > F critical value, rotation of the knee joint specimen is a significant factor in the determination of the intrameniscal stresses at 95% confidence.

The P-value is 0.00164; therefore, the result is significant at 99.98% confidence.

The statistical analysis shows that internal or external rotation of the knee joint specimen is a factor in determining the intrameniscal stresses and that higher stresses occur at external rotation.

4.2 Static Experiment -Variation of intrameniscal stress with time

The purpose of this experiment is to monitor the stress variations within the menisci of porcine knee specimens as static pressure was exerted on the joint.

4.2.1 Methodology

The materials used were porcine knee specimens, the pressure conductive sensor system, the custom made frame structure (Figure 25), steel rods, ropes and fixed weights. The static experiment setup is shown in Figure 38. Experiments were conducted on five porcine knee specimens.

The knee specimen was first mounted on the structure. Afterwhich, a pressure conductive sensor was inserted into one of the meniscal locations shown in Figure 17. A steel rod was inserted through a channel proximal to the roof of the intercondylar fossa, to avoid compromising the integrity of the femoral attachments of the cruciate ligaments and collateral ligaments. A 20N weight was attached to the steel rod on each side of the knee specimen.

Intrameniscal force was recorded by the sensor system from the point of load application to the point of load removal. The cycle of load application and removal was repeated five times at the interval of thirty minutes.

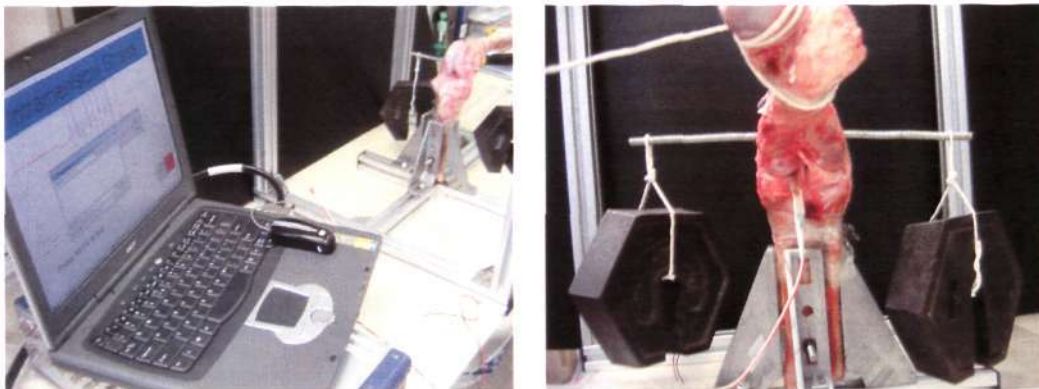


Figure 38: Static Experiment Setup

Pressure conductive sensor was also inserted between the articular cartilages to obtain the contact stress at the articular cartilage-articular cartilage interface (Figure 39).

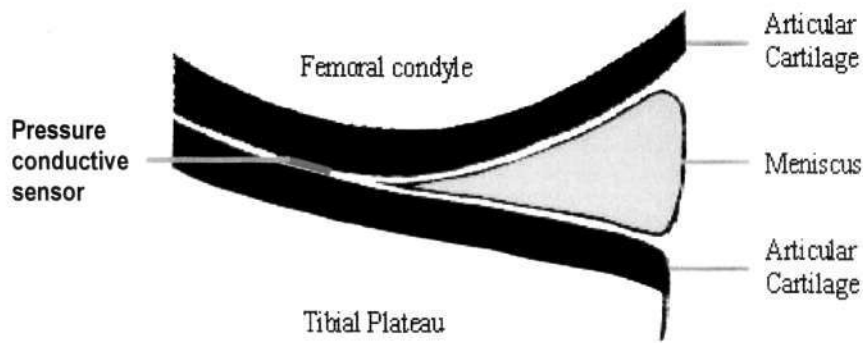


Figure 39: Position of pressure conductive sensor between the articular cartilages

Similarly, phosphate buffer solution was dripped onto the joint at regular interval to maintain the water content during the experiment. After each experiment, the sensor locations in the menisci were checked to ensure that the sensor was well embedded inside the menisci as described in section 4.1.1 at page 50 of the report.

4.2.2 Results

The intrameniscal force and articular cartilage contact force was again divided by the sensing area of the sensor to obtain the intrameniscal stress and articular cartilage contact stress. The intrameniscal stress and articular cartilage contact stress was plotted against time to observe the shift in stress with time. As the intrameniscal stress vs. time graphs show similar trend, only three slightly different graphs are shown.

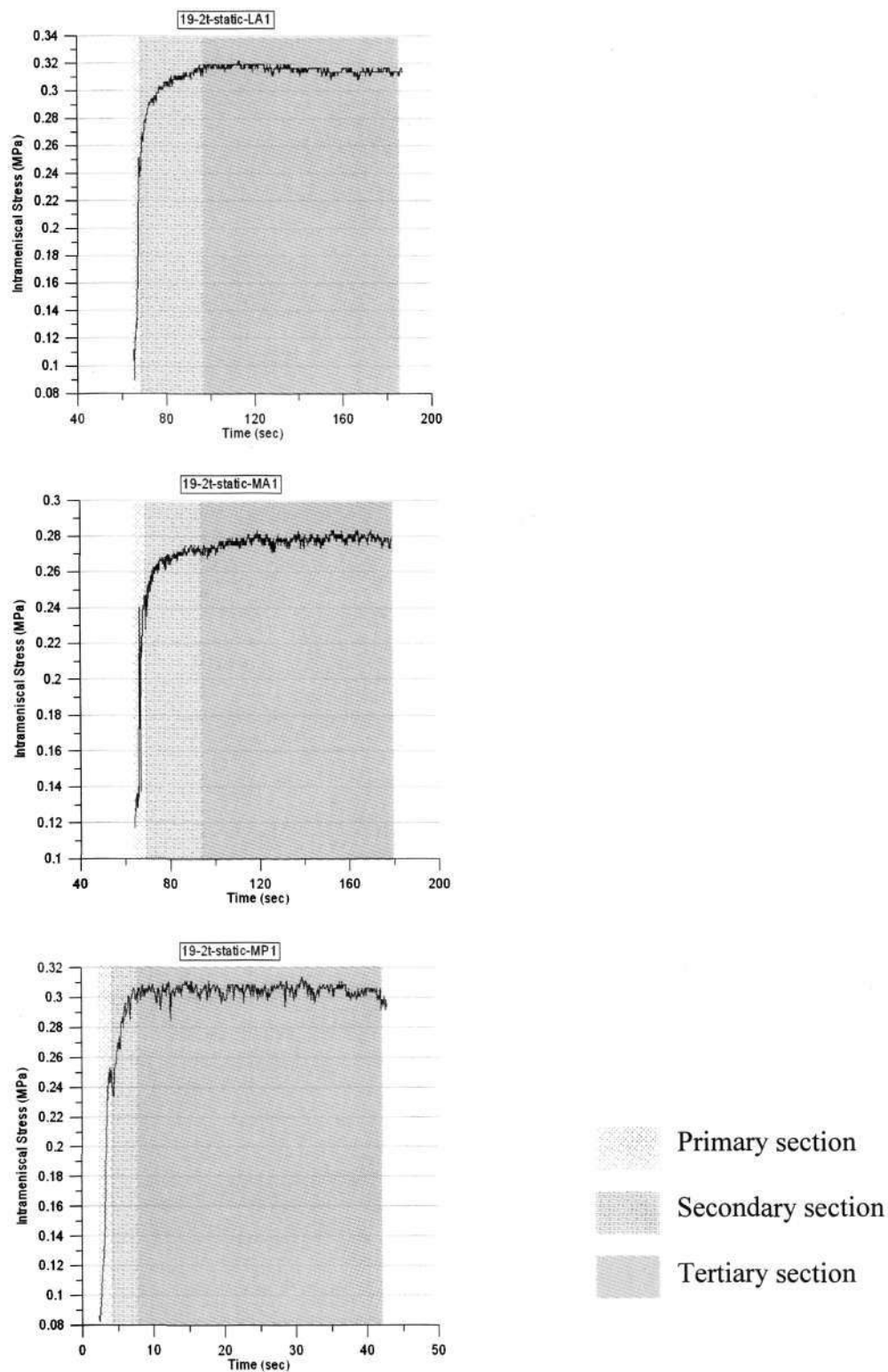


Figure 40: Graphs of Intrameniscal stress vs time at each position

Only general trend of the variation of intrameniscal stress with time is considered in this study. It must be noted that the speed of increase in the intrameniscal stress depends on the location as well as the load applied to it.

The general trend of the intrameniscal stress vs. time graph obtained is a sharp increase which lasts for less than 5 seconds, after which, the gradient of the curve decreases until a steady state is reached. For most of the results, the steady state region is a plateau (third graph in Figure 40), while for others; the steady state region may be a very slight positive (second graph of Figure 40) or negative gradient (first graph of Figure 40). For ease of discussion, the stress variation is divided into three sections. The primary section is the sharp increase in intrameniscal stresses on loading. The secondary section is the gradual decrease in gradient of the rise of intrameniscal stress. The tertiary section is where some of the results give a plateau, while others give a slight gradient which can be positive or negative.

The primary section shows the increase in intrameniscal stress as the load was applied. The sections of interest are the secondary and the tertiary sections.

As observed from the results shown in Figure 40, the intrameniscal stress increased in secondary section for all of the experimental results. If the intrameniscal stress increases, the stress must decrease in some other load bearing location. Therefore, the contact stress between the articular cartilages was measured. The result is shown in Figure 41. Due to low friction and an inclination of the articular cartilage-articular cartilage interface, only a few sets of data could be successfully collected.

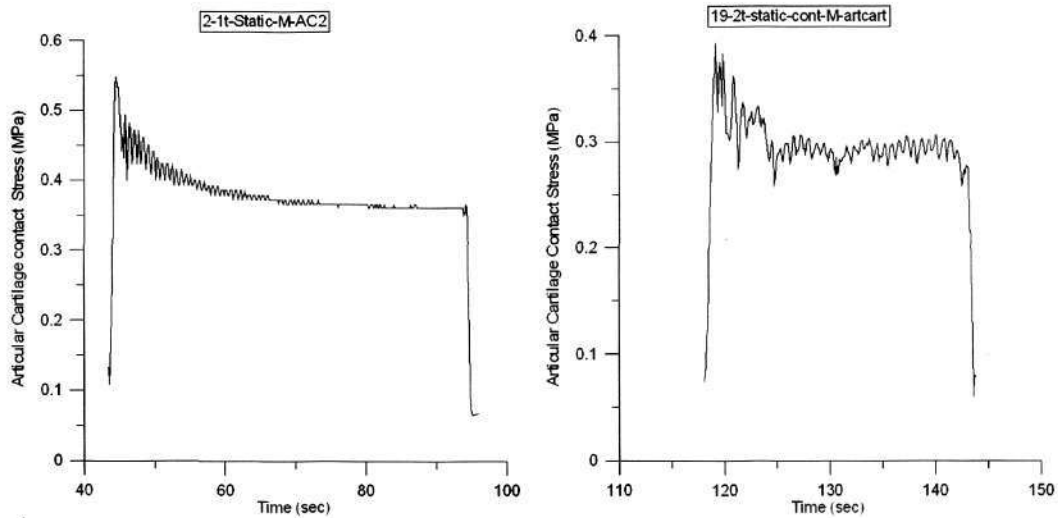


Figure 41: Graphs of articular cartilage contact stress vs time

As observed in Figure 41, the contact stress on the articular cartilage decreased with time. This implies that there was a load transfer from the articular cartilage to the meniscus with time.

The behaviour of stress with time in the tertiary section were varied, and this may be due to the different material property at different test site on the menisci [51].

Mathematical models can be developed from experimental results to explain the load shift between the meniscus and the articular cartilage. The models can also be used to explain the variation of load-time behaviour in the tertiary section with meniscal material property.

4.3 Material Testing

4.3.1 Methodology

The stress relaxation behaviour was investigated next through unconfined compression tests to aid in the formulation of mathematical models. The stress relaxation tests were conducted on extracted pieces of meniscus and articular cartilage on an Instron machine (model 3366). Special care was taken during extraction to ensure a flat and regular surface for all the test specimens. Phosphate buffer solution was used to prevent the specimens from drying up which will alter the mechanical properties. The dimensions of the specimens were measured with a measuring ruler and noted down before test. The specimen was then placed at the centre of the force plate and loaded to 0.2kN at 5mm/min and hold for 10 minutes.

Eight meniscus specimens and eight articular cartilage specimens were tested.



Figure 42: Material test setup

4.3.2 Results

Normalised stress is plotted against time, where normalised stress is $\frac{\text{Measured stress}}{\text{Initial applied stress}}$.

It is observed from the results obtained that the articular cartilage and the meniscus exhibit power-law stress relaxation behaviour. The normalised stress vs. time graph have an equation of the form $\sigma=At^B$. Parameters for the articular cartilage power-law equation are A and B where A is the constant of proportionality and B is the exponent of the power law equation. For the meniscus, C and D are the parameter for the power law equation where C is the constant of proportionality and D is the exponent of the power law equation. Values of parameters A, B, C and D for the power-fit curves for articular cartilage and meniscus samples are listed in Table 2 and Table 3.

The normalised stress-time graph for articular cartilage sample 1 (AC1) is shown in Figure 43 and the normalised stress-time graph for meniscus sample 11 (m11) is shown in Figure 44 as examples of the stress relaxation graphs. The power-fit curve is shown in red.

Table 2: Parameters of the articular cartilage power-fit curves for stress relaxation tests

$\sigma=At^B$	AC1	AC2	AC3	AC4	AC5	AC6	AC7	AC8
A	0.1817	0.1913	0.1638	0.1329	0.1644	0.1346	0.2205	0.1854
B	-0.5110	-0.5525	-0.5293	-0.5462	-0.6772	-0.5945	-0.6476	-0.5126
R-squared values	0.99612	0.98937	0.98314	0.98858	0.98414	0.99534	0.9827	0.99149

Mean of A: 0.1718; std dev: 0.02941

Mean of B: -0.5714; std dev: 0.06258

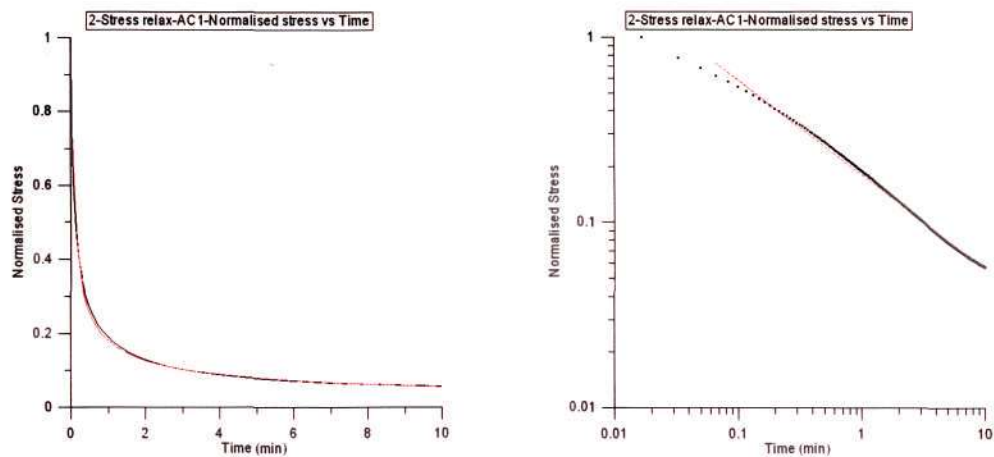


Figure 43: Stress Relaxation Graph for articular cartilage specimen AC1

Table 3: Parameters of the meniscus power-fit curves for stress relaxation tests

$\sigma = Ct^D$	m5	m6	m8	m9	m10	m11	m12	m13
C	0.09420	0.1026	0.1581	0.1635	0.1426	0.1107	0.07518	0.1011
D	-0.8532	-0.7759	-0.5984	-0.6142	-0.7719	-0.6503	-0.7654	-0.8035
R-squared values	0.98958	0.99294	0.99279	0.99284	0.98681	0.99679	0.99767	0.99265

Mean of C: 0.1185 std dev: 0.03219

Mean of D: -0.7291 std dev: 0.09469

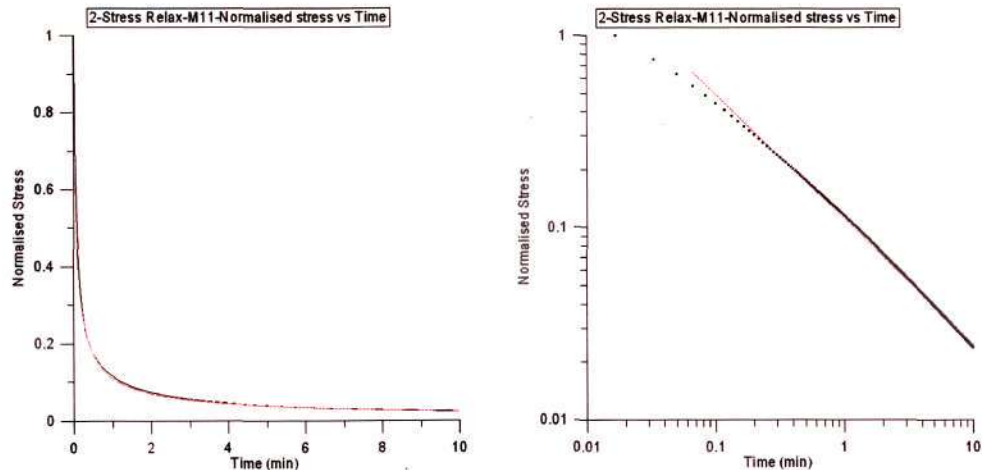


Figure 44: Stress Relaxation Graph for meniscus specimen M11

The variations in the stress relaxation properties shown by parameter A, B, C and D were due to the difference in the extracted locations of the specimen.

The stress relaxation graphs for the specimens are included in Appendix B.

5.0 MATERIAL MODEL

Three models were created to explain the results from the static experiments. The models were derived using force and displacement parameters for ease of formulation. As the intrameniscal stresses were determined by dividing the intrameniscal forces with a constant sensing area, the behaviour of the intrameniscal stress and intrameniscal force are comparable. The force versus time graphs of all models were compared with the static experimental results. Attention was focused in comparing the secondary and tertiary sections of the experimental results with the results from the models.

5.1 The Standard Linear Solid Model

A commonly utilized model, the standard linear solid (SLS) was first formulated. K_{m1} , K_{m2} and η_m are the parameters for elements in the meniscus component. K_{ac1} , K_{ac2} and η_{ac} are the parameters for elements in the articular cartilage component.

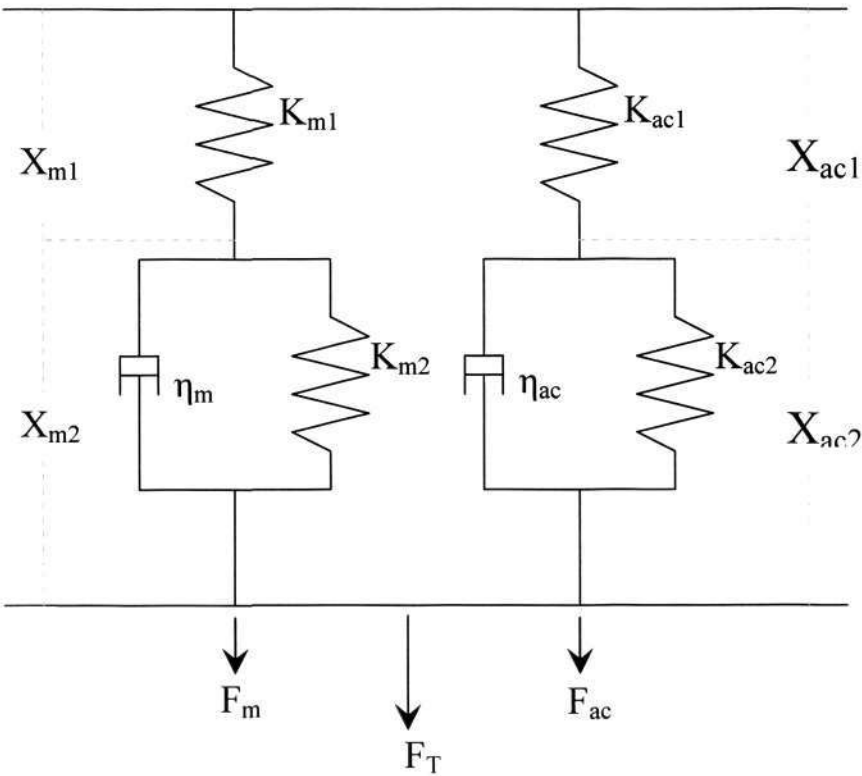


Figure 45: Standard Linear Solid model

where,

X_{ac1} : the displacement by the articular cartilage series spring element

X_{ac2} : the displacement by the articular cartilage dashpot and spring element

X_{m1} : the displacement by the meniscus series spring element

X_{m2} : the displacement by the meniscus dashpot and spring element

F_{ac} : the force applied on the articular cartilage

F_m : the force applied on the meniscus

F_T : the total force

K_{m1} : the spring stiffness for the series spring element in the meniscus component

K_{m2} : the spring stiffness for the parallel spring element in the meniscus component

η_m : the viscosity of the dashpot element in the meniscus component

K_{ac1} : the spring stiffness for the series spring element in the articular cartilage component

K_{ac2} : the spring stiffness for the parallel spring element in the articular cartilage component

η_{ac} : the viscosity of the dashpot element in the articular cartilage component.

Total displacement:

$$X = X_{m1} + X_{m2} = X_{ac1} + X_{ac2} \quad (5.1.1)$$

$$\text{Hooke's Law:} \quad (5.1.2)$$

$$F_m = X_{m1} K_{m1}$$

$$F_{ac} = X_{ac1} K_{ac1} \quad (5.1.3)$$

$$\text{Hooke's Law and Newton's Law:} \quad (5.1.4)$$

$$F_m = X_{m2} K_{m2} + \eta_m \dot{X}_{m2}$$

$$F_{ac} = X_{ac2} K_{ac2} + \eta_{ac} \dot{X}_{ac2} \quad (5.1.5)$$

The total force carried by the meniscus and articular cartilage components is defined as the summation of the forces of each individual component:

$$F_T = F_{ac} + F_m \quad (5.1.6)$$

Laplace Transformation for equations (5.1.2)-(5.1.6) and rearrange:

$$\begin{aligned} \hat{X}_{m1} &= \frac{\hat{F}_m}{K_{m1}} \\ \hat{X}_{ac1} &= \frac{\hat{F}_{ac}}{K_{ac1}} \\ \hat{X}_{m2} &= \frac{\hat{F}_m}{K_{m2} + s\eta_m} \\ \hat{X}_{ac2} &= \frac{\hat{F}_{ac}}{K_{ac2} + s\eta_{ac}} \\ \hat{F}_T &= \hat{F}_{ac} + \hat{F}_m \end{aligned}$$

Using Laplace Transformation for equations (5.1.2)-(5.1.5) and equation 5.1.1:

$$\begin{aligned} \hat{X} &= \hat{F}_m \left(\frac{1}{K_{m1}} + \frac{1}{K_{m2} + s\eta_m} \right) \\ \rightarrow \hat{F}_m &= \frac{\hat{X}(K_{m1}K_{m2} + sK_{m1}\eta_m)}{K_{m1} + K_{m2} + s\eta_m} \end{aligned} \quad (5.1.7)$$

$$\begin{aligned} \hat{X} &= \hat{F}_{ac} \left(\frac{1}{K_{ac1}} + \frac{1}{K_{ac2} + s\eta_{ac}} \right) \\ \rightarrow \hat{F}_{ac} &= \frac{\hat{X}(K_{ac1}K_{ac2} + sK_{ac1}\eta_{ac})}{K_{ac1} + K_{ac2} + s\eta_{ac}} \end{aligned} \quad (5.1.8)$$

Substituting equations (5.1.7) and (5.1.8) into Laplace Transformation of (5.1.6):

$$\begin{aligned}\hat{F}_T &= \hat{F}_m + \hat{F}_{ac} \\ &= \frac{\hat{X}(K_{m1}K_{m2} + sK_{m1}\eta_m)}{K_{m1} + K_{m2} + s\eta_m} + \frac{\hat{X}(K_{ac1}K_{ac2} + sK_{ac1}\eta_{ac})}{K_{ac1} + K_{ac2} + s\eta_{ac}} \\ \rightarrow \hat{X} &= \frac{F_T}{s} \left(\frac{(K_{m1} + K_{m2} + s\eta_m)(K_{ac1} + K_{ac2} + s\eta_{ac})}{(K_{m1}K_{m2} + sK_{m1}\eta_m)(K_{ac1} + K_{ac2} + s\eta_{ac}) + (K_{ac1}K_{ac2} + sK_{ac1}\eta_{ac})(K_{m1} + K_{m2} + s\eta_m)} \right)\end{aligned}\quad (5.1.9)$$

Let:

$$A = K_{m1}$$

$$B = K_{m2}$$

$$C = \eta_m$$

$$D = K_{ac1}$$

$$E = K_{ac2}$$

$$F = \eta_{ac}$$

Substituting the above notations into equation (5.1.9) and rearrange:

$$\hat{X} = F_T \left\{ \frac{s^2(CF) + s(AF + BF + CD + CE) + (AD + AE + BD + BE)}{s[s^2(ACF + DCF) + s(ABF + ACD + ACE + DCE + ADF + BDF) + (ABD + ABE + ADE + BDE)]} \right\}\quad (5.1.9a)$$

Substituting the notations above into equation (5.1.7):

$$\hat{F}_m = \hat{X} \frac{AB + sAC}{A + B + sC}\quad (5.1.10)$$

To obtain \hat{F}_m , substitute equation (5.1.9a) into equation (5.1.10):

$$\begin{aligned}\hat{F}_m &= \\ F_T &\left\{ \frac{s^2(CF) + s(AF + BF + CD + CE) + (AD + AE + BD + BE)}{s[s^2(ACF + DCF) + s(ABF + ACD + ACE + DCE + ADF + BDF) + (ABD + ABE + ADE + BDE)]} \right\} \left(\frac{AB + sAC}{A + B + sC} \right)\end{aligned}\quad (5.1.11)$$

From equation (5.1.11), F_m is obtained using inverse Laplace transformation on MatLab.

Solution of Inverse Laplace Transformation from MatLab:

$$F_m = F_T N [K - De^{Gt} (M \cosh(IHt) + L \sinh(IHt))] \quad (5.1.12)$$

where,

$$G = -\frac{ABF + CAD + CAE + CDE + DFA + DFB}{2CF(A + D)}$$

$$H = (C^2A^2D^2 + A^2B^2F^2 + 2A^2BF^2D + 2C^2A^2DE - 4ABCDEF + 2AB^2F^2D - 2A^2BFCD - 2A^2BFCE + 2C^2AD^2E + 2CA^2D^2F + C^2D^2E^2 + 2C^2AE^2D + C^2A^2E^2 - 2CAD^2FB - 2CA^2EDF - 2CD^2EFA + 2D^2F^2AB + D^2F^2A^2 - 2CD^2EFB + D^2F^2B^2)^{0.5}$$

$$I = \frac{1}{2CF(A + D)}$$

$$J = ABD + ABE + DEA + DEB$$

$$K = BHAD + BHD^2 + BHAE + BHDE$$

$$L = DCA^2E + 2D^2CAE + CA^2E^2 + DCAE^2 - 2DFA^2B - D^2FBA - DFB^2A - D^2FB^2 + D^2CBE - D^2FAEB + D^2CBA + DCBAE - DFA^2E - FA^2EB$$

$$M = DHB + HAE$$

$$N = \frac{A}{JH(A + D)}$$

$$F_{ac} = F_T - F_m \quad (5.1.13)$$

F_m and F_{ac} are plotted with time and compared with the results obtained from the experiment on variation of intrameniscal stress with time.

In the setting of the values of the parameters (K_{m1} , K_{m2} , η_m , K_{ac1} , K_{ac2} , η_{ac}), the basic rule that was followed was that $K_{m1} + K_{ac1} = 5$, $K_{m2} + K_{ac2} = 5$ and $\eta_m + \eta_{ac} = 5$. K_{m1} and K_{ac1} are set to be constant and equal spring stiffness. In the determination of K_{m2} , K_{ac2} , η_m and η_{ac} , the rule followed was that $\eta_m > \eta_{ac}$ and $K_{m2} < K_{ac2}$. This is because it was assumed that articular cartilage has a lower dashpot viscosity and is stiffer than the meniscus.

Following the rules, let:

F_T	t	K_{m1}	K_{m2}	η_m	K_{ac1}	K_{ac2}	η_{ac}
10	10	2.5	1	4	2.5	4	1

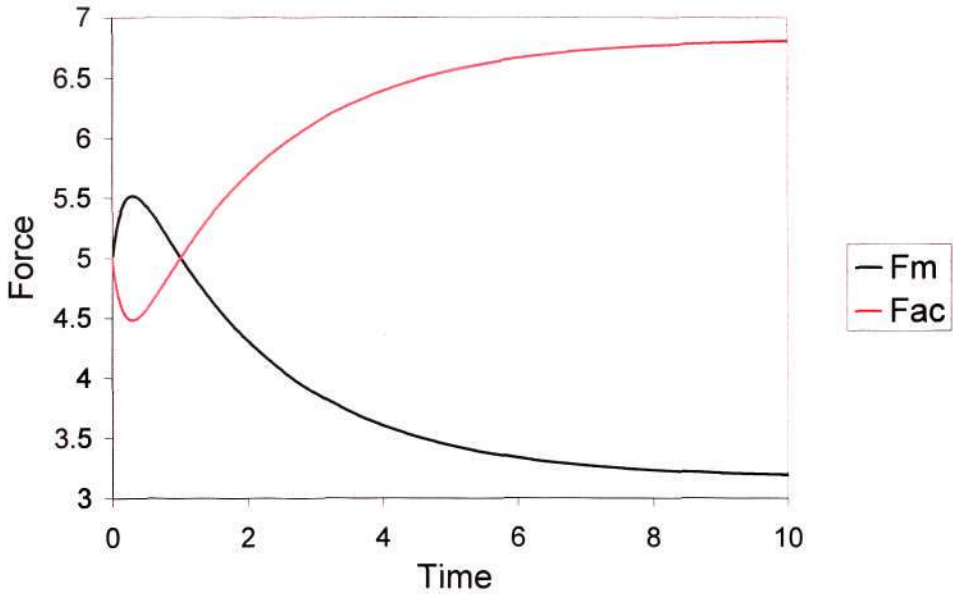


Figure 46: Result of SLS model

Results from the SLS model have different trends compared to the results obtained from the experiments on variation of intrameniscal stress and articular cartilage contact stress with time (Figure 40 and Figure 41).

The meniscal stress with time graph (F_m in Figure 46) decreases sharply after reaching a peak. This is different from the experimental results of intrameniscal stress measurement which reaches a stabilized state (tertiary section) after a gradual increase (secondary section) (Figure 40). Similarly, the curve of articular cartilage force (F_{ac} in Figure 46) behaves differently compared to the experimental result on articular cartilage contact stress (Figure 41). Instead of decreasing to a level plateau, the load on articular cartilage from the SLS model, F_{ac} decreases to a sharp valley and then increases to a level plateau.

From the comparison, the SLS model may not be the correct model to be used. Since, the stress relaxation material test results for the meniscus and articular cartilage specimens showed a power-law fit instead of an exponential fit, a new model based on power-law was derived.

5.2 First Viscoelastic Power Model

A one-dimensional nonlinear viscoelastic power model is used to explain the load shift phenomenon in the menisci and articular cartilage. The model consists of the meniscus and articular cartilage components which are arranged in parallel and each incorporates a spring element and a nonlinear viscoelastic element that depends on the state of the structure (Figure 47).

From the literature [114-116], both stress relaxation and creep behaviour of ligament follow power law. As the material tests conducted on the extracted specimens of articular cartilage and meniscus showed power-law stress relaxation behaviour, force-time behavior of the viscoelastic element were assumed to follow power law during structural creep. As the behaviour of the viscoelastic element is dependent on the force applied to it, a force term was added to the equation for viscoelastic element.

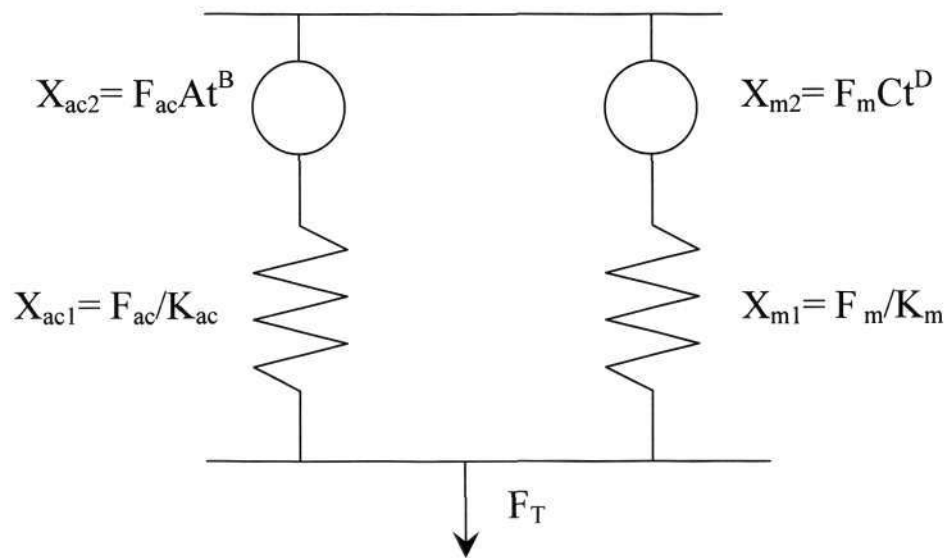


Figure 47: First Viscoelastic Power model

where,

- X_{ac1} : the displacement by the articular cartilage spring element
- X_{ac2} : the displacement by the articular cartilage viscoelastic element
- X_{m1} : the displacement by the meniscus spring element
- X_{m2} : the displacement by the meniscus viscoelastic element
- F_{ac} : the force applied on the articular cartilage
- F_m : the force applied on the meniscus
- F_T : the total force

- K_{ac} : articular cartilage spring stiffness.
 K_m : meniscus spring stiffness
A: the constant of proportionality for the power law equation for articular cartilage viscoelastic element
B: the exponent of the power law equation for articular cartilage viscoelastic element
C: the constant of proportionality for the power law equation for meniscus viscoelastic element
D: the exponent of the power law equation for meniscus viscoelastic element

The total force carried by the meniscus and articular cartilage components is defined as the summation of the forces of each individual component:

$$F_T = F_{ac} + F_m \quad (5.2.1)$$

Let

$$\frac{1}{K_{ac}} + At^B = G$$

$$\frac{1}{K_m} + Ct^D = H$$

Total displacement for articular cartilage component:

$$X = \frac{F_{ac}}{K_{ac}} + F_{ac} At^B$$

$$X = F_{ac} G$$

$$\rightarrow F_{ac} = \frac{X}{G} \quad (5.2.2)$$

Total displacement for meniscus component:

$$X = \frac{F_m}{K_m} + F_m Ct^D$$

$$X = F_m H$$

$$\rightarrow F_m = \frac{X}{H} \quad (5.2.3)$$

Substituting Equation (5.2.2) and (5.2.3) into (5.2.1):

$$F_T = F_{ac} + F_m$$

$$F_T = X \left(\frac{1}{G} + \frac{1}{H} \right)$$

$$F_T = F_{ac} G \left(\frac{1}{G} + \frac{1}{H} \right)$$

$$F_{ac} = \frac{F_T}{G \left(\frac{1}{G} + \frac{1}{H} \right)}$$

$$F_{ac} = \frac{F_T}{G \left(\frac{H+G}{HG} \right)}$$

$$F_{ac} = \frac{F_T H}{H+G}$$

$$\rightarrow F_{ac} = F_T \left(\frac{\frac{1}{K_m} + Ct^D}{\frac{1}{K_m} + Ct^D + \frac{1}{K_{ac}} + At^B} \right) \quad (5.2.4)$$

$$F_m = \frac{F_T G}{H+G}$$

$$\rightarrow F_m = F_T \left(\frac{\frac{1}{K_{ac}} + At^B}{\frac{1}{K_m} + Ct^D + \frac{1}{K_{ac}} + At^B} \right) \quad (5.2.5)$$

Let:

F_T	t	A	B	C	D	K_{ac}	K_m
10	10	0.2	0.57	0.1	0.73	2.5	2.5

where,

K_{ac} and K_m are equal, random spring stiffness. The material parameters A, B, C and D are approximately the values obtained from the material tests. Note that B and D are absolute values. The basic rules used for the choice of the values of A, B, C and D are derived from the material tests results where $B > A$, and $D > C$; $A > C$, and $D > B$.

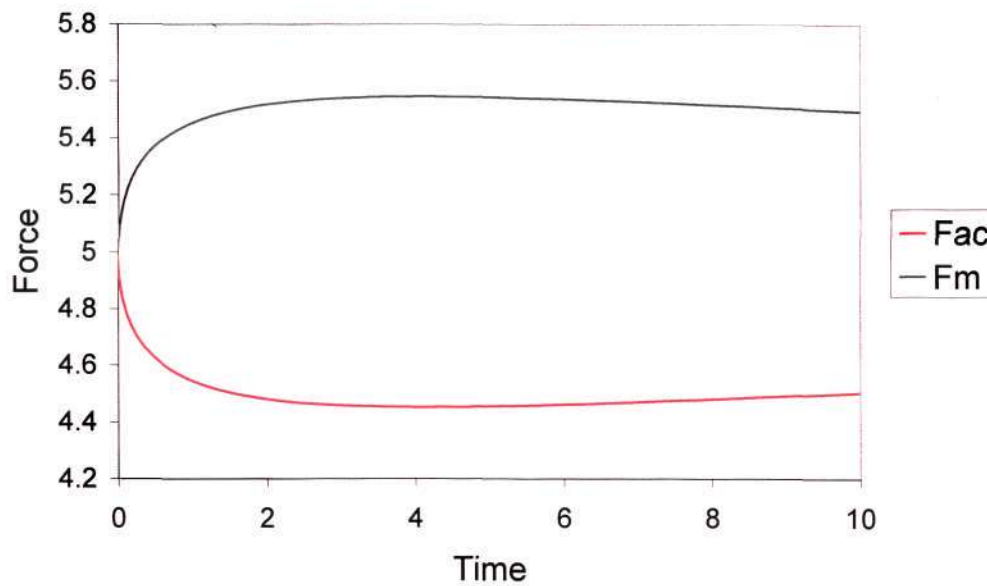


Figure 48: Result of the First Viscoelastic Power model

By plotting out the derived equations using the values of A , B , C , D , K_m and K_{ac} stated above, it can be observed that the general trend of the meniscus and articular cartilage force –time behaviour is similar to the experimental results. In the model predication, the load shifts from the articular cartilage to the meniscus which is shown in the secondary section of the experimental results.

In the meniscal graph (F_m in Figure 48) obtained, there is a slightly negative gradient of -0.0107 with R -squared value= 0.998153 between the 6th and the 10th time unit (tertiary section). The meniscal graph of the first viscoelastic power model have similar trend as compared to the first graph in Figure 40. The tertiary section of the articular cartilage curve has an upward slope which was not observed in the experiment.

This model does not consider that the load on the menisci is applied through the articular cartilage. Therefore, a second viscoelastic power-law model with an additional articular cartilage component was formulated.

5.3 Second Viscoelastic Power Model

Articular cartilage and meniscus components each include a spring and a power-law viscoelastic element. The model has an articular cartilage component in series with a meniscus component, parallel with another articular cartilage component.

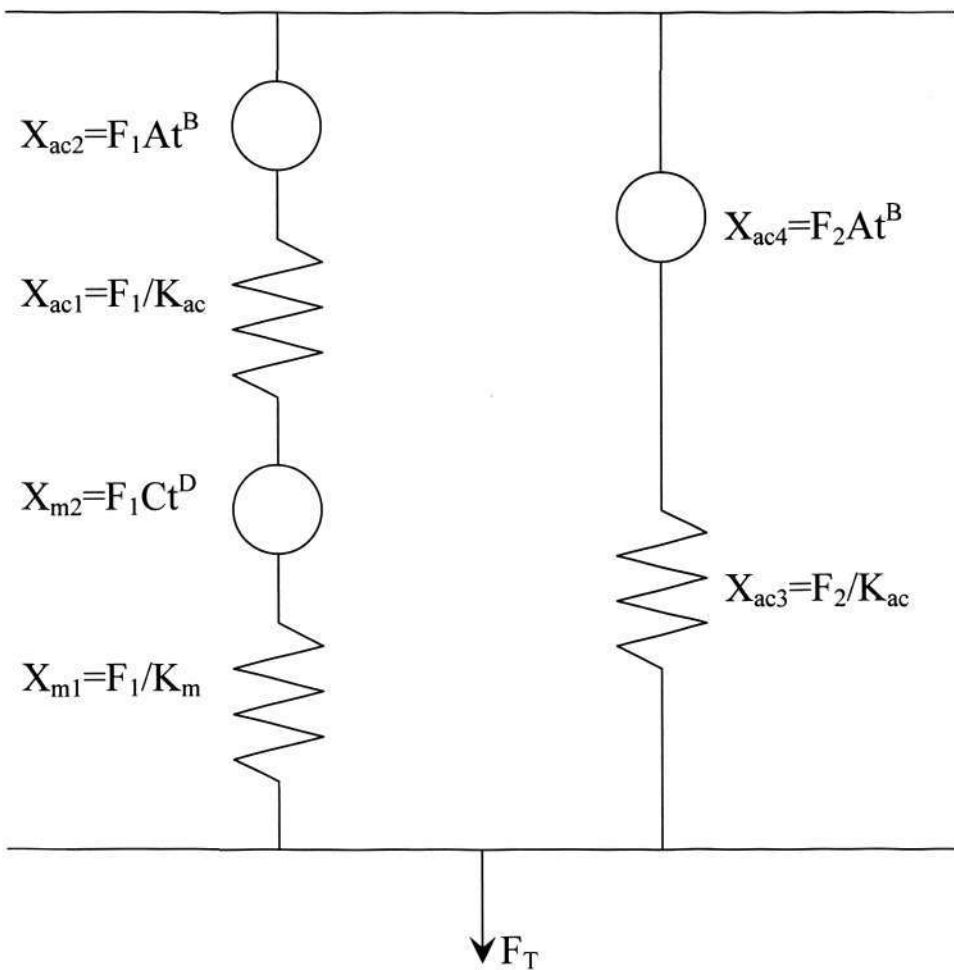


Figure 49: Second Viscoelastic Power Model

where,

- X_{ac1} : the displacement by the articular cartilage spring element
- X_{ac2} : the displacement by the articular cartilage viscoelastic element
- X_{m1} : the displacement by the meniscus spring element
- X_{m2} : the displacement by the meniscus viscoelastic element
- X_{ac3} : the displacement by the second articular cartilage spring element
- X_{ac4} : the displacement by the second articular cartilage viscoelastic element
- F_1 : the force applied on the meniscus element and the first articular cartilage element
- F_2 : the force applied on the second articular cartilage element
- F_T : the total force
- K_{ac} : articular cartilage spring stiffness
- K_m : meniscus spring stiffness
- A: the constant of proportionality for the power law equation for articular cartilage viscoelastic element
- B: the exponent of the power law equation for articular cartilage viscoelastic element
- C: the constant of proportionality for the power law equation for meniscus viscoelastic element
- D: the exponent of the power law equation for meniscus viscoelastic element

The total force carried by the meniscus and articular cartilage components is defined as the summation of the forces:

$$F_T = F_1 + F_2 \quad (5.3.1)$$

Sum of displacement:

$$X = F_1 \left(\frac{1}{k_{ac}} + At^B + \frac{1}{K_m} + Ct^D \right)$$

$$\rightarrow F_1 = \frac{X}{\left(\frac{1}{k_{ac}} + At^B + \frac{1}{K_m} + Ct^D \right)} \quad (5.3.2)$$

Sum of displacement:

$$X = F_2 \left(\frac{1}{k_{ac}} + At^B \right)$$

$$\rightarrow F_2 = \frac{X}{\left(\frac{1}{k_{ac}} + At^B \right)} \quad (5.3.3)$$

Substitute equations (5.3.2) and (5.3.3) into equation (5.3.1):

$$F = \frac{X}{\frac{1}{k_{ac}} + At^B + \frac{1}{K_m} + Ct^D} + \frac{X}{\frac{1}{k_{ac}} + At^B}$$

$$\rightarrow X = \frac{F}{\frac{1}{\frac{1}{k_{ac}} + At^B + \frac{1}{K_m} + Ct^D} + \frac{1}{\frac{1}{k_{ac}} + At^B}} \quad (5.3.4)$$

Substitute equation (5.3.4) into (5.3.2) and (5.3.3):

$$F_1 = \frac{F \left(\frac{1}{k_{ac}} + At^B \right)}{\left(\frac{1}{k_{ac}} + At^B + \frac{1}{K_m} + Ct^D \right) + \left(\frac{1}{k_{ac}} + At^B \right)} \quad (5.3.5)$$

$$F_2 = \frac{F \left(\frac{1}{k_{ac}} + At^B + \frac{1}{K_m} + Ct^D \right)}{\left(\frac{1}{k_{ac}} + At^B + \frac{1}{K_m} + Ct^D \right) + \left(\frac{1}{k_{ac}} + At^B \right)} \quad (5.3.6)$$

Let

F_T	t	A	B	C	D	K_{ac}	K_m
10	10	0.2	0.57	0.1	0.73	2.5	2.5

where,

A, B, C and D were kept close to the values obtained from the material tests. The basic rules derived from the material tests results in choosing the values of A, B, C and D are that $B > A$ and $D > C$; $A > C$ and $D > B$. Note that absolute values were used for B and D.

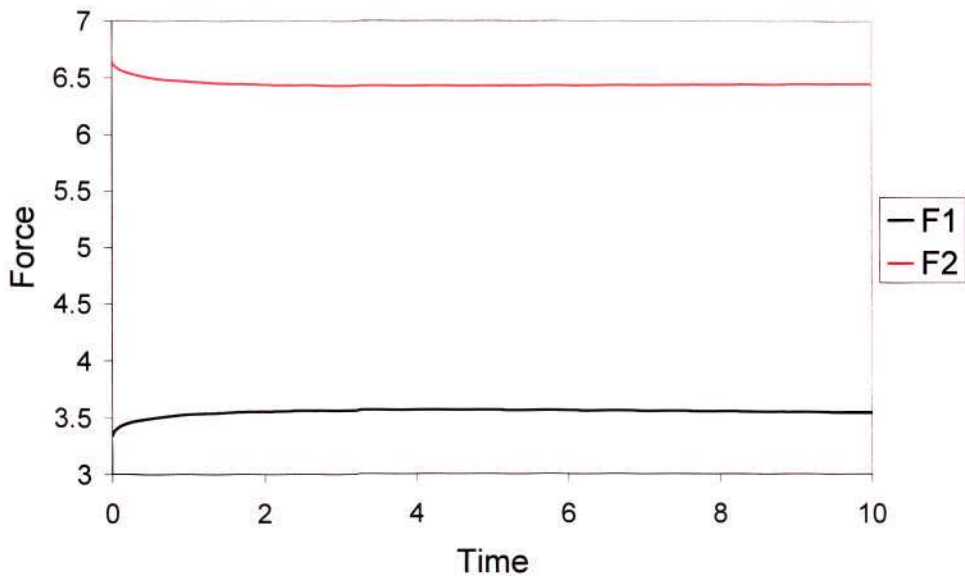


Figure 50: Result of Second Viscoelastic Power-law model with $D=0.73$

The articular cartilage and meniscus force vs. time graph from the second viscoelastic power-law model (Figure 50) is similar to the experimental results (Figure 40 and Figure 41). The secondary section of the meniscal force-time graph (F_1 from Figure 50) increases with time and reaches a stable state. The tertiary section have a slight negative slope of -0.00445 from the 6th to the 10th time unit (R-squared value= 0.998094) when D was set to 0.73.

As the material property of meniscus depends on the experimented location [51], the exponent of the power law equation for meniscus viscoelastic element was increased and then decreased by 20% to observed the effect on the force vs. time behaviour.

By increasing parameter D to 0.88, a tertiary section with a downward slope in the meniscal load vs. time graph is observed (F_1 from Figure 51). The gradient for the last 4 time units of the meniscal load vs. time graph is -0.0251 with R-squared value= 0.999519

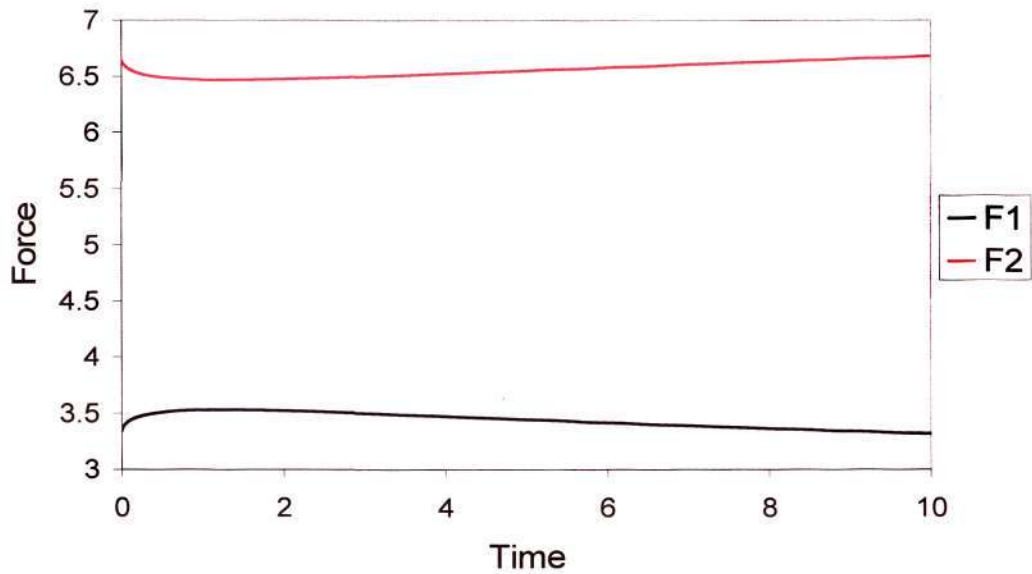


Figure 51: Result of Second Viscoelastic Power-law model with D=0.88

By decreasing parameter D to 0.58, a tertiary section, with an upward slope in the meniscal load vs. time graph is observed. The gradient for the last 4 time units of the meniscal load vs. time graph is 0.0109 with R-squared value= 0.99463

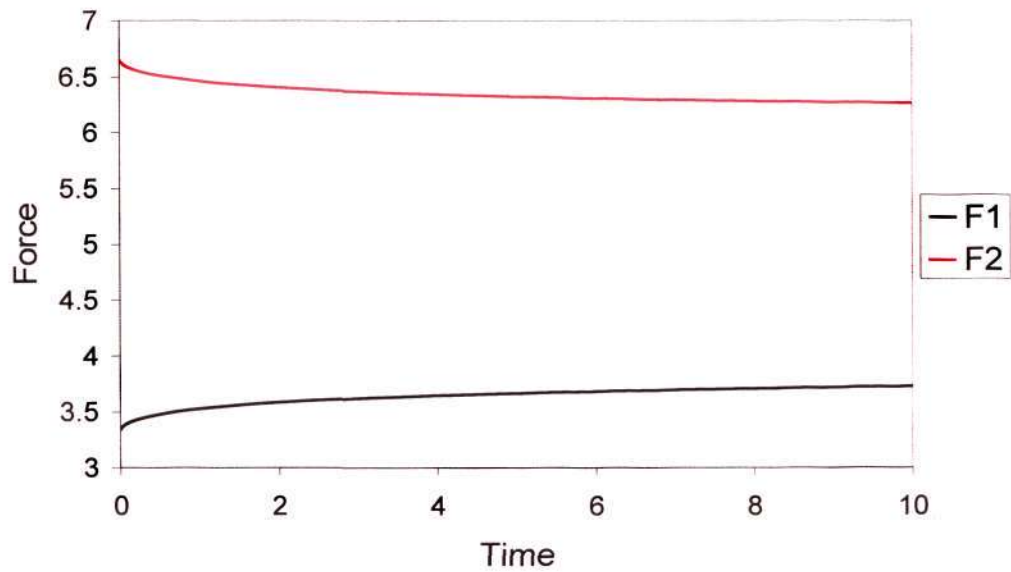


Figure 52: Result of Second Viscoelastic Power-law model with D=0.58

Through the variation of D , the exponent of the power law equation for meniscus viscoelastic element, the trend of the tertiary section of the force vs. time graph was altered. This can explain the differences in the tertiary section of the static experiment results. From the model, it can be observed that by varying only D , the load on the meniscus over time may be constant, gradually increase or gradually decrease. The change from positive to negative gradient in the tertiary section of the meniscal load vs. time graph for the second viscoelastic power model occurs when value of parameter D is between 0.69 and 0.7. This means that the variation of the meniscus material properties in different location of the meniscus plays a large part in the load transfer phenomenon between the meniscus and the articular cartilage.

Although simple structural models were used, it is capable of qualitatively describing the experimental observations for the nonlinear response of the meniscus and articular cartilage.

6.0 DISCUSSION

Knee mechanics have been studied extensively [4, 8-38]. However, there have been no studies on the measurement of knee joint intrameniscal stresses. This study includes the measurement of the intrameniscal stresses in porcine knee specimens during the variation of knee angulations with torque applied at terminal knee positions; measurement of variation of the intrameniscal stresses with time during mid flexion when constant load was applied on the joint; and the formulation of mathematical models with material test data.

Results from the experiments on porcine knee joints were used to draw an analogous relationship to human knee joint in the discussion. Expected physiological load exerted on the human knee joint have been calculated to be more than five times body weight in normal daily activities [1, 2]. As an animal model is used, a smaller load is used in the experiment. Therefore, the intrameniscal stresses in human knee can be expected to be much higher during daily activities as compared to the intrameniscal stress values obtained from the experiments. The assessment for the dynamic experiments is made by comparing the stress at different meniscal locations, at different knee positions and different applied torque. For the static experiments, assessment is made by comparing the intrameniscal stress-time relationship with the articular cartilage contact stress- time relationship. In this way, parallel comparisons can be drawn from the experimental results to the intrameniscal stresses in a human knee joint.

Acute meniscal injuries occur during sport activities where there is a sudden flexion, extension, rotation or a combined extension or flexion with rotation of the knee joint. Chronic meniscal injuries occur when there is a long period of repeated exposure to an injurious force which may take place during normal daily activities like work or sports [64-66]. From the dynamic experimental results, locations of high stress-moment ratio can be found, indicating possible injury sites. The knee positions which created high stress-moment ratio should be noted to lessen injury occurrences.

From the results for dynamic variation of joint angulations, it was found that high peaks in intrameniscal stress occurred at terminal knee positions (hyperextension,

hyperflexion, maximal internal and external rotation). This was expected since the applied moment was highest at terminal positions. This finding is in agreement with past studies where human meniscal injuries were found to frequently occur due to knee joint hyperextension and hyperflexion with rotation [117]. Several injury mechanisms were associated to tibial torque and knee flexion angle. In these positions, the menisci experience high load, leading to higher rate of injuries [118].

From the results of dynamic experiments on intrameniscal stress, it was observed that lateral-anterior region experienced the highest stress-moment ratio at hyperextension. This implied that this region is most likely to be injured during hyperextension compared to the other regions. During flexion, lateral -posterior and medial -posterior regions have the highest stress-moment ratio. From literature [71], it was found that patients who were in occupations that required squatting or crouching down during work were more likely to sustain posterior medial meniscal lesions. This is in accordance with the high stress-moment ratio experienced by the medial-posterior regions during hyperflexion in the experiments.

Knee joint is frequently injured during sport activities and it was found that soccer and skiing are the two activities that show high occurrence of knee injuries [119]. Typically, in these sport activities, knee joint is loaded during internal and external rotation which cause high intrameniscal stress.

From experimental results, highest intrameniscal stress occurs at lateral-anterior region during external rotation and at lateral-posterior region during internal rotation. On average, higher stress-moment ratio occurred during external rotation compared to internal rotation of the porcine knee joint. Considering a typical soccer kick movement, the knee joint is externally rotated and is fully extended on contact between the foot and the ball. In an analogical sense, high intrameniscal stress will be experienced in the knee joint according to the experimental results as high stress-moment ratio was observed during external rotation and hyperextension of the knee joint. This finding indicates that the knee menisci experience high intrameniscal stresses during a typical soccer kick.

Although anterior cruciate ligament injuries are the more prevalent injuries sustained during skiing, medial meniscus lesion have a high rate of occurrences [119]. This is because injury mechanisms during skiing are typically valgus-external rotation, flexion-internal rotation and hyperextension-internal rotation [120]. External rotation, flexion-internal rotation and hyperextension-internal rotation would also cause high intrameniscal stress according to the experimental results. These positions that cause anterior cruciate ligament injuries will most likely lead to meniscus lesions.

Another sport which has occurrences of meniscal injuries is Judo, where the athletes rotate their knee to execute a technique or flex their knee abruptly to avoid a hit [121]. The sudden shift to terminal knee position will cause high stress in the menisci. Also, in rock climbing, certain positions taken by climbers can lead to meniscal injuries. One of the most common situations is where the climber extends their knees from a hyperflexion and external rotation position [122]. According to the experimental results, high intrameniscal stress occurs during external rotation and hyperflexion of the knee joint. When the climber starts to extend his/her knee, the axial load on the knee joint increases leading to an increase in stress within the menisci. Additionally, extension during external rotation may lead to the trapping of the meniscus between the femoral condyle and tibial plateau leading to meniscal injuries.

From the results for variation of intrameniscal stresses due to dynamic variation of joint angulations, it can be concluded that such measurement techniques can be used for locating areas of high intrameniscal stresses in various knee positions. Applications of such techniques on human cadaveric knee would indicate the meniscal areas under high stress and the respective joint positions. The experimental results can be used as a gauge on the injury site based on injury mechanism. This experimental technique can also be used to investigate mechanism of secondary tears in the menisci. This is done by investigating the effects of injuries in knee structures on intrameniscal stress. This is especially significant in ACL damages as it is closely linked to meniscal injuries [46]. The pattern of variations of intrameniscal stress during cyclic loading of the knee joint can also be found and the change of intrameniscal stress with moment and angle can also be analysed to provide better understanding of the knee joint mechanics.

The static experiment on the variation of the intrameniscal stresses with time was conducted next to investigate in the effect prolong loading of the knee joint. For the experiment, the joint was loaded in mid-flexion.

The stress-time relationship under constant load is separated into three sections. The primary section is the sharp increase in intrameniscal stresses on loading. The secondary section is the gradual fall in the speed of increase in the intrameniscal stress. There is some variation in the tertiary section. The majority of the results give a plateau, while some results give a slight gradient which can be positive or negative. The increase in stresses within the meniscus can only mean that there is a decrease in stresses in another structure of the knee joint. Therefore, the contact stresses between the articular cartilages were measured. It was found that there was indeed a decrease in contact stresses as time increases. This implies that there is a load shift from the articular cartilage to the meniscus. If similar shift in load can be observed in human cadaveric knee joint, this may imply that patients with injured or recently repaired meniscus should avoid loading the knee for long period of time. This also indicates that the articular cartilage is protected during static loading of the knee joint.

The difference in the tertiary section of the result may be due to the slight differences in the mechanical properties of the meniscus in different locations. The local variation in tissue structures and compositions contributes to the variability in measurement in the meniscus [123].

To clarify the load shift phenomenon and the difference in the tertiary section of the resultant stress vs. time graphs, mathematical models were formulated. Material tests were first conducted to find the stress-time behaviour to develop the models. Specimens of articular cartilage and meniscus were extracted and tested using unconfined compression tests. It was found that similar to many biological materials, the meniscus and the articular cartilage follow power law in the stress vs. time graphs. From the literature [114-116], both stress relaxation and creep behaviour of knee joint ligaments follow power law with correlation in the rate of change in stress and strain with time.

Standard linear solid model was first created as a comparison. It was found that the resultant load vs. time behaviour is different from the results from the static experiments. This indicates that the standard linear solid model may not be suitable to model the load transfer behaviour between the menisci and the articular cartilage. The reason is that the SLS models an exponential behaviour while the material test results indicate that the articular cartilage and meniscus material follow power-law stress-time behaviour.

Viscoelastic power models were developed as a result of the stress relaxation tests. The force-time relationship was assumed to follow the power-law due to the result from the material test conducted and the finding on the relationship between creep and stress relaxation behaviour of ligament [114-116]. Meniscus and articular cartilage components were assumed to include a spring and a viscoelastic element. As the behaviour of the viscoelastic elements depends on the load applied on it, the power-law equations were multiplied by the load. Meniscus and articular cartilage components were assumed to be parallel in the first viscoelastic power model. The first viscoelastic power model is able to give a resultant graph which is similar to the stress vs. time graph from the static tests. The model shows a shift in load from the articular cartilage component to the meniscus component as time increases. However, this model does not consider that the load on the menisci is applied through the articular cartilage.

In the second viscoelastic power model, an articular cartilage component is connected in series with a meniscus component. It is then connected in parallel with another articular cartilage component. The resultant stress vs. time behaviour from the model is similar to the results from the static experiments. In the secondary section, load on the meniscus component increases with time and load on the parallel articular cartilage component decreases with time, exhibiting load transfer from the articular cartilage to the meniscus.

By variation of the material parameters, the tertiary section of the stress vs. time graph can be a straight line with zero, a small positive or negative gradient. This explains the differences in the tertiary section in the static experiments results. From the second viscoelastic power model, it can be observed that by varying the material

parameter of the meniscus, D , the load transfer mechanism can be slightly altered. This indicates that at different location of the meniscus, the load transfer mechanism is different due to the composition and structure of the tissue.

For locations in the meniscus with the exponent of the power law equation for the viscoelastic element, D ranging from around 0.69 to 0.7, the tertiary section levels off, thereby retaining the stress on the meniscus. When D is more than 0.7, the articular cartilage will be loaded more gradually over time. When D is less than 0.7, the load on the meniscus will increase over time. It must be noted that the variation also depends on the material properties of the articular cartilage. In the second viscoelastic power model, the material parameters of the articular cartilage are kept constant, varying only the exponent of the power law equation for the meniscus viscoelastic element.

From the second viscoelastic power model, the dependence of the load change behaviour on the material properties can be observed. Effect of geometry of the meniscus can be introduced into the model. The effect of the “wedge” shape of the meniscus can be observed by adding articular cartilage and meniscus components to the model. The model is shown in Figure 53.

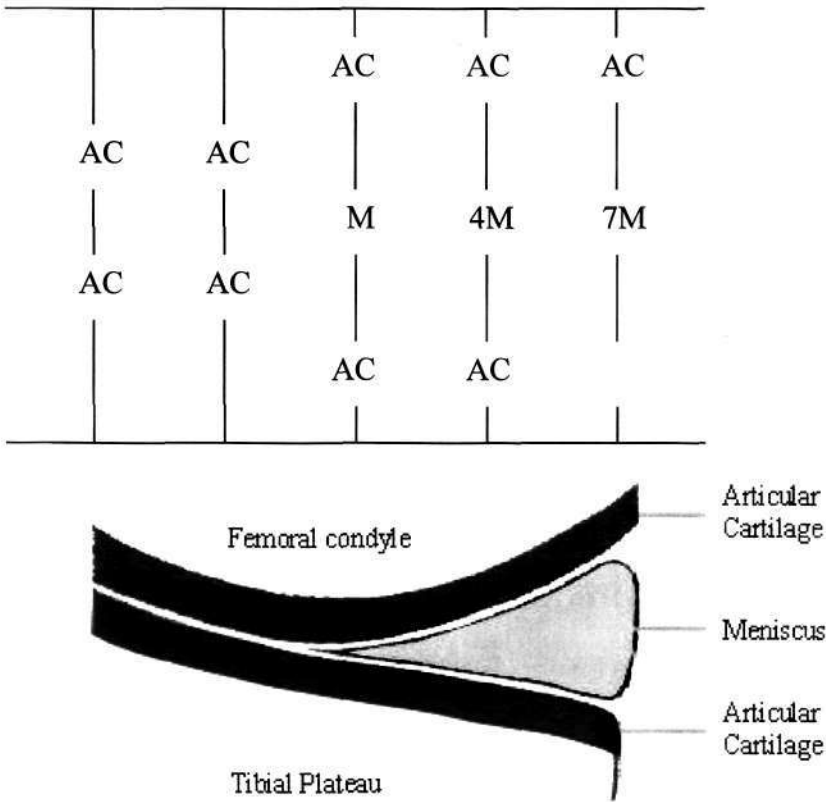


Figure 53: Model and schematics of joint interfaces

The ratio of meniscus components and articular cartilage components used in the model will be dependent on the species due to the geometry variation of the meniscus between species [113]. The effect of geometry on the load transfer phenomenon can be determined from such model.

In general, this study indicates that extreme knee position should be avoided and articular cartilage is protected when there is static loading on the knee joint. It is also shown that models can be derived to explain the load vs. time behaviour of the meniscus and articular cartilage.

7.0 CONCLUSION AND RECOMMENDATIONS

In conclusion, measurement of the stresses within the meniscus during dynamic variation of the knee position and during static exertion of pressure is possible. From the experiment conducted in the measurement of the intrameniscal forces, it was shown that the pressure conductive sensor can be used with some modification to measure dynamic pressure variation. The study introduces a new experimental technique for investigation in the knee mechanics.

In this report, variation of intrameniscal stress with joint angulations, applied torque and time were determined. The locations in the menisci, at which the highest stress occurs during dynamic load application, can be determined at different joint position. The terminal knee positions examined were hyperextension, hyperflexion, maximal internal and maximal external rotation. From the experimental results, high intrameniscal stresses were experienced during terminal positions. This indicates that extreme positions with high applied moment on the knee joint should be avoided. It is significant to note that a lower applied moment at a combination of extreme positions of the knee joint, for example external rotation with maximal extension, will cause high stress to be experienced within the meniscus.

The variations of stress with time in the menisci and in the articular cartilage-articular cartilage interface were determined. The result strongly implies that the stress shifted from the articular cartilage to the meniscus in the porcine knee specimens as time increases. This finding suggests that load on the articular cartilage will be reduced during static standing. This load shift behaviour will protect the articular cartilage if the knee joint is under static loading. This phenomenon was studied through the formulation of mathematical models.

The mathematical models derived are the standard linear solid model and two viscoelastic power models. From the models, it was shown that results yielded by the static load experiment and the stress relaxation tests can be explained by the non linear viscoelastic power model. Load shift in the structures were displayed by both the viscoelastic power models. The different behaviour of the stress variation at tertiary stage can be modelled by changing the exponent of the power law equation

for meniscus viscoelastic element, which is shown in the second viscoelastic power-law model.

Measurement of the forces in the knee joint is invaluable to the understanding of the knee mechanics. This can aid in the validation of theoretical models and will benefit in the designs and establishments of preventive and corrective measures in knee injuries.

The measurement of the intrameniscal stresses and derivation of mathematical model should be conducted on human cadaveric knee to get more understanding in the meniscus mechanics and its injuries. By comparing the pattern of intrameniscal stress variation with the applied moment and joint position, more insight on the human knee mechanics can be gained. In addition, the mathematical model can be formulated by considering the 'wedge' shape geometry of the meniscus to investigate in the effect of geometry on meniscus mechanics.

8.0 PAPERS PUBLISHED/IN-REVIEW

- P. K. Goh, F. K. Fuss, A. C. Ritchie, D. T. T. Lie, S. C. Tjin Intrameniscal forces determined by Fibre Bragg Grating sensors. 7th Annual NTU-SGH Symposium (Singapore 2005), Symposium Paper Published
- P. K. Goh, F. K. Fuss, T. Yanai, A. C. Ritchie, D. T. T. Lie, S. C. Tjin Determination of intrameniscal stresses. 12th International Conference on BioMedical Engineering (Singapore 2005), Conference Paper Published
- P. K. Goh, F. K. Fuss, T. Yanai, A. C. Ritchie Dynamic Intrameniscal Stresses Measurement in the Porcine Knee. International Conference on Biomedical and Pharmaceutical Engineering (Singapore 2006), Conference Paper Published
- P. K. Goh, F. K. Fuss, T. Yanai, A. C. Ritchie Time-Dependent Change of Load Sharing between Two Non-Linear Visco-Elastic Materials: Experiment and Model. International Conference on Biomedical and Pharmaceutical Engineering (Singapore 2006), Conference Paper Published
- P. K. Goh, F. K. Fuss, T. Yanai, A. C. Ritchie, D. T. T. Lie, S. C. Tjin Measurement of Intrameniscal Forces and Stresses by Two Different Miniature Transducers. Journal of Mechanics in Medicine and Biology Vol. 7, No. 1 (2007) 65–74, Journal Paper Published

9.0 REFERENCES

1. Seireg, A. and Arvikar, R.J., *The prediction of muscular load sharing and joint forces in the lower extremities during walking*. Journal of Biomechanics, 1975. **8** (2):89-102.
2. Fu, F.H. and Thompson, W.O., *Motion of the Meniscus During Knee Flexion*, in *Knee Meniscus: Basic and Clinical Foundation*, V.C. Mow, S.P. Arnoczky, and D.W. Jackson, Editors. 1992, Raven Press, Ltd: New York. p. 75-89.
3. *Changi General Hospital Performs Singapore's First Meniscal Transplant*. [http://www.cgh.com.sg/public/caring/Apr2002_issue72/pg1.htm]. Changi General Hospital 2002. (Accessed: October 2005)
4. Hollis, J.M., Pearsall IV, A.W. and Niciforos, P.G., *Change in meniscal strain with anterior cruciate ligament injury and after reconstruction*. The American Journal of Sports Medicine, 2000. **28** (5):700-704.
5. Medlar, R.C., Mandiberg, J.J. and Lyne, E.D., *Meniscectomies in children. Report of long-term results (mean, 8.3 years) of 26 children*. American Journal of Sports Medicine, 1980. **8** (2):87-92.
6. Brindle, T., Nyland, J. and Johnson, D.L., *The Meniscus: Review of Basic Principles with Application to Surgery and Rehabilitation*. Journal of Athletic Training, 2001. **36** (2):160-169.
7. Arnoczky, S.P. and McDevitt, C.A., *The Meniscus: Structure, Function, Repair, and Replacement*, in *Orthopaedic Basic Science: Biology and Biomechanics of the Musculoskeletal System*, J.A. Buckwalter, T.A. Einhorn, and S.R. Simon, Editors. 2000, American Academy of Orthopaedic Surgeons: Rosemont.
8. Bendjaballah, M.Z., Shirazi-Adl, A. and Zukor, D.J., *Biomechanics of the human knee joint in compression: reconstruction, mesh generation and finite element analysis*. The Knee, 1995. **2** (2):69-79.

9. Meakin, J.R., Shrive, N.G., Frank, C.B. and Hart, D.A., *Finite element analysis of the meniscus: The influence of geometry and material properties on its behaviour*. Knee, 2003. **10** (1):33-41.
10. Pena, E., Calvo, B., Martinez, M.A., Palanca, D. and Doblare, M., *Finite element analysis of the effect of meniscal tears and meniscectomies on human knee biomechanics*. Clinical Biomechanics, 2005. **20**:498-507.
11. Perie, D. and Hobatho, M.C., *In vivo determination of contact areas and pressure of the femorotibial joint using non-linear finite element analysis*. Clinical Biomechanics, 1998. **13**:394-402.
12. Wilson, W., van Rietbergen, B., van Donkelaar, C.C. and Huiskes, R., *Pathways of load-induced cartilage damage causing cartilage degeneration in the knee after meniscectomy*. Journal of Biomechanics, 2003. **36**:845-851.
13. Donahue, T.L.H., Hull, M.L., Rashid, M.M. and Jacobs, C.R., *How the stiffness of meniscal attachments and meniscal material properties affect tibio-femoral contact pressure computed using a validated finite element model of the human knee joint*. Journal of Biomechanics, 2003. **36**:19-34.
14. LeRoux, M.A. and Setton, L.A., *Experimental and Biphase FEM Determinations of the Material Properties and Hydraulic Permeability of the Meniscus in Tension*. Journal of Biomechanical Engineering, 2002. **124** (3):315-321.
15. Donahue, T.L.H., Hull, M.L., Rashid, M.M. and Jacobs, C.R., *A Finite Element Model of the Human Knee Joint for the Study of Tibio-Femoral Contact*. Journal of Biomechanical Engineering, 2002. **124** (3):273-280.
16. Spilker, R.L., Donzelli, P.S. and Mow, V.C., *A transversely isotropic biphasic finite element model of the meniscus*. Journal of Biomechanics, 1992. **25** (9):1027-1045.

17. Lengsfeld, M., *Stresses at the meniscomfemoral joint: Elastostatic investigations on the applicability of interface elements*. Journal of Biomedical Engineering, 1993. **15** (4):324-328.
18. Bendjaballah, M.Z., Shirazi-Adl, A. and Zukor, D.J., *Biomechanical response of the passive human knee joint unders anterior-posterior forces*. Clinical Biomechanics, 1998. **13**:625-633.
19. Bendjaballah, M.Z., Shirazi-Adl, A. and Zukor, D.J., *Finite element analysis of human knee joint in varus-valgus*. Clinical Biomechanics, 1997. **12** (3):139-148.
20. Pfeiler, T.W., Shirazi-Adl, A., Kasra, M. and Cates, H.E. *Finite element dynamic response analysis of the human knee joint*. in *Advances in Bioengineering*. 2004.
21. Moglo, K.E. and Shirazi-Adl, A., *Biomechanics of passive knee joint in drawer: Load transmission in intact and ACL-deficient joints*. Knee, 2003. **10** (3):265-276.
22. Penrose, J.M.T., Holt, G.M., Beaugonin, M. and Hose, D.R., *Development of an Accurate Three-dimensional Finite Element Knee Model*. Computer methods in biomechanics and biomedical engineering, 2002. **5** (4):291-300.
23. Mesfar, W. and Shirazi-Adl, A., *Biomechanics of the knee joint in flexion under various quadriceps forces*. The Knee, 2005. **12**:424-434.
24. Jilani, A., Shirazi-Adl, A. and Bendjaballah, M.Z., *Biomechanics of human tibio-femoral joint in axial rotation*. The Knee, 1997. **4**:203-213.
25. Wismans, J., Veldpaus, F. and Janssen, J., *A three-dimensional mathematical model of the knee joint*. Journal of Biomechanics, 1980. **13**:677-685.
26. Ahmed, A.M., *The Load-Bearing Role of the Knee Menisci*, in *Knee Meniscus: Basic and Clinical Foundations*, V.C. Mow, S.P. Arnoczky, and D.W. Jackson, Editors. 1992, Raven Press, Ltd.: New York. p. 59-73.

27. Huang, A., Hull, M.L. and Howell, S.M., *The level of compressive load affects conclusions from statistical analyses to determine whether a lateral meniscal autograft restores tibial contact pressure to normal: A study in human cadaveric knees*. Journal of Orthopaedic Research, 2003. **21** (3):459-464.
28. Kaufman, K.R., Kovacevic, N., Irby, S.E. and Colwell, C.W., *Instrumented implant for measuring tibiofemoral forces*. Journal of Biomechanics, 1996. **29** (5):667-671.
29. D'Lima, D.D., Townsend, C.P., Arms, S.W., Morris, B.A. and Colwell, J., Clifford W., *An implantable telemetry device to measure intra-articular tibial forces*. Journal of Biomechanics, 2005. **38** (2):299-304.
30. Crottet, D., Maeder, T., Fritschy, D., Bleuler, H., Nolte, L.-P. and Pappas, I.P., *Development of a Force Amplitude- and Location- Sensing Device Designed to Improve the Ligament Balancing Procedure in TKA*. IEEE Transactions on Biomedical Engineering, 2005. **52** (9):1609-1611.
31. Amirouche, F., Aram, L., Gonzalez, M., Giachetti, R. and Mahr, C. *The fitting of the Human Joint through Micro Implanted Sensors*. in *1st Annual International IEEE-EMBS Special Topic Conference on Microtechnologies in Medicine & Biology*. 2000. Lyon, France.
32. Uezaki, N., Kobayashi, A. and Matsushige, K., *The viscoelastic properties of the human semilunar cartilage*. Journal of Biomechanics, 1979. **12** (1):65-73.
33. Sweigart, M.A. and Athanasiou, K.A., *Tensile and compressive properties of the medial rabbit meniscus*. Journal of Engineering in Medicine, 2005. **219**:337-347.
34. Sweigart, M.A., Zhu, C.F., Agrawal, C.M., Clanton, T.C. and Athanasiou, K.A. *Biomechanical properties of the medial meniscus in experimental animal models*. in *Proceedings of the Second Joint EMBS/BMES Conference*. 2002. Houston, United States.

35. Becker, R., Wirz, D., Wolf, C., Gopfert, B., Nebelung, W. and Friederich, N., *Measurement of meniscomfemoral contact pressure after repair of bucket-handle tears with biodegradable implants*. Archives of Orthopaedic and Trauma Surgery, 2005. **125** (4):254-260.
36. Anderson, I.A., MacDiarmid, A.A., Harris, M.L., Gillies, R.M., Phelps, R. and Walsh, W.R., *A novel method for measuring medial compartment pressures within the knee joint in-vivo*. Journal of Biomechanics, 2003. **36** (9):1391-1395.
37. Andrish, J.T., Kambic, H.E., Valdevit, A.D.C., Kuroda, R., Parker, R.D., Aronowitz, E. and Elster, T., *Selected knee osteotomies and meniscal replacement: Effects on dynamic intra-joint loading*. Journal of Bone and Joint Surgery - Series A, 2001. **83** (SUPPL. 2 II):142-150.
38. Jones, R.S., Keene, G.C.R., Learmonth, D.J.A., Bickerstaff, D., Nawana, N.S., Costi, J.J. and Percy, M.J., *Direct measurement of hoop strains in the intact and torn human medial meniscus*. Clinical Biomechanics, 1996. **11** (5):295-300.
39. Komistek, R.D., Kane, T.R., Mahfouz, M., Ochoa, J.A. and Dennis, D.A., *Knee mechanics: a review of past and present techniques to determine in vivo loads*. Journal of Biomechanics, 2005. **38** (2):215-228.
40. McGinty, G., Irrgang, J.J. and Pezzullo, D., *Biomechanical considerations for rehabilitation of the knee*. Clinical Biomechanics, 2000. **15** (3):160-166.
41. Tortora, G.J. and Grabowski, S.R., *Principles of anatomy and physiology*. 9th ed. 2000, Wiley:New York ; Chichester.
42. Hay, J.G. and Reid, J.G., *Anatomy, mechanics, and human motion*. 2nd ed. 1988, Prentice Hall:Englewood Cliffs, N.J.
43. O'Connor, J.J., Shercliff, T.L., Biden, E. and Goodfellow, J.W., *Geometry of the knee in the sagittal plane*. Proceedings of the Institution of Mechanical Engineers, Part H: Journal of Engineering in Medicine, 1989. **203** (4):223-203.

44. Fuss, F.K., *Anatomy of the cruciate ligaments and their function in extension and flexion of the human knee joint*. American Journal of Anatomy, 1989. **184** (2):165-176.
45. Fuss, F.K., *Biomechanics of the child's knee (Biomechanik des kindlichen kniegelenks)*. Acta Chirurgica Austriaca, 1996. **28** (SUPPL. 120):7-10.
46. Yao, J., Snibbe, J., Maloney, M. and Lerner, A.L., *Stresses and strains in the medial meniscus of an ACL deficient knee under anterior loading: A finite element analysis with image-based experimental validation*. Journal of Biomechanical Engineering, 2006. **128** (1):135-141.
47. Weissengruber, G.E., Fuss, F.K., Egger, G., Stanek, G., Hittmair, K.M. and Forstenpointner, G., *The elephant knee joint: Morphological and biomechanical considerations*. Journal of Anatomy, 2006. **208** (1):59-72.
48. Fuss, F.K., *Voluntary rotation in the human knee joint*. Journal of Anatomy, 1991. **179**:115-125.
49. Platzer, W., *Bewegungsapparat*, in *Atlas der Anatomie*, W. Kahle, H. Leonhardt, and W. Platzer, Editors. 1979, Thieme: Stuttgart.
50. Koh, J.S.B., Nagai, T., Motojima, S., Sell, T.C.a. and Lephart, S.M., *Concepts and measurement of in vivo tibiofemoral kinematics*. Operative Techniques in Orthopaedics, 2005. **15** (1):43-48.
51. Messner, K. and Gao, J., *The menisci of the knee joint. Anatomical and functional characteristics, and a rationale for clinical treatment*. Journal of Anatomy, 1998. **193** (2):161-178.
52. Mow, V.C. and Ratcliffe, A., *Structure and Function of Articular Cartilage and Meniscus*, in *Basic Orthopaedic Biomechanics*, V.C. Mow and W.C. Hayes, Editors. 1997, Lippincott-Raven: Philadelphia. p. 113-178.
53. McKinley, M. and O'Loughlin, V.D., *Human Anatomy*. 2006, McGraw-Hill:New York.

54. Fuss, F.K.: *Anatomy, BG2051, 1009*, Nanyang Technological University, Singapore; 2006 (Lecture notes)
55. Gray, H., *The Complete Gray's Anatomy*. Sixteenth ed. T.P. Pick and R. Howden. 2003, Merchant Book Company:East Molesey.
56. Smith, L.K., Weiss, E.L. and Lehmkuhl, L.D., *Brunnstrom's Clinical Kinesiology*. Fifth ed. 1996, F.A. Davis:Philadelphia.
57. Arnoczky, S.P., *Gross and Vascular Anatomy of the Meniscus and Its role in Meniscus Healing, Regeneration, and Remodeling*, in *Knee Meniscus: Basic and Clinical Foundation*, V.C. Mow, S.P. Arnoczky, and D.W. Jackson, Editors. 1992, Raven Press,Ltd: New York. p. 1-14.
58. Gupte, C.M., Bull, A.M.J., Thomas, R.D.W. and Amis, A.A., *A review of the function and biomechanics of the meniscofemoral ligaments*. Arthroscopy - Journal of Arthroscopic and Related Surgery, 2003. **19** (2):161-171.
59. Beaupre, A., Choukroun, R. and Guidouin, R., *Knee menisci: Correlation between microstructure and biomechanics*. Clinical Orthopaedics and Related Research, 1986. **208**:72-75.
60. Kapandji, I.A., *The Physiology of the joints*. Vol. 2. 1970, Churchill Livingstone:New York.
61. Ritchie, A.C.: *Biomechanics of the Meniscus*, Singapore; 2005 (Personal Communication)
62. Levy, I.M., Torzilli, P.A. and Fisch, I.D., *The contribution of the meniscus to the stability of the knee*, in *Knee Meniscus: Basic and Clinical Foundations*, V.C. Mow, S.P. Arnoczky, and D.W. Jackson, Editors. 1992, Raven Press, Ltd: New York. p. 107-115.
63. Blauvelt, C.T. and Nelson, F.R.T., *A Manual of Orthopaedic Terminology*. Sixth ed. 1998, Mosby Inc.:St Louis.
64. Schlosser, V. and Kuner, E., *Traumatologie*. Third ed. 1980, Thieme:Stuttgart.

65. Heim U, B.J., *Checkliste Traumatologie*. 1981, Thieme:Stuttgart.
66. Burri, C., Beck, H., Ecke, H., Jungbluth, K.H., Kuner, E.H., Pannike, A., Schmit-Neuerburg, K.P., Schweiberer, L., Schweikert, C.H., Spier, W. and Tscherne, H., *Unfallchirurgie*. Third ed. 1982, Springer:Berlin.
67. Seeley, R.R., Stephens, T.D. and Tate, P., *Anatomy & physiology*. 6th ed. 2003, McGraw-Hill:Dubuque, IA.
68. Hall, S.J., *Basic Biomechanics*. 2nd ed. 1995, Brown and Benchmark:Madison.
69. Lento, P.H. and Akuthota, V., *Meniscal injuries: A critical review*. Journal of Back and Musculoskeletal Rehabilitation, 2000. **15** (2-3): 55-62.
70. Drosos, G.I. and Pozo, J.L., *The causes and mechanisms of meniscal injuries in the sporting and non-sporting environment in an unselected population*. Knee, 2004. **11** (2):143-149.
71. Childress, H.M., *Diagnosis of Posterior Lesions of the Medial Meniscus*. American Journal of Surgery, 1957. **93**:782-787.
72. McDermott, I.D., *Meniscal tears*. Current Orthopaedics, 2006. **20** (2):85-94.
73. Peters, G. and Wirth, C.J., *The current state of meniscal allograft transplantation and replacement*. Knee, 2003. **10** (1):19-31.
74. Kobayashi, M., Chang, Y.-S. and Oka, M., *A two year in vivo study of polyvinyl alcohol-hydrogel (PVA-H) artificial meniscus*. Biomaterials, 2005. **26** (16):3243-3248.
75. Felix, N.A. and Paulos, L.E., *Current status of meniscal transplantation*. The Knee, 2003. **10**:13-17.
76. Bergmann, G., Graichen, F. and Rohlmann, A., *Hip joint loading during walking and running, measured in two patients*. Journal of Biomechanics, 1993. **26** (8):969-990.

77. Brand, R.A., Pedersen, D.R., Davy, D.T., Kotzar, G.M., Heiple, K.G. and Goldberg, V.M., *Comparison of hip force calculations and measurements in the same patient*. The Journal of Arthroplasty, 1994. **9** (1):45-51.
78. Skyhar, M.J., Warren, R.F., Ortiz, G.J., Schwartz, E. and Otis, J.C., *The effects of sectioning of the posterior cruciate ligament and the posterolateral complex on the articular contact pressures within the knee*. Journal of Bone and Joint Surgery - Series A, 1993. **75** (5):694-699.
79. Wang, C. L., Cheng, C.K., Chen, C.W., Lu, C.M., Hang, Y.S. and Liu, T.K., *Contact areas and pressure distributions in the subtalar joint*. Journal of Biomechanics, 1995. **28** (3):269-279.
80. McNamara, J.L., Collier, J.P., Mayor, M.B. and Jensen, R.E., *A comparison of contact pressures in tibial and patellar total knee components before and after service in vivo*. Clinical Orthopaedics and Related Research, 1994. (299):104-113.
81. Zdero, R., Fenton, P.V., Rudan, J. and Bryant, J.T., *Fuji Film and Ultrasound Measurement of Total Knee Arthroplasty Contact Areas*. The Journal of Arthroplasty, 2001. **16** (3):367-375.
82. Orr, J.F. and Shelton, J.C., *Optical measurement methods in biomechanics*. 1st ed. 1997, Chapman & Hall:London ; New York.
83. Liao, J.J., Cheng, C.K., Huang, C.H. and Lo, W.H., *Effect of Fuji pressure sensitive film on actual contact characteristics of artificial tibiofemoral joint*. Clinical Biomechanics, 2002. **17**:698-704.
84. Thambyah, A., Goh, J.C.H. and Das De, S., *Contact stresses in the knee joint in deep flexion*. Medical Engineering and Physics, 2005. **27** (4):329-335.
85. *Map and Sensor model number: 4000*.
[<http://www.tekscan.com/medical/catalog/4000.html>]. Tekscan Inc. ©2005.
(Accessed: November 2005)

86. *Map and Sensor model number: 6900.*
[<http://www.tekscan.com/medical/catalog/6900.html>]. Tekscan Inc. ©2005.
(Accessed: November 2005)
87. Hollis, J.M., Pearsall IV, A.W. and Niciforos, P.G., *Change in meniscal strain with anterior cruciate ligament injury and after reconstruction.* The American Journal of Sports Medicine, 2000. **28** (5):700-704.
88. Wu, J.Z., Herzog, W. and Epstein, M., *Effects of inserting a pressensor film into articular joints on the actual contact mechanics.* Journal of Biomechanical Engineering, 1998. **120** (5):655-659.
89. Stachowiak, G.W. and Batchelor, A.W., *Engineering Tribology.* 2001, Butterworth Heinemann:Boston.
90. Havey, R.M., Patwardhan, A.G., Meade, K.P. and Gavin, T.M., *Methodology - Measurements, part II: Instrumentation and apparatus.* Journal of Prosthetics and Orthotics, 1996. **8** (2):50-64.
91. Gloeckner, P.J. and Kostrzewsky, G.J., *An overview of obtaining quantitative pressure distributions and loads from pressure-sensitive films.* Experimental Techniques, 2002. **26** (1):27-30.
92. Omega Engineering Inc.: *Transactions in measurement and control-Volume 3 Force related measurement,* 2003
93. Chung, D.D.L., *Comparison of submicron-diameter carbon filaments and conventional carbon fibers as fillers in composite materials.* Carbon, 2001. **39** (8):1119-1125.
94. Taya, M., Kim, W.J. and K., O., *Piezoresistivity of a short fiberrelastomer matrix composite.* Mechanics of materials, 1998. **28**:53-59.
95. Niggs, B.M., *Measurement techniques- Pressure Distribution,* in *Biomechanics of the Musculo-skeletal system*, B.M. Niggs and W. Herzog, Editors. 1999, John Wiley and Sons: Chichester. p. 281-285.

96. *Flexiforce Force sensor* [<http://www.tekscan.com/flexiforce/flexiforce.html>]. Tekscan Inc. ©2005. (Accessed: September 2005)
97. Fregly, B.J. and Sawyera, W.G., *Estimation of discretization errors in contact pressure measurements*. Journal of Biomechanics, 2003. **36**:609–613.
98. Kendall, M.: *K-scan sensors*, Boston; 2005 (Personal Communication)
99. Niihara, K., Choa, Y.-H., Hussain, M., Nishida, H., Hamahashi, Y. and Kawahara, K. (2003) *Deformable conductive elastomer and manufacturing method thereof*. United States. US 6,558,577 B1
100. *Inastomer (pressure conductive sensor)*. [http://www.inabarubber.co.jp/en/b_products/inastomer/index.html]. Inaba Rubber Co., L. 2004. (Accessed: 2005)
101. Ashruf, C.M.A., *Thin flexible pressure sensors*. Sensor Review, 2002. **22** (4):322-327.
102. Fernandes, C.P., Glantz, P.-O.J., Svensson, S.A. and Bergmark, A., *A novel sensor for bite force determinations*. Dental Materials, 2003. **19** (2):118-126.
103. Gilbertson, L., Goel, V.K., Patwardhan, A.G., Havey, R., Morris, T. and Gavin, T. *Biomechanical function of 'three-point' hyperextension orthoses*. in *American Society of Mechanical Engineers, Bioengineering Division (Publication) BED*. 1991.
104. *FSR Integration Guide Notes*. [<http://www.steadlands.com/interlink/interlinkpages/fsr.htm>]. Steadlands International Marketing Ltd 2005. (Accessed: September 2005)
105. Lee, B., *Review of the present status of optical fiber sensors*. Optical Fiber Technology, 2003. **9**:57-79.
106. Tjin, S.C., Mohanty, L., Lie, D.T.T. and Paganiban, S. *Tibiofemoral pressure mapping with fiber grating sensor*. in *7th Annual NTU-SGH Symposium*. 2005. Singapore.

107. Krohn, D.A., *Fiber optic sensors : Fundamentals and Applications*. 3rd ed. 2000, ISA:Research Triangle Park, NC.
108. Urbanczyk, W., *Selected applications of fiber-optic sensors*. Proceedings of SPIE - The International Society for Optical Engineering, 1999. **3820**:221-234.
109. Othonos, A. and Kalli, K., *Fiber Bragg gratings : fundamentals and applications in telecommunications and sensing*. Artech House optoelectronics library. 1999, Artech House:Boston.
110. Baek, S., Jeong, Y. and Lee, B., *Characteristics of short-period blazed fiber Bragg gratings for use as macro-bending sensors*. Applied Optics, 2002. **41** (4):631-636.
111. Othonos, A., *Fiber Bragg gratings*. Review of Scientific Instruments, 1997. **68** (12):4309-4341.
112. Fuss, F.K.: *Meniscus of different species*, Singapore; 2006 (Personal Communication)
113. Fuss, F.K., *Fibrous tissue on the tibia plateau of the kangaroo: A theory on the pressure absorption of joint surfaces*. Anatomical Record, 1994. **238** (3):297-303.
114. Hingorani, R.V., Provenzano, P.P., Lakes, R.S., Escarcega, A. and Vanderby Jr., R., *Nonlinear viscoelasticity in rabbit medial collateral ligament*. Annals of Biomedical Engineering, 2004. **32** (2):306-312.
115. Provenzano, P.P., Lakes, R.S., Keenan, T. and Vanderby Jr, R., *Nonlinear Ligament Viscoelasticity*. Annals of Biomedical Engineering, 2001. **29**:908-914.
116. Lakes, R.S. and Vanderby, R., *Interrelation of creep and relaxation: A modeling approach for ligaments*. Journal of Biomechanical Engineering, 1999. **121** (6):612-615.

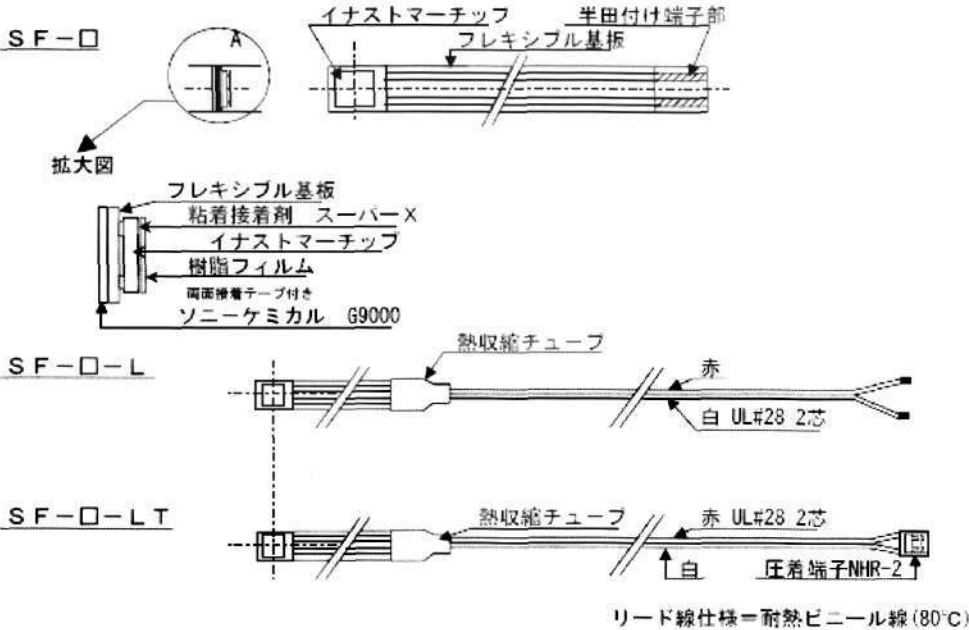
117. Hayes, C.W., Brigido, M.K., Jamadar, D.A. and Propeck, T., *Mechanism-based Pattern Approach to Classification of Complex Injuries of the Knee Depicted at MR Imaging*. RadioGraphics, 2000. **20**:S121 - S134.
118. Senter, C. and Hame, S.L., *Biomechanical analysis of tibial torque and knee flexion angle: Implications for understanding knee injury*. Sports Medicine, 2006. **36** (8):635-641.
119. Majewski, M., Susanne, H. and Klaus, S., *Epidemiology of athletic knee injuries: A 10-year study*. Knee, 2006. **13** (3):184-188.
120. Järvinen, M., Natri, A., Laurila, S. and Kannus, P., *Mechanisms of anterior cruciate ligament ruptures in skiing*. Knee Surgery, Sports Traumatology, Arthroscopy, 1994. **2** (4):224-228.
121. Souzaa, M., Monteiroa, H., Del Vecchiob, F. and Gonçalvesb, A., *Referring to judo's sports injuries in São Paulo State Championship*. Science & Sports, 2006. **21**:280–284.
122. Peters, P., *Orthopedic problems in sport climbing*. Wilderness and Environmental Medicine, 2001. **12** (2): 100-110.
123. Adams, M.E. and Hukins, D.W.L., *The Extracellular Matrix of the Meniscus*, in *Knee Meniscus: Basic and Clinical Foundations*, V.C. Mow, S.P. Arnoczky, and D.W. Jackson, Editors. 1992, Raven Press: New York. p. 15-28.

APPENDIX A

仕様書

1. 品名 イナストマー SFタイプ (2、3、4、5)

2. 外形寸法



項目	定格
(1) 使用温度範囲	-5~50℃
(2) 使用湿度範囲	30~85%RH
(3) 保存温度範囲	-40~70℃
(4) 保存湿度範囲	10~95%RH
(5) 最大許容負荷	3~5kgf (サイズにより変更)
(6) 最大許容電圧	30V
(7) 最大許容電流	20mA

4. 電気的特性

項目	仕様	条件
(1) 無負荷抵抗値	40MΩ以上	0kgf
(2) 最大負荷抵抗値	1.0kΩ以下	3000gf

5. F-R特性

(1) 押し方向

規格値 (参考値)

負荷 [gf]	0	50	100	250	500	1500	3000
抵抗値 [Ω]	40M以上	300k~150k	100k~60k	50k~25k	8.0k~4.0k	3.0k~1.3k	1.0k以下

(2) 戻し方向

「各荷重点から負荷の開放に対して、下記で定める仕様を満足すること」

条件	仕様
負荷が加わった状態から0gfへ開放する	1 sec以内に10MΩ以上に復帰すること

6. 機械的特性

- (1) 最大荷重 ... 5.0 k g f
- (2) 推奨荷重 ... 3.0 k g f
- (3) リード線引っ張り強度...2.0 k g f

7. 耐久性

1.0kgfの負荷において、1秒ON－3秒OFFの連続耐久試験において10万回終了異常ないこと。

8. 温度特性

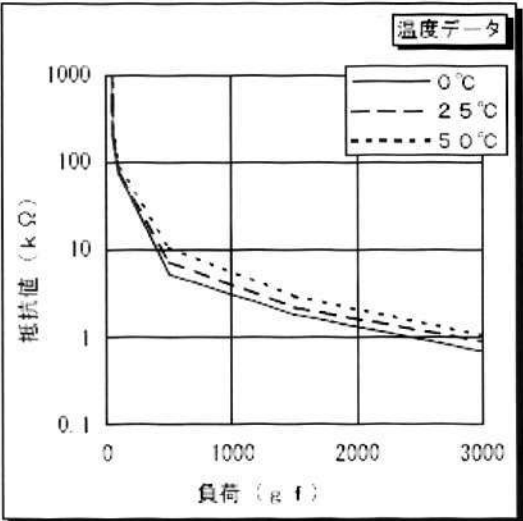
使用温度範囲 0～50℃

参考データ：SF-5

g f	0℃	25℃	50℃
0	1.65E+12	1.65E+12	1.65E+12
50	180.17	206.24	262.30
100	71.92	72.37	86.40
500	5.24	7.24	10.47
1500	1.82	2.19	2.95
3000	0.69	0.89	1.05

(単位：kΩ)

※温度補正回路により変化を少なくすることが可能



※個体間、製造ロット間でのばらつきがあります。

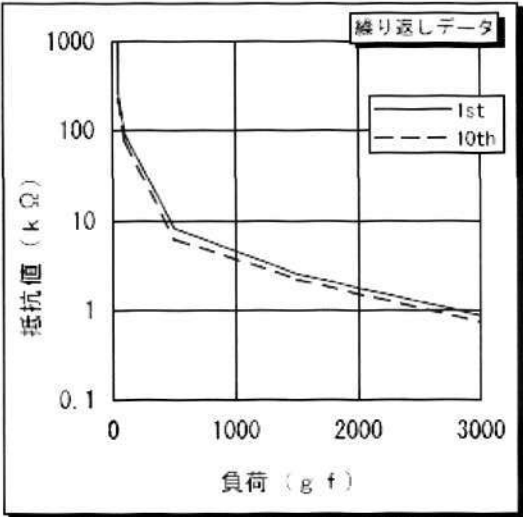
9. 繰り返し加圧復帰特性

初期から10回加圧までの特性変化

参考データ：SF-5

g f	1st	10th
0	1.65E+12	1.65E+12
50	256.87	223.89
100	92.66	73.78
500	8.13	6.18
1500	2.51	2.19
3000	0.86	0.72

(単位：kΩ)



※個体間、製造ロット間でのばらつきがあります。

The maximum force that can be applied to a single sensor = 4 kgf [39 N]

The maximum force allowed for accurate measurements = 3 kgf [27 N]

The maximum current that can be applied = 20 mA

The maximum voltage that can be applied = 30 V

The range of temperature in which the sensor can be used = -5 ~ 50 degrees Celsius

The range of the environmental humidity in which the sensor can be used = 30 ~ 85 %

APPENDIX B

